ELECTRONIC SPECTROSCOPY OF ISOELECTRONIC MOLECULES. II. LINEAR TRIATOMIC GROUPINGS CONTAINING SIXTEEN VALENCE ELECTRONS*†

J. W. RABALAIS,‡ J. M. McDONALD, V. SCHERR,§ AND S. P. McGLYNN**

Coates Chemical Laboratories, Louisiana State University, Baton Rouge, Louisiana 70803

Received April 15, 1970 (Revised Manuscript Received August 12, 1970)

Contents

Foreword

This work contains original material; it also possesses many characteristics of a review article. The review nature stems from the consideration of older data, the collation of this older material into a coherent whole, the provision of missing information where needed, and the reinterpretation of the entirety of old and new data in an internally consistent fashion.

The plan of the article requires comment:

(i) The general approaches found useful are outlined in section I.

(ii) The theoretical aspects and all methods used in the interpretive effort are discussed in section II. While the utility of these methods is illustrated at appropriate points in the text, their full applicability will not be evidenced until section IV.

(iii) Section III provides information on instrumentation, chemical sources, and purification procedures. The experimental aspects of the molecular electronic spectra of each isoelectronic entity are discussed. The electronic transitions are labeled in terms of state assignments which are not fully validated. Thus, the assignments made here for individual electronic transitions may seem premature; we excuse ouselves for this tactic by noting the textual cohesion which it provides and the fact that the use of other names (*i.e.*, α band, p band, V ← N transition, etc.) is evaded.

(iv) The material of sections II and III is conjoined in section IV. The discussion given may seem brief—perhaps superficial; this, however, is a consequence of the prior sections II and III and a desire not to be overly repetitive.

I. Introduction

The electronic spectra of triatomic 16-valence-electron molecules have been much investigated. Nonetheless, few state identifications exist. The best attempts at assigning the excited electronic states of these molecules have been made by Mulliken[1] and Walsh.[2] However, these authors had access to limited amounts of data, and their correlations left questions unanswered. The purpose of the present work is to elicit good electronic absorption spectra (*i.e.*, to ~11 eV) and to characterize and identify excited electronic states.

The molecules considered are

$D_{\infty h}$ point group—CO_2, CS_2, NNN^-, NO_2^+, CN_2^{2-}, $HgCl_2$, $HgBr_2$, HgI_2

$C_{\infty v}$ point group—OCS, NNO, NCO^-, NCS^-, NCCl, NCBr, NCI

* This work was supported by contract between the U. S. Atomic Energy Commission—Biology Branch and the Louisiana State University. The computational work reported herein was performed under the aegis of a U. S. Air Force contract with the Louisiana State University.

† Part I of this series is concerned with bent triatomics such as O_3, NO_2, $HCOO^-$, peptide linkage, etc.: H. J. Maria, D. Larson, M. E. McCarville, and S. P. McGlynn, *Accounts Chem. Res.*, 3, 368 (1970).

‡ Present address: Institute of Physics, University of Uppsala, Uppsala, Sweden. This work was done in partial fulfillment of the requirements for the degree of Doctor of Philosophy at the Louisiana State University.

§ Present address: Department of Chemistry, University of Wisconsin—Parkside, Kenosha, Wis. 53140.

** To whom correspondence concerning this material should be addressed.

(1) R. S. Mulliken, *Can. J. Chem.*, 36, 10 (1958); *Rev. Mod. Phys.*, 14, 204 (1942); *J. Chem. Phys.*, 3, 720 (1935); *J. Chim. Phys.*, 46, 497, 675 (1949); *Phys. Rev.*, 41, 751 (1932); 43, 279 (1933); 60, 512 (1941); *Chem. Rev.*, 41, 219 (1947).

(2) A. D. Walsh, *J. Chem. Soc.*, 2266 (1953).

D_{2d} point group—H_2CCCH_2
C_{2v} point group—H_2CCO, H_2NCN, $(CH_3)_2NCN$, H_2CNN
C_s point group—HNNN, HNCO, HNCS, CH_3CH_2NCO, $C_5H_{11}NNN$

All of these molecules or ions contain 16 valence electrons Nearly all are triatomic; those few which are not consist of a dominant triatomic grouping to which are attached σ-bonded H atoms or alkyl groups. The triatomic grouping is always linear in the ground state of the system.

Some of the spectra presented here have been measured previously; our remeasurements were made to provide a single representation of the entire absorption region, to evaluate unknown extinction coefficients and oscillator strengths, and to provide missing data relating to energies, band shapes, vibrational structure, and Rydberg transitions.

Three techniques have been employed in assigning electronic spectra: (i) symmetry considerations; (ii) semiempirical molecular orbital calculations; and (iii) specific identifications. Each method is separately useful for making state identifications; however, consistent agreement between the three methods can provide unique assignments. These methods are as follows.

(*i*) *Symmetry Considerations.* The main differences in the molecules of interest arise from the atomic make-up of the triatomic grouping and the slight perturbations supplied by the off-axis attachment of H atoms or alkyl groups. The grouping of spectroscopic significance is the linear triatomic entity. The off-axis perturbation supplied by appended groups removes many of the electronic degeneracies associated with the linear triatomic chain—but does so in such a way as to retain the widely spread distribution of states characteristic of the linear entity. Consequently, degeneracies inherent in the states of $D_{\infty h}$ and $C_{\infty v}$ molecules should resolve in predictable ways as one proceeds to lower molecular symmetries. Furthermore, many transitions, which are dipole-forbidden in the high-symmetry molecules, may attain considerable dipole-allowedness in the lower symmetry entities. Given the persistence of recognizable trends from molecule to molecule, the removal of degeneracies and of dipole-forbiddenness can provide important diagnostic tools for state identifications.

(*ii*) *Semiempirical Molecular Orbital Calculations.* Electronic structure and spectroscopy can be discussed in terms of LCAO MO calculations. Mulliken–Wolfsberg–Helmholz (MWH) calculations are useful in discussing such properties as molecular wave functions, one-electron orbital energies as a function of angle (Walsh diagrams), total electronic energy as a function of angle, transition energies, charge densities, etc. Variable-electronegativity self-consistent-field (VESCF) and configuration interaction (CI) calculations provide useful theoretical energies and wave functions for states of $\pi \rightarrow \pi^*$ type. Oscillator strengths and lifetimes of singlet ← singlet and triplet ← singlet transitions can be calculated using the properly antisymmetrized MWH or VESCF state functions. Such computed information for any one molecule is neither particularly credible nor useful. However, if applied to a series of molecules and if used to predict trends in the electronic spectroscopy, it can be of help in correlating and assigning the observed states. It is in this facet of empirical quantum-chemical schemes that their importance lies.

(*iii*) *Specific Identifications.* Some of the observed electronic states can be identified uniquely using vibrational and/or rotational analyses. Band shapes, Franck–Condon considerations, forbiddenness and allowedness of transition origins, polarizations, and intensity considerations can also provide information which is useful in this context. Where possible, such information will be used in discussing state assignments.

Another item of interest is also broached. This concept relates to the use of *quantum defects* as an aid to the assignment of Rydberg states: specifically, the quantum defects for molecules which consist of second-row atoms differ from those for molecules which are composed solely of third-row atoms; furthermore, the quantum defects for molecules which consist of both second- and third-row atoms are intermediate (this finding has significance for virtual orbital interactions and for Rydberg identification methods).

II. Theory

A. MOLECULAR ORBITALS

The electronic structure is described in terms of molecular orbitals (MO's). The semiempirical Mulliken–Wolfsberg–Helmholz (MWH) technique is used to calculate the MO's. The calculations are similar to those of Carroll, *et al.*[3-7] Such calculations extend the semiempirical one-electron nature of simple Hückel theory to all valence electrons and are also known[8] as "extended Hückel theory." Solution of the secular equation $|H_{ij} - EG_{ij}| = 0$ results in eigenvalues of an effective one-electron Hamiltonian. The H_{ii} matrix elements are approximated as the negative of the atomic valence-state ionization potentials (VSIP's). Following Viste and Gray,[9] the VSIP's are calculated as functions of atomic charge and orbital population and take into account changes in the atomic environment within a molecule. Resonance integrals are calculated using the Cusachs approximation[10]

$$H_{ij} = (2 - |S_{ij}|)(H_{ii} + H_{jj})S_{ij}/2 \qquad (1)$$

where the S_{ij}'s are overlap integrals. The Cusachs approximation is chosen in preference to others[7,11] because it contains no external parameters which are arbitrarily variable. Clementi double-zeta functions were used as an atomic orbital basis.[12] All MWH calculations were processed to charge self-consistency using a heavily damped iterative procedure.[3]

The following atomic orbital basis sets are used in the calculations reported here.

H	1s
C	2s, $2p_x$, $2p_y$, $2p_z$
N	2s, $2p_x$, $2p_y$, $2p_z$
O	2s, $2p_x$, $2p_y$, $2p_z$
S	3s, $3p_x$, $3p_y$, $3p_z$
Cl	3s, $3p_x$, $3p_y$, $3p_z$

(3) D. G. Carroll, A. T. Armstrong, and S. P. McGlynn, *J. Chem. Phys.*, 44, 1865 (1966).
(4) J. R. McDonald, V. M. Scherr and S. P. McGlynn, *ibid.*, 51, 1723 (1969).
(5) J. W. Rabalais, J. R. McDonald, and S. P. McGlynn, *ibid.*, 51, 5095, 5103 (1969).
(6) J. R. McDonald, J. W. Rabalais, and S. P. McGlynn, *ibid.*, 52, 1332 (1970).
(7) M. Wolfsberg and L. Helmholz, *ibid.*, 20, 837 (1952).
(8) R. Hoffmann, *ibid.*, 39, 1397 (1963).
(9) A. Viste and H. B. Gray, *Inorg. Chem.*, 3, 1113 (1964).
(10) L. C. Cusachs, *J. Chem. Phys.*, 43, S157 (1965).
(11) C. J. Ballhausen and H. B. Gray, *Inorg. Chem.*, 1, 111 (1962).
(12) E. Clementi, IBM Research Paper R·J·256 and Supplement, Sept 6, 1963.

The geometries, point groups, and coordinates of all molecules are listed in Figure 1.[18-22]

1. Correlation of the Orbitals of the United Atom, the Separated Atom, and the Linear Molecule

The correlation of orbitals between large and small internuclear distances, as exemplified by carbon dioxide, is shown in Figure 2. The K-shell electrons are omitted because they lie very low on the energy scale. However, these K-shell electrons are considered in the serial numbering of orbitals used in Figure 2. The atomic orbitals of carbon and oxygen are shown at the extreme right of the diagram. As these atoms are brought together to form CO_2, the orbitals become bonding, nonbonding, or antibonding. The ordering of molecular orbitals in the molecule is also affected by the repulsion between pairs of orbitals of the same type ($3\sigma_g$ and $4\sigma_g$; $1\pi_u$ and $2\pi_u$; $3\sigma_u$ and $4\sigma_u$) arising from atomic orbitals of nearly the same energy. The orbitals of the united atom (Ar) are shown at the extreme left of the diagram. When the atoms of CO_2 coalesce to form Ar, eight of the electrons increase their n values in order to satisfy the Pauli principle. The electrons with $n = 2$ are shifted down the energy scale by the increased, concentrated nuclear charge. The $n = 3$ electrons retain approximately the same energies as they had in the molecule. In Figure 2, the molecular orbitals are connected by dashed lines to the major contributory atomic orbitals of the separated atoms. The MWH calculations agree with the correlations of Figure 2. However, the MWH results do indicate that contributions from other AO's are also significant.

In any case, the correlation of Figure 2 provides rather complete validation of the MWH MO energy level diagrams for CO_2. Similar validation is obtained for other simple triatomics.

2. Correlation of the Molecular Orbitals of Linear and Bent Molecules

A correlation of the symmetry representations of the MO's of the various molecules considered is given in Table I. The MO eigenvalues, from MWH calculations, are presented in Table II. The highest occupied and lowest unoccupied MO's of the linear molecules are doubly degenerate π MO's which split into two components in molecules of lower symmetry. The magnitude of this splitting is dependent upon the size and type of the off-axis perturbation employed (*i.e.*, on the number of off-axis H atoms or alkyl groups and the degree of nonlinearity which they introduce).

The behavior of the electronic MO wave functions with change of angle are especially useful in understanding the

Table I

Correlation of Symmetry Representations of Molecular Orbitals among the Point Groups of Importance[a]

$D_{\infty h}$	$C_{\infty v}$	D_{2d}	C_{2v}	C_s
$4\sigma_u$	9σ	$4b_2$	$5b_2$	12a′
$5\sigma_g$	8σ	$5a_1$	$7a_1$	11a′
			$2b_1$	3a″
$2\pi_u$	3π	3e		
			$6a_1$	10a′
			$1a_2$	2a″
$1\pi_g$	2π	2e		
			$4b_2$	9a′
$3\sigma_u$	7σ	$3b_2$	$3b_2$	8a′
			$1b_1$	1a″
$1\pi_u$	1π	1e		
			$5a_1$	7a′
$4\sigma_g$	6σ	$4a_1$	$4a_1$	6a′
$2\sigma_u$	5σ	$2b_2$	$2b_2$	5a′
$3\sigma_g$	4σ	$3a_1$	$3a_1$	4a′

[a] The double-dashed line across the body of the table separates the filled lower MO's from the unfilled upper MO's appropriate to the ground-state electronic configuration.

electronic properties of these molecules. A one-electron orbital energy *vs.* angle schematization (*i.e.*, a Walsh diagram) is shown in Figure 3 for CO_2 in its ground-state configuration. Schematic representations of the molecular orbitals in the linear and 90° bent molecule are also presented in Figure 3.

a. $3\sigma_g(3a_1)$ Molecular Orbital

The first valence orbital, $3\sigma_g(3a_1)$, is strongly bonding in linear and bent geometries. In the linear conformation, the main contributors to this MO are $2s_O$ and $2s_C$ atomic orbitals, with a very small contribution from the $2p_{zO}$ AO's. Bending leads to a bond between the $2p_{zO}$ AO's, and this is accompanied by some increase in the $2p_{yN}$ AO involvement. Thus, bending leads to an increase in end-atom bonding and this stabilizes the $3\sigma_g(3a_1)$ MO.

b. $2\sigma_u(2b_2)$ Molecular Orbital

The $2\sigma_u(2b_2)$ MO is antibonding between the two end atoms and possesses a node through the central atom. In the linear configuration, this MO is composed of $2s_O$ AO's and a $2p_{zC}$ AO. Bending causes an increase in both the kinetic and electronic repulsion energies of electrons in this MO and, as a result, the MO energy increases with decreasing angle.

c. $4\sigma_g(4a_1)$ Molecular Orbital

The $4\sigma_g(4a_1)$ MO, in the linear conformation, is composed of $2s_O$, $2p_{zO}$, and $2s_C$ AO's arranged such that nodes intersect both of the O–C bonds. Bending causes a large shift of electron charge out of the $2p_{zO}$ AO's into the $2p_{yO}$ AO's, and a strong bond develops between the $2p_{yO}$ and $2s_C$ AO's. Thus, the en-

(13) L. E. Sutton, "Tables of Interatomic Distances and Configurations in Molecules and Ions," The Chemical Society, London, 1958.
(14) F. A. Cotton and G. Wilkinson, "Advanced Inorganic Chemistry," 2nd ed, Wiley, New York, N. Y., 1966.
(15) P. Gray and T. C. Waddington, *Trans. Faraday Soc.*, 53, 901 (1957).
(16) E. L. Wagner, *J. Chem. Phys.*, 43, 2728 (1965).
(17) A. D. McLean and M. Yoshimine, "Tables of Linear Molecule Wavefunctions," IBM, San Jose, Calif., 1967.
(18) R. N. Dixon and G. H. Kirby, *Trans. Faraday Soc.*, 64, 2002 (1968).
(19) A. Pellegatti, *Theor. Chim. Acta*, 8, 128 (1965).
(20) H. F. Henneike and R. S. Drago, *J. Amer. Chem. Soc.*, 90, 5112 (1968).
(21) R. N. Dixon and G. H. Kirby, *Trans. Faraday Soc.*, 62, 1406 (1966).
(22) B. L. Evans, A. D. Yoffe, and P. Gray, *Chem. Rev.*, 59, 515 (1959).

Table II

Results of MWH Calculations for the Ground-State MO's of Some Molecules of Interest[a]

CO_2 $D_{\infty h}$	CS_2 $D_{\infty h}$	NO_2^+ $D_{\infty h}$	N_3^- $D_{\infty h}$	HN_3 C_s	CN_2^{2-} $D_{\infty h}$	HCN_2^- C_s	H_2CN_2 C_{2v}	H_2CCCH_2 D_{2d}
				−7.024(3a″)		−4.035(3a″)	−5.515($2b_1$)	
−6.909($2\pi_u$)	−6.326($2\pi_u$)	−11.634($2\pi_u$)	−4.428($2\pi_u$)		−1.539($2\pi_u$)			−6.041(3e)
				−7.751(10a′)		−4.459(10a′)	−6.192($6a_1$)	
				−11.841(2a″)		−7.898(2a″)	−11.434($1a_2$)	
−14.050($1\pi_g$)	−11.330($1\pi_g$)	−19.242($1\pi_g$)	−7.768($1\pi_g$)		−3.494($1\pi_g$)			−11.657(2e)
				−12.765(9a′)		−8.410(9a′)	−12.245($4b_2$)	
−14.927($3\sigma_u$)	−12.608($3\sigma_u$)	−21.554($3\sigma_u$)	−9.529($3\sigma_u$)	−14.491(8a′)	−3.910($3\sigma_u$)	−9.170(8a′)	−12.442($3b_2$)	−12.737($3b_2$)
				−17.190(7a′)		−10.597(1a″)	−14.792($1b_1$)	
−17.680($1\pi_u$)	−14.440($1\pi_u$)	−25.564($1\pi_u$)	−12.409($1\pi_u$)		−5.268($1\pi_u$)			−14.718(1e)
				−17.360(1a″)		−11.015(7a′)	−17.133($5a_1$)	
−18.059($4\sigma_g$)	−15.320($4\sigma_g$)	−25.139($4\sigma_g$)	−12.623($4\sigma_g$)	−18.298(6a′)	−6.640($4\sigma_g$)	−12.755(6a′)	−17.331($4a_1$)	−15.752($4a_1$)

H_2CCO C_{2v}	N_2O $C_{\infty v}$	OCS $C_{\infty v}$	$NCCl$ $C_{\infty v}$	NCO^- $C_{\infty v}$	$HNCO$ C_s	NCS^- $C_{\infty v}$	$HNCS$ C_s
−5.492($2b_1$)					−6.052(3a″)		−5.865(3a″)
	−7.713(3π)	−6.544(3π)	−6.073(3π)	−4.235(3π)		−4.242(3π)	
−7.521($6a_1$)					−6.784(10a″)		−6.541(10a′)
−11.487($1a_2$)					−12.498(2a″)		−11.379(2a″)
	−13.323(2π)	−12.548(2π)	−12.335(2π)	−8.586(2π)		−7.871(2π)	
−13.629($4b_2$)					−12.833(9a′)		−11.714(9a′)
	−15.175(7σ)	−13.673(7σ)	−12.615(7σ)	−9.205(3σ)	−14.387(8a′)	−8.592(7σ)	−13.337(8a′)
−15.582($1b_1$)					−16.158(1a″)		−14.674(1a″)
	−18.581(6σ)	−15.901(1π)	−16.264(1π)	−11.330(1π)		−10.383(1π)	
−16.087($5a_1$)					−16.221(7a′)		−14.824(7a′)
−16.661($4a_1$)	−18.807(1π)	−16.496(6σ)	−17.426(6σ)	−12.231(6σ)	−17.654(6a′)	−11.785(6σ)	−16.529(6a′)

[a] The eigenvalues are in electron volts and are followed by the symmetry notation of the orbital. Orbitals above the double-dashed line are unoccupied in the ground state.

ergy of the $4\sigma_g(4a_1)$ MO is expected to decrease as the O–C–O angle becomes smaller.

d. $1\pi_u(1b_1$ and $5a_1)$ Molecular Orbital

The $1\pi_u(1b_1)$ MO consists of an out-of-plane in-phase combination of $2p_x$ AO's from all three centers. This MO is bonding throughout the molecular extent. The central atom contributes the largest amount of electron density in the linear conformation; however, upon bending, the charge distributes itself more evenly throughout the $2p_x$ AO's, and a slight decrease in energy occurs because of the greater electronegativity of the end atoms.

The $1\pi_u(5a_1)$ MO is similar to the $1\pi_u(1b_1)$ orbital in the linear conformation—except that it consists of $2p_y$ AO's. Bending of the molecule results in a gradual increase in energy of this MO followed by a slight decrease at ~100°. The gradual increase in energy arises from a decrease in the extent of $2p_y$ π-bonding caused by bending. The decrease in energy at smaller angles is due to the increased bonding which sets in between the $2p_{zO}$ AO's and the $2p_{yC}$ AO; this latter interaction produces a bonding region which is localized within the molecular triangle.

e. $3\sigma_u(3b_2)$ Molecular Orbital

The $3\sigma_u(3b_2)$ MO is composed, in the linear conformation, of $2p_z$ AO's on all atoms; it also possesses a small amount of $2s_O$ AO character. These orbitals are arranged such that they are strongly bonding in the O–C bond region, with nodes passing through each of the three atoms. Bending shifts most of the charge to the $2p_{yO}$ AO's and $2p_{zC}$ AO and produces a small decrease in energy. The nodes through each atom remain intact in the bent conformation.

f. $1\pi_g(1a_2$ and $4b_2)$ Molecular Orbital

The $1\pi_g(1a_2)$ MO is composed of an antibonding combination of $2p_{xO}$ AO's. Its energy is approximately independent of angle.

The $1\pi_g(4b_2)$ MO is the highest occupied MO; it is similar to the $1\pi_g(1a_2)$ MO in the linear conformation—except that it is composed of $2p_{yO}$ AO's. Bending causes a large shift of electron density from the $2p_{yO}$ AO's to the $2p_{zO}$ AO's with a small further amount going to the $2p_{zC}$ AO. These AO's are arranged in an antibonding manner, and this antibonding characteristic grows larger as the angle grows smaller. *The sharp increase of energy of this MO caused by bending is responsible for the stability of the linear ground-state conformation of the molecules under consideration.*

g. $2\pi_u(6a_1$ and $2b_1)$ Molecular Orbital

The first unoccupied MO is the $2\pi_u(6a_1)$ MO. It consists of considerable $2p_{yC}$ AO and a little $2p_{yO}$ character. These are arranged in an antibonding manner, with nodes intersecting each bond and with the molecular axis also lying in a nodal plane. When the molecule is bent, electronic charge is shifted from the $2p_{yC}$ AO to the $2p_{zC}$ and $2p_{yO}$ AO's and a strong bond develops between the C–O centers. Thus, bending results in a decrease of MO energy to an extent which causes this MO to drop below the $1\pi_g(4b_2)$ MO. *The increased bonding provided by the $2\pi_u(6a_1)$ MO in the bent conformation is responsible for the nonlinearity of triatomic groups which contain 17 or 18 valence electrons.*

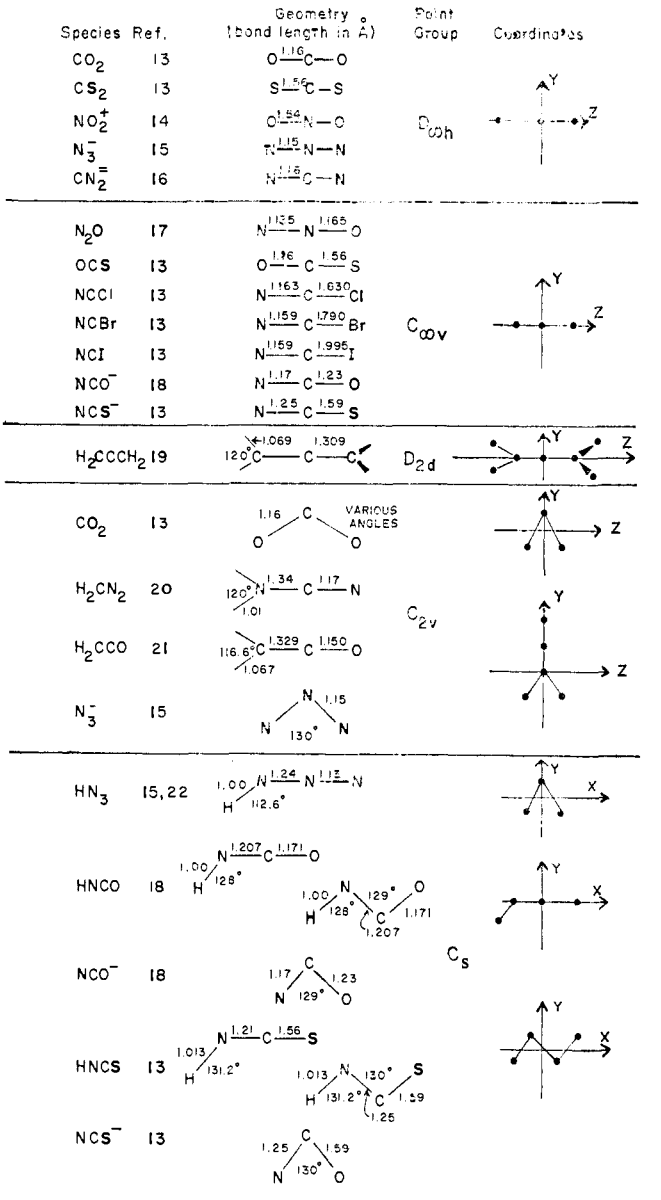

Figure 1. Molecular geometries. Distances are in ångstrom units.

The $2\pi_u(2b_1)$ MO is similar to the $2\pi_u(6a_1)$ MO but is composed of $2p_x$ instead of $2p_y$ AO's. Its energy remains approximately independent of the degree of bending.

h. $5\sigma_g(7a_1)$ Molecular Orbital

The $5\sigma_g(7a_1)$ MO is composed of a $2s_C$ AO and $2s_O$ and $2p_{zO}$ AO's arranged in an antibonding nammer; nodes intersect the two O atoms and the two bonds in planes perpendicular to the molecular axis. This MO lies above the ionization potential of the molecule. Bending of the molecule shifts electron density into the $2p_{yC}$ and $2p_{yO}$ AO's. This MO is heavily antibonding; since the electron repulsion interaction becomes stronger as the angle grows smaller, a large increase in orbital energy results upon bending.

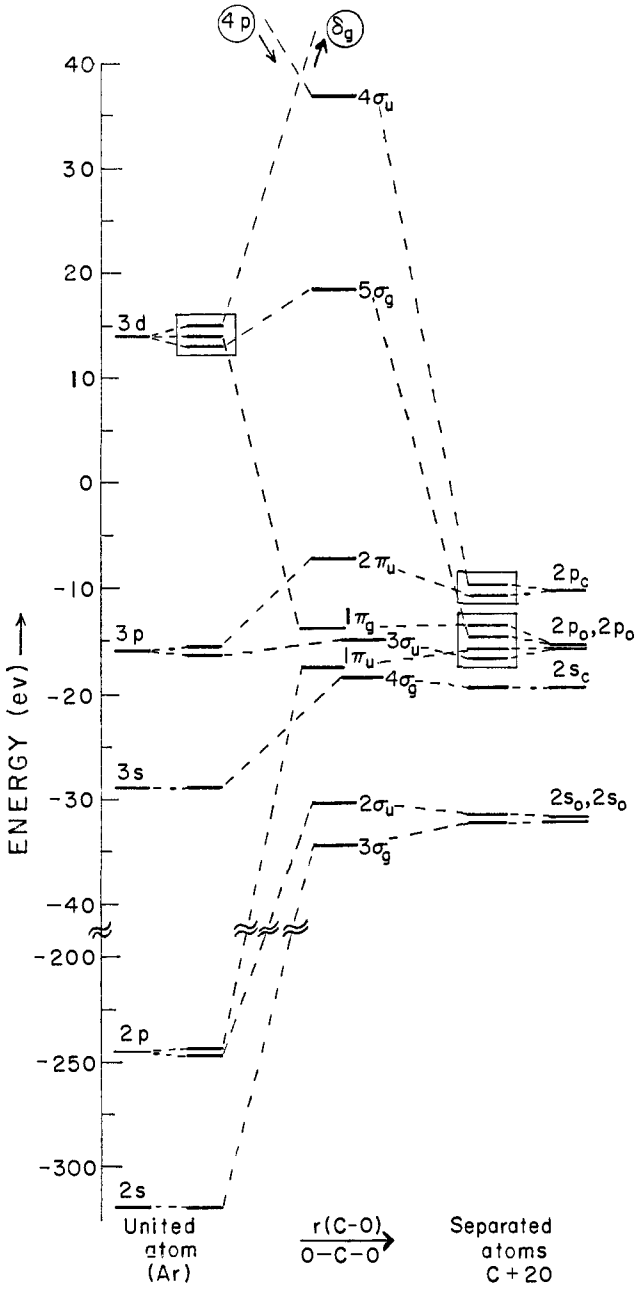

Figure 2. Correlation of orbitals between large and small internuclear distances in CO_2. Enclosure of levels in frames indicates gross expansion of the energy scale. Carbon dioxide molecular orbitals are taken from MWH calculations. Atomic energy levels are from K. Siegbahn, *et al.*, *Nova Acta Regiae Soc. Sci. Upsal., Ser. IV*, 20, 1 (1967). The energy of the 3d atomic orbital of Ar is from "Atomic Energy Levels," National Bureau of Standards Circular 467, U. S. Government Printing Office, Washington, D. C., June 15, 1949.

i. $4\sigma_u(5b_2)$ Molecular Orbital

The $4\sigma_u(5b_2)$ MO also lies above the ionization potential of CO_2. It is composed of $2p_z$ AO's from all three atoms as well as a $2s_O$ AO contribution. Bending of the molecule causes a shift of some electron density into the $2p_{yO}$ AO's and the strong electron repulsions present in the linear conformation decreases. The result is a decrease in the MO energy so large that this MO and the $5\sigma_g(7a_1)$ MO invert their relative energies at smaller angles.

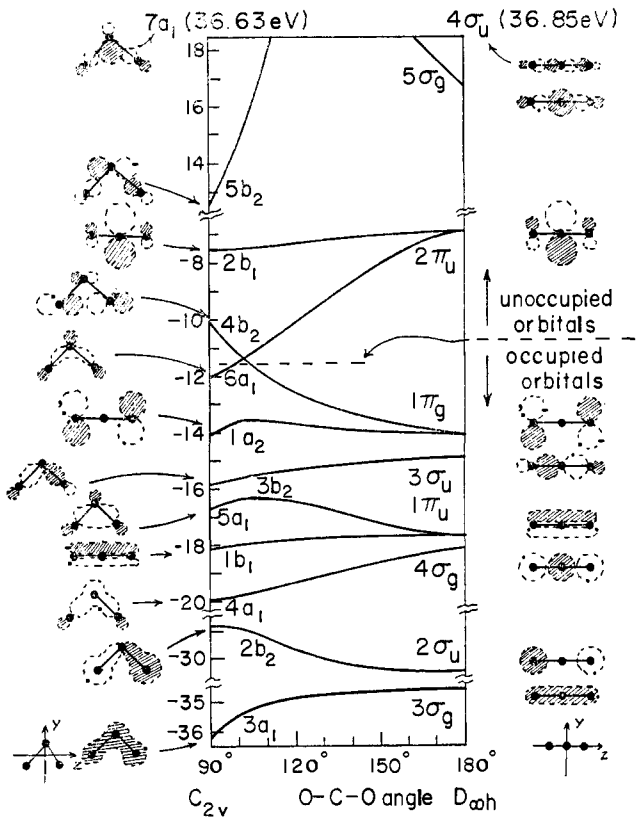

Figure 3. Walsh diagram of CO_2 in the ground state. Schematic MO's are also indicated. The hatched areas represent regions of negative amplitude. Only one member of each pair of the degenerate $1\pi_u$, $1\pi_g$, and $2\pi_u$ orbitals is shown. The other member of each pair is identical with the one shown, except that it is rotated by 90° about the internuclear axis. In the 90° conformation, except for the $1b_1$, $1a_2$, and $2b_1$ orbitals, the molecule is shown in the *yz* plane and all orbitals are in this same plane. For the $1b_1$, $1a_2$, and $2b_1$ orbitals, the molecule is shown in the *xz* plane and the orbitals are in this same plane (*i.e.*, the orbitals are perpendicular to the plane of the molecule).

3. *Correlation of the Molecular Orbitals of Triatomics with and without Off-Axis Groups*

Alkyl adducts induce much the same sort of effects as do hydrogen atom adducts. When such groups are added to a linear triatomic, as in $NCS^- + H^+ \rightarrow HNCS$, the adduct adopts an off-axis location at one end of the triatomic grouping. The primary bonding occurs between one constituent of each of the doubly degenerate π MO's of the linear triatomic and the σ orbitals of the appended group. We designate the interacting π components as $1\pi_u(5a_1)$ and $1\pi_g(4b_2)$; these components immediately lose their "π purity." On the other hand, the $1\pi_u(1b_1)$ and $1\pi_g(1a_2)$ MO's retain their identity as pure π MO's of the triatomic skeleton.

The $1\pi_g(4b_2)$ MO of the linear triatomics and their protonated or alkylated congeners bears a direct relationship to the "nonbonding" or n MO of carbonyl-containing compounds. This relationship is illustrated in Figure 4 where the $2b_2$ (*i.e.*, nonbonding) MO of formaldehyde is compared to the $1\pi_g(9a'$ and $4b_2)$ MO's of NCO^-, HNCO, and H_2CCO. The $2b_2$ MO is nonbonding in the C–O region of formaldehyde. In NCO^- and HNCO, on the other hand, the corresponding MO possesses a considerable amplitude in the in-plane $2p_O$ AO. The

$1\pi_g$(9a′) MO is weakly bonding in the N–C region and slightly antibonding in the C–O region. For H_2CCO, the $1\pi_g(4b_2)$ MO contains a small amount of $2p_C$ AO character; however, the $4b_2$ MO is bonding in the C–O region and antibonding in the C–C region. This weak bonding between the two end atoms also occurs in H_2NCN, $(CH_3)_2NCN$, and H_2CNN. Thus, in the linear triatomic molecules, with and without off-axis groups, the $1\pi_g$(9a′ and $4b_2$) MO is weakly bonding in some regions and weakly antibonding in other regions. For this reason, this MO is clearly not as "nonbonding" as is the $2b_2$ MO of formaldehyde.

The shifts and splittings experienced by the molecular orbitals of the linear molecule when an off-axis group is added are shown in Figure 5 for NCS^- and HNCS. The a′ MO of HNCS is of lower energy than the a″ MO because of the stabilization caused by mixing of the $1s_H$ AO and the a′ component of the π MO. In the bent ion, where there is no proton available for σ bonding, the a′ MO is of higher energy than the a″ MO. The unoccupied orbitals retain the ordering a′ < a″ in all instances.

Similar results are obtained for NCO^- and HNCO (see ref 5) and for NNN^- and HNNN (see ref 6).

B. MOLECULAR ELECTRONIC STATES

From Tables I and II, the transitions which should be of interest in the near- and vacuum ultraviolet regions are

$D_{\infty h}$: $1\pi_g \rightarrow 2\pi_u$ and $3\sigma_u \rightarrow 2\pi_u$

$C_{\infty v}$: $2\pi \rightarrow 3\pi$ and $7\sigma \rightarrow 3\pi$

D_{2d}: $2e \rightarrow 3e$ and $3b_2 \rightarrow 3e$

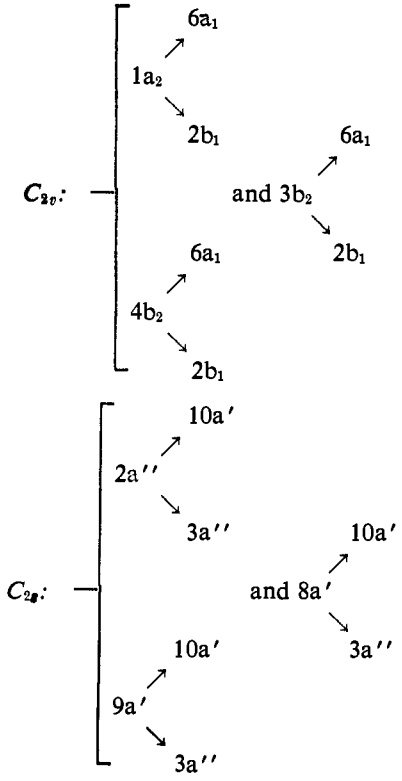

The lowest energy MO excitation of $D_{\infty h}$ molecules is expected to be $1\pi_g \rightarrow 2\pi_u$; it gives rise to $^{1,3}\Sigma_u^-$, $^{1,3}\Delta_u$, and $^{1,3}\Sigma_u^+$ excited states. The $3\sigma_u \rightarrow 2\pi_u$ excitation which gives rise to $^{1,3}\Pi_g$ excited states is also expected to be of low energy.

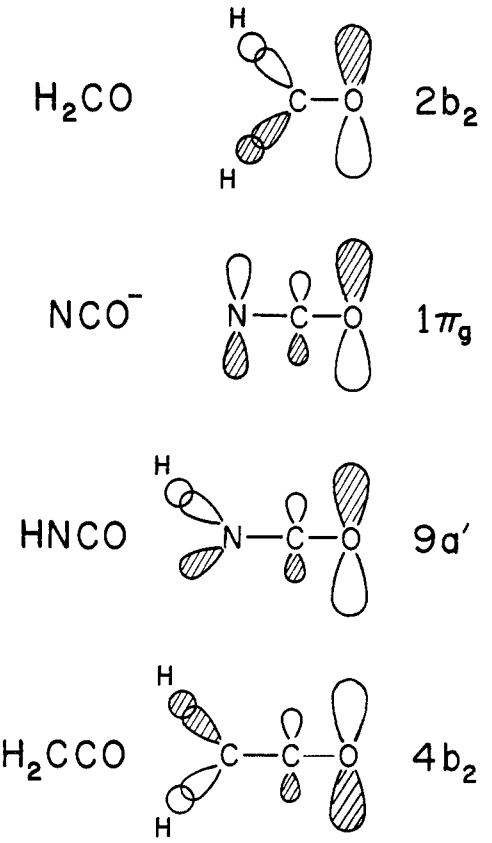

Figure 4. Comparison of the $2b_2$ "nonbonding" molecuar orbitals of formaldehyde with the $1\pi_g$, 9a′, and $4b_2$ MO's of NCO^-, HNCO, and H_2CCO. The hatched areas denote regions of negative MO amplitudes.

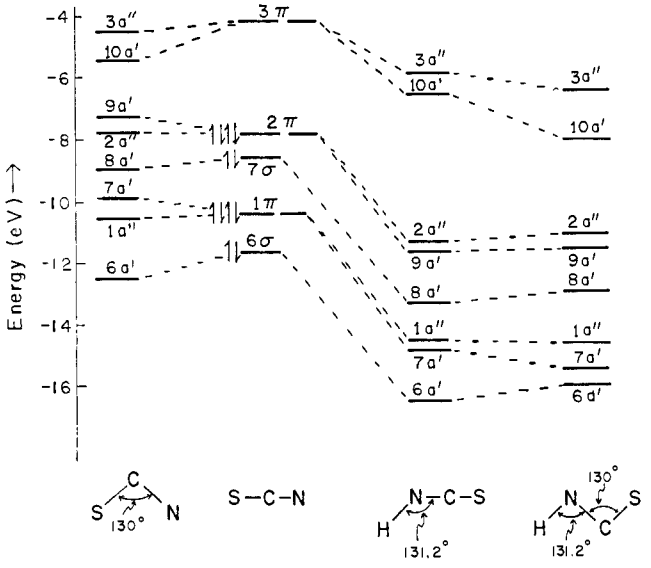

Figure 5. A correlation of the molecular orbitals of HNCS (linear and bent NCS group) with those of linear and bent NCS^-. The filled MO's of the ground-state configuration are indicated by arrows.

These states should span an energy region of the spectrum of ~10 eV.

It is known experimentally in the cases of CO_2, OCS, and CS_2 that the $1\pi_u$ MO is of higher energy than the $3\sigma_u$ MO.

Thus, the $1\pi_u \rightarrow 2\pi_u$ MO excitation, which generates $^{1,3}\Sigma_g^-$, $^{1,3}\Delta_g$, and $^{1,3}\Sigma_g^+$ excited states, should be considered also. Transitions to these excited states are unlikely to be observed for the following reasons:

(i) All of these transitions are parity-forbidden. Forbiddenness exists even when the parity selection rule is relaxed for the Σ^- and Δ states.

(ii) The energies of these states should approximate those of the states derived from the $3\sigma_u \rightarrow 2\pi_u$ MO excitation and the higher energy states derived from the $1\pi_g \rightarrow 2\pi_u$ MO excitation. Furthermore, the en rgetic ordering of these states is expected to be similar to the ordering derived from the $1\pi_g \rightarrow 2\pi_u$ MO excitation, that is, $E(^1\Sigma^-) < E(^1\Delta) < E(^1\Sigma^+)$. Thus, the highly forbidden transitions to the $^{1,3}\Sigma_g^-$, $^{1,3}\Delta_g$, and $^3\Sigma_g^+$ states are expected to be completely submerged below the more intense transitions to the $^1\Sigma_u^+$, $^1\Pi_g$, and Rydberg states. The transition to the $^1\Sigma_g^+$ state should lie at very high energies—probably beyond the short-wavelength limit of our measurements—and should be submerged beneath the stronger Rydberg bands and the dissociative continuum.

(iii) As indicated in item ii, we expect to observe the transition $^1\Pi_g \rightarrow {}^1\Sigma_g^+$ but not any of those derived from the $1\pi_u \rightarrow 2\pi_u$ MO excitation. Since the $^1\Pi_g \rightarrow {}^1\Sigma_g^+$ is also a forbidden transition, such an expectation requires some validation. Such validation runs as follows: (1) the $^1\Pi_g \rightarrow {}^1\Sigma_g^+$ transition becomes allowed when parity restrictions are relaxed; (2) the $^1\Pi_g \rightarrow {}^1\Sigma_g^+$ transition may gain intensity by vibronic coupling mediated by π_u vibrational modes; (3) the $^1\Pi_g \rightarrow {}^1\Sigma_g^+$ transition usually occurs in a region of the spectrum which is relatively free of Rydberg excitations and dissociative continua.

1. Correlation of Electronic States

A correlation of the excited electronic state representations between point groups is shown in Table III. The doubly degenerate $^1\Delta_u$ and $^1\Pi_g$ states split into two components in the point groups of low symmetry. Such splittings should be detectable.

Table III

Correlation of Electronic State Representations among Various Point Groups

Point group	*Ground state*	$\pi \rightarrow \pi^*$ *states*			$\sigma \rightarrow \pi^*$ *state(s)*
$D_{\infty h}$	$^1\Sigma_g^+$	Σ_u^-	Δ_u	Σ_u^+	Π_g
$C_{\infty v}$	$^1\Sigma^+$	Σ^-	Δ	Σ^+	Π
D_{2d}	$^1A_1$	B_1	A_2 A_1	B_2	E
C_{2v}	$^1A_1$	A_2	A_2 B_2	B_2	A_2 B_2
C_s	$^1A'$	A''	A'' A'	A'	A'' A'

The correlations of Table III form a strong basis for state identifications. Each electronic state has its own unique properties which distinguish it from all others. These are:

(i) The $^1\Sigma_u^+ \leftarrow {}^1\Sigma_g^+$ transition is the only one that is allowed in all point groups and does not split into two components in molecules of low symmetry.

(ii) The $^1\Delta_u \leftarrow {}^1\Sigma_g^+$ transition is the only one that splits into two components in the D_{2d}, C_{2v}, and C_s molecules, that is forbidden in $D_{\infty h}$, $C_{\infty v}$, and D_{2d}, and that has one allowed component in C_{2v} and two allowed components in C_s.

(iii) The $^1\Sigma_u^- \leftarrow {}^1\Sigma_g^+$ transition is the only one that is forbidden in all point groups except C_s and does not split into two components in low-symmetry molecules.

(iv) The $^1\Pi_g \leftarrow {}^1\Sigma_g^+$ transition is the only one that splits into two components in C_{2v} and C_s molecules, that is forbidden in $D_{\infty h}$ and allowed in $C_{\infty v}$ and D_{2d}, and that has one allowed component in C_{2v} and two allowed components in C_s.

Transition energies can be estimated, in a very preliminary approximation, as the difference of MWH MO energies. In the case of transitions involving degenerate MO's, the MWH MO energy differences provide, at most, the barycenter of the resulting excited states. For example, the MWH MO energy of $(1\pi_g)^3(2\pi_u)^1$ configuration is the barycenter of the states shown schematically in Figure 6. Since the MWH calculations are one-electron in nature and neglect much electron repulsion and correlation effects, they should not be used to predict the spectroscopy of any one molecule. Instead, they should be used in a correlative fashion—and even then, warily.

2. Symmetry- and Spin-Adapted Wave Functions

Proper symmetry-adapted and spin-adapted state wave functions for the molecular orbital excitations have been constructed. These state wave functions can be used to calculate state energies;[23] for example, we find

$$E(^1\Sigma^-) = \langle \Psi(^1\Sigma^-) | \mathcal{H} | \Psi(^1\Sigma^-) \rangle \qquad (2)$$

where $\mathcal{H}$, the total Hamiltonian, now contains explicit electron-repulsion terms. These adapted wave functions are used to compute transition moments (*i.e.*, oscillator strengths) and state energies. The former were evaluated by transforming all MO's to a Lowdin basis, following the procedures of Cusachs and Trus;[24] the resulting MO's were then converted to a proper symmetry-adapted state basis. The calculated oscillator strengths are presented in Table IV.

The oscillator strengths of Table IV illustrate the allowedness, forbiddenness, and splitting characteristics of the electronic transitions. The most intense transition in all molecules is expected to be the $^1\Sigma_u^+ \leftarrow {}^1\Sigma_g^+$ and its analog excitations. The expected high intensity of this transition should allow easy identification. The $^1\Sigma_u^- \leftarrow {}^1\Sigma_g^+$ and its correlating transitions are expected to be forbidden in most molecules and, even when allowed, should remain extremely weak. The expected low-intensity characteristics of this transition should provide its most distinguishing feature. Considering the $^1\Pi_g$ and $^1\Delta_u$ states, the oscillator strengths for the $^1\Pi_g \leftarrow {}^1\Sigma_g^+$ transition are expected to be higher than those for the $^1\Delta_u \leftarrow {}^1\Sigma_g^+$ transition for all molecules except ones of C_s symmetry. Experimental results do indeed indicate that the transition to the $^1\Pi_g$ state is always more intense than that to the $^1\Delta_u$ state. The reason is associated with the fact that the $^1\Pi_g \leftarrow {}^1\Sigma_g^+$ transition gains much of its intensity through vibronic coupling with π_u modes whereas the $^1\Delta_u \leftarrow {}^1\Sigma_g^+$ transition is forbidden by all first-order vibronic coupling routes.

(23) S. P. McGlynn, L. Vanquickenborne, M. Kinoshita, and D. G. Carroll, "Introduction to Applied Quantum Chemistry," Holt, Rinehart and Winston, New York, N. Y., 1971.

(24) L. C. Cusachs and B. L. Trus, *J. Chem. Phys.*, 46, 1532 (1967).

Table IV

Oscillator Strengths for Transitions from the Ground State to the Indicated Upper States[a]

	$^1\Sigma_u^-$		$^1\Delta_u$		$^1\Sigma_u^+$		$^1\pi_g$	
ONO^+	0		0		0.519		0	
OCO	0		0		0.417		0	
SCS	0		0		0.502		0	
NNN^-	0		0		0.278		0	
NCN^{2-}	0		0		0.151		0	
OCS	0		0		0.482		1.22×10^{-4}	
NNO	0		0		0.386		7.61×10^{-4}	
NCS^-	0		0		0.302		3.59×10^{-4}	
NCO^-	0		0		0.286		1.44×10^{-3}	
H_2CCCH_2	0		0		0.344		3.84×10^{-3}	
H_2NCN	0	0		1.09×10^{-3}	0.355	0		0.259
H_2CCO	0	0		4.09×10^{-3}	0.420	0		0.391
HNCS	9.81×10^{-5}	1.92×10^{-4}		0.383	0.458	9.64×10^{-4}		8.21×10^{-2}
HNNN	3.86×10^{-4}	1.13×10^{-3}		0.317	0.385	5.03×10^{-3}		3.97×10^{-2}
HNCO	5.02×10^{-4}	1.33×10^{-3}		0.328	0.411	8.48×10^{-5}		2.43×10^{-3}

[a] For identification of states in molecules other than $D_{\infty h}$ symmetry, see Table III.

3. Geometry of Excited States

Certain excited states of these molecules are expected to be bent while others should be linear. MWH calculations were performed on NCS^- at various angles ranging from 180 to 120°; these calculations were iterated to charge self-consistency using a ground-state electronic configuration. Orbital energies from the ground-state calculations were then used to calculate the total energy of each excited configuration as a function of angle. The results are shown in Figure 7. A specific predicted geometry of each excited state is implicit in this diagram. A similar type of computation was performed on CO_2; however, in this instance, the MWH calculation was iterated to self-consistency for each open-shell excited configuration as a function of angle. Results, shown in Figure 8, are similar to those of Figure 7.

The calculations indicate that the ground state, $^1\Sigma_g^+(^1A_1)$, and the $^1\Delta_u(^1A_2)$, $^1\Sigma_u^+(^1B_2)$, and $^1\Pi_g(^1A_2)$ excited states should be linear whereas the $^1\Delta_u(^1B_2)$, $^1\Sigma_u^-(^1A_2)$, and $^1\Pi_g(^1B_2)$ excited states should be bent. It should be reemphasized that such conclusions are qualitative and merely indicative of tendencies toward the presence or absence of linearity. However, these conclusions, coupled with vibrational analysis, Franck–Condon analysis, and band shapes, do lead to reasonably secure predictions of excited-state geometries.

4. Configuration Interaction and Singlet–Triplet Energy Splittings

Energies of excited states were calculated for ten species using a Pariser–Parr–Pople process in which the σ-electron charge density provided by the MWH method was assumed fixed and productive of the potential field in which the π electrons move. The π-electron subset was then iterated to charge self-consistency using the "variable electronegativity" concept (VESCF). A configuration interaction computation yielded energies for the $^1\Sigma_u^+ \rightarrow {}^1\Sigma_g^+$ and $^3\Sigma_u^+ \rightarrow {}^1\Sigma_g^+$ transitions. Only these transitions could be handled because of the inability of the VESCF CI program to treat π orbitals in different planes. The results are shown in Table V. The calculated energy of the $^1\Sigma_u^+$ and $^3\Sigma_u^+$ states and the corresponding singlet–triplet (S–T) splittings provide good qualitative trends for the ordering of excited-state energies. Considering the neutral molecular species, the S–T split increases as the size of the molecule decreases (*e.g.*, the S–T split increases in the order H_2CCCH_2 < H_2NCN < H_2CCO < HNCO < NNO < CO_2). Smaller splittings are also observed for molecules containing atoms

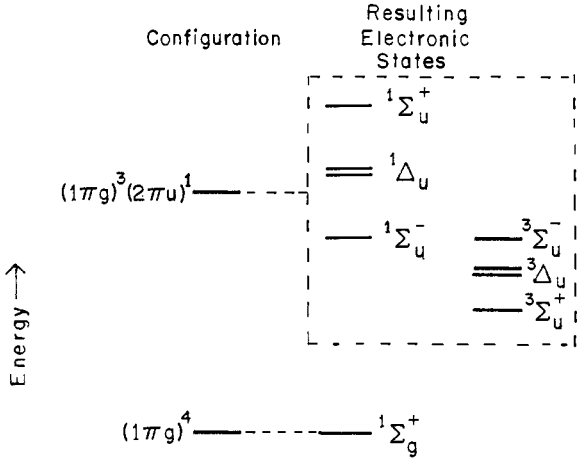

Figure 6. Schematic representation of the electronic states resulting from the $(1\pi_g)^3(2\pi_u)^1$ electron configuration of a $D_{\infty h}$ molecule.

Table V

Energies of the $^1\Sigma_u^+$ Excited States of Various Molecular Species from VESCF CI Calculations

Species	$^1\Sigma_u^+$ (*eV*)	$^3\Sigma_u^+$ (*eV*)	*S–T split* (*eV*)
NCN^{2-}	7.96	5.20	2.76
NNN^-	7.13	4.06	3.07
OCO	6.72	1.97	4.75
HNCO	6.53	2.11	4.42
NNO	6.20	1.58	4.62
ONO^+	6.16	0.65	5.51
$HNCN^-$	6.12	2.49	3.65
H_2NCN	5.96	2.52	3.44
H_2CCO	5.87	1.77	4.10
H_2CCCH_2	5.61	2.97	2.64

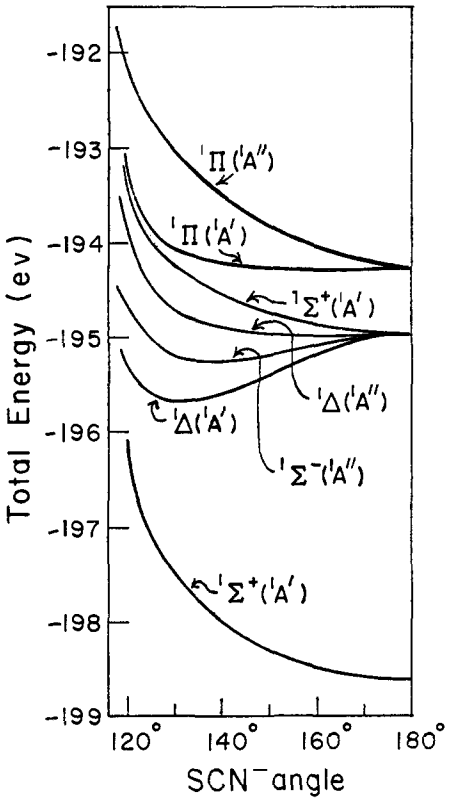

Figure 7. Total energies of electronic states in NCS^- as a function of angle (ground-state iteration only).

from the third row of the periodic table, *i.e.*, OCS and CS_2. These smaller splittings are due to a reduction in the exchange integrals which is, in turn, attributable to the increase in the molecular "box size" when H atoms are added or when larger, diffuse sulfur orbitals are involved.

Calculations on the lower electronic states of CO_2 using Roothaan's LCAO SCF method have been reported by Mulligan.[25] The calculations on the $\pi \rightarrow \pi^*$ and $\sigma \rightarrow \pi^*$ MO excitations render the following excited state energies (in eV): $^3\Sigma_u^+$ (7.6), $^3\Delta_u$ (8.4), $^3\Sigma_u^-$ (9.2), $^1\Sigma_u^-$ (9.2), $^1\Delta_u$ (9.5), $^1\Sigma_u^+$ (22.1), $^3\Pi_g$ (14.6), and $^1\Pi_g$ (14.6). The singlet–triplet splitting in the $^{1,3}\Sigma_u^-$ and $^{1,3}\Pi_g$ states was zero within the accuracy of the calculation. The splitting in the case of the $^{1,3}\Sigma_u^+$ states was abnormally large.

Although the energies of the excited states as calculated by Mulligan are too high, the energetic ordering is meaningful. From these computations, we expect the $^3\Sigma_u^+$ state to be the lowest energy excited state. The $^3\Delta_u$ and $^3\Sigma_u^-$ states should lie slightly higher in energy. The $^1\Sigma_u^-$ state is expected to be the lowest energy excited singlet state. The $^1\Delta_u$ state should lie slightly higher and the $^1\Pi_g$ and $^1\Sigma_u^+$ states should be the two highest energy states. Thus, from the predicted intensities of the various transitions as given in Table IV and the energetic ordering predicted here, we might expect to obtain considerable insight into the spectra of these 16-valence-electron molecules. We expect the long-wavelength bands ($^3\Sigma_u^+$, $^{1,3}\Sigma_u^-$, $^{1,3}\Delta_u \leftarrow {}^1\Sigma_g^+$) to be of low intensity and the shorter wavelength bands ($^1\Pi_g$, $^1\Sigma_u^+ \leftarrow {}^1\Sigma_g^+$) to be of higher intensity.

(25) J. F. Mulligan, *J. Chem. Phys.*, **19**, 1428 (1951).

5. *Ionization Potentials*

Orbital energies from ground-state calculations are frequently used as ionization potentials (IP's). The first ionization potential of all species calculated here is from a π MO with the values decreasing in the order cations > molecules > anions > dianions, as expected. These trends can be observed in Table II. In all cases where bent and linear species were calculated (*e.g.*, NCS^-), the bent species possesses the lowest IP; it is for this same reason that the bent species is less stable.

Sichel and Whitehead[26] have presented a correlation of computed IP's with experimental values. For CO_2, CS_2, OCS, and N_2O they concluded that the CNDO method gave the best fit with experiment. Values for the first four IP's of these molecules (as calculated by CNDO, extended Hückel method (EHM), Hartree–Fock, and the present MWH methods) are tabulated along with experimental values in Table VI. The ordering of calculated IP's does not agree with the experimental ordering unless, as in the case of the Hartree–Fock calculation, an extended basis set is used in the computation. Thus, lack of correspondence of IP ordering is found even with minimal basis set Hartree–Fock, and is to be expected also in semiempirical calculations. This deficiency in the semiempirical calculations is due to the neglect of "atoms-in-molecules" effects and the effects of σ–π separability as discussed by Armstrong, *et al.*[27] However, MWH values for the first ionization potential are in much closer agreement with experiment than the EHM, CNDO, or Hartree–Fock values.

C. RYDBERG STATES

We suppose that Rydberg MO's are formed from linear combinations of virtual atomic orbitals (LCVAO's) pertaining to the various atomic centers in the molecule. We will refer to such LCVAO's as "bonding" or "antibonding," but we use this terminology only with reference to a barycenter energy of the constituent VAO's; for example, in the case of CS_2, this barycenter for the lowest energy s-type Rydberg is

$$[\mathrm{VSIE}(3s_C) + 2\mathrm{VSIE}(4s_S)]/3 = [(-3.66) + 2(-3.76)]/3 = -3.73 \text{ eV} \quad (3)$$

If all the atoms composing a molecule belong to the same row of the periodic table, the VAO's comprising a Rydberg do, for the most part, refer to the same principal quantum number. Hence, we speak of 3s, 3p, 3d Rydbergs, etc., for CO_2. In the case of CS_2, however, our computations indicate that the lowest energy Rydberg orbital of s type is composed of 33% $3s_C$ character and 67% $4s_S$ character. The question immediately arises: What value of n, the principal quantum number, should be used for such an orbital? If we choose, based on the dominance of the $4s_S$ character, to set $n = 4$, it is clear that this rather arbitrary choice must later be reflected in the value of the quantum defect required to provide correspondence with experiment.

Molecular Rydberg states are generated by promoting a valence electron to an orbital so diffuse that it engulfs the whole molecule. The energy of this type of transition is

$$E_n = A - R/(n - \delta)^2 \quad (4)$$

(26) J. M. Sichel and M. A. Whitehead, *Theor. Chim. Acta*, **11**, 239 (1968).

(27) A. T. Armstrong, B. Bertus, and S. P. McGlynn, *Spectrosc. Lett.*, **1**, 43 (1968).

Table VI

Comparison of the Lower Ionization Potentials (eV) of Selected Molecules

	Expt[a]		*MWH, calcd*		*Extended*[b] *Hückel, calcd*		*CNDO,*[b] *calcd*		*Hartree–Fock,*[c] *calcd*	
OCO	π_g	13.78	π_g	14.05	π_g	17.20	π_g	14.55	π_g	14.81
	π_u	17.32	σ_u	14.93	σ_u	17.51	σ_u	14.55	π_u	19.45
	σ_u	18.08	π_u	17.68	π_u	18.14	π_u	16.83	σ_u	20.23
	σ_g	19.40	σ_g	18.06	σ_g	19.56	σ_g	21.01	σ_g	21.77
NNO	π	12.89	2π	13.32	π	15.27	π	13.58	π	13.37
	σ	16.38	7σ	15.18	σ	16.16	σ	15.35	σ	19.01
	π	17.65	6σ	15.58	π	18.16	π	16.63	π	20.73
	σ	20.11	1π	18.81	σ	19.85	σ	23.83	σ	22.63
OCS	π	11.20	2π	12.55	π	13.14	π	12.26		
	π	15.08	7σ	13.67	σ	14.67	σ	13.81		
	σ	16.04	1π	15.90	π	17.76	π	15.36		
	σ	17.96	6σ	16.50	σ	18.40	σ	19.32		
SCS	π_g	10.09	$1\pi_g$	11.33	π_g	12.24	π_g	11.33		
	π_u	12.69	$3\sigma_g$	12.61	σ_u	13.48	σ_u	12.59		
	σ_u	14.47	$1\pi_u$	14.44	π_u	14.18	π_u	13.28		
	σ_g	16.19	$4\sigma_g$	15.32	σ_g	15.72	σ_g	18.23		
NCCl			2π	12.33	π	14.48	π	13.08		
			7σ	12.61	σ	14.88	σ	13.69		
			1π	16.26	π	15.77	π	14.93		
			6σ	17.43	σ	17.70	σ	20.00		
H_3CCCH_3	2e	10.19	2e	11.66						
HNNN	2a''	11.5	2a''	11.84						
H_2CCO	$1a_2$	9.60	$1a_2$	11.49						

[a] References 6, 28, 29, 30. [b] Reference 26. [c] Reference 20.

where A is the valence-electron ionization energy, R is the Rydberg constant, n is the principal quantum number of the AO which dominates the constitution of the Rydberg orbital, and δ is a quantum defect. The Rydberg states of homopolar diatomic molecules have been discussed by Mulliken;[31] the nature of the quantum defect δ has been treated briefly by Walsh.[32]

The magnitude of the quantum defect depends upon the extent of orbital penetration into the interior of the molecule. The deeper this penetration, the larger is the effective core charge seen by electrons in the orbital and the larger is the quantum defect. Thus, for molecules composed of second-row atoms, the quantum defects are $\delta \simeq 1.0$, 0.5, and 0.1 for s-, p-, and d-type Rydberg MO's, respectively. Since core-shielding is less effective in the third-row atoms, the corresponding quantum defects for molecules composed of such atoms are larger and are given by $\delta \simeq 2.0$, 1.5, and 0.4, respectively. The sets of δ's given above are experimental and of reasonable generality. The question of interest now is the set of δ values to be used in a molecule such as CS_2. In the case of the s-type Rydberg MO we have discussed, if we choose $n = 4$, it follows that δ should lie in the range $1.0 < \delta < 2.0$ and that similar intermediacies might also apply to p- and d-type Rydbergs in such molecules. We have observed such intermediary δ's in CS_2 and OCS; they are of value in characterizing Rydberg series and in deriving estimates of the VAO composition of Rydbergs in molecules consisting of atoms from different rows of the periodic table. Since these two molecules (*i.e.*, CS_2 and OCS) provide the only two known examples of intermediary quantum defects, it is clear that further study is in order.

The calculations performed on CS_2, CO_2, NCCl, and NCO^- included certain VAO's from the various atomic centers on the molecule. These calculations accord with the mixed nature of the Rydberg MO's. They invariably predict that the lowest Rydberg state should be of s type and that it should lie at higher energies than the lower energy $\pi \rightarrow \pi^*$ states.

D. ELECTRONEGATIVITY CONSIDERATIONS

Certain of the molecules discussed here absorb at much lower energies than others. A rationalization of these differences has been given by Walsh:[2] the lowest energy electronic transition takes place from an orbital largely localized on the end atoms ($1\pi_g$, see Figure 3) to an orbital largely localized on the central atom ($2\pi_u$). Considering N_2O and CO_2, the orbital largely localized on the end atoms should be less tightly bound in NNO than OCO because of the lower electronegativity of the N atom relative to the O atom. However, the orbital largely localized on the central atom should be more tightly bound in NNO than OCO because the N atom is more electronegative than the C atom. The electronic excitation in N_2O, therefore, should require less energy than that in CO_2. This, of course, is the situation observed experimentally.

We wish to expand Walsh's proposal in order to predict usable qualitative trends in the energies of absorption spectra. The molecules studied here are divided into two groups: the XCX′ and the XNX′ groups. The sum of the Pauling electronegativities of X and X′ are listed in the second column of Table VII. The barycenters of the $1\pi_g \rightarrow 2\pi_u$ and $3\sigma_u \rightarrow 2\pi_u$

(28) C. R. Brundle and D. W. Turner, *Int. J. Mass Spectrom. Ion Phys.*, 2, 195 (1969).

(29a) D. W. Turner and D. P. May, *J. Chem. Phys.*, 46, 1156 (1967).

(29b) M. I. Al-Joboury, D. P. May, and D. W. Turner, *J. Chem. Soc.*, 6350 (1965).

(30) G. Herzberg, "Molecular Spectra and Molecular Structure. Vol. III. Electronic Spectra and Electronic Structure of Polyatomic Molecules," Van Nostrand, New York, N. Y., 1967.

(31) R. S. Mulliken, *J. Amer. Chem. Soc.*, 86, 3183 (1964); 88, 1849 (1966).

(32) A. D. Walsh, *J. Phys. Radium*, 15, 501 (1954).

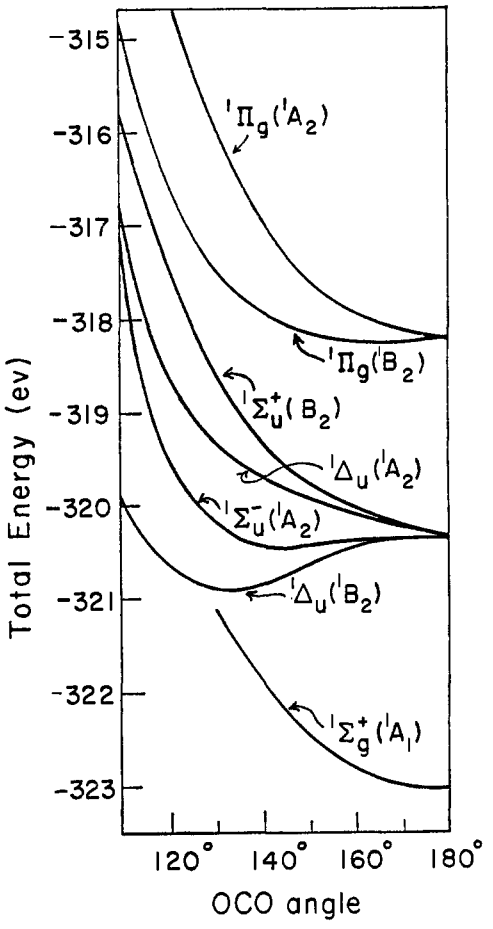

Figure 8. Total energies of electronic states in CO_2 as a function of angle (open-shell iteration).

transitions, from MWH calculations, are listed in columns 3 and 4.

It is evident that, when the central atom remains unchanged, the transition energy should vary according to the electronegativity of the two end atoms. This prediction results from the complete localization of the $1\pi_g$ molecular orbital on the two end atoms in CO_2 and its almost complete similar localization in NNO. The degree of this localization is demonstrated by the MWH MO eigenvectors in eq 5. The $3\sigma_u$ orbital, although

$$O_{(1)}CO_{(2)}:\Psi(1\pi_g) =$$

$$-\begin{bmatrix}0.7071(2p_{xO_{(1)}}) - 0.7071(2p_{xO_{(2)}})\\ 0.7071(2p_{yO_{(1)}}) - 0.7071(2p_{yO_{(2)}})\end{bmatrix} \quad (5)$$

$$N_{(1)}N_{(2)}O:\Psi(2\pi) =$$

$$-\begin{bmatrix}0.6315(2p_{xN_{(1)}}) + 0.1281(2p_{xN_{(2)}}) - 0.7647(2p_{xO})\\ 0.6315(2p_{yN_{(1)}}) + 0.1281(2p_{yN_{(2)}}) - 0.7647(2p_{yO})\end{bmatrix}$$

not so heavily localized on the end atoms, is expected to be affected in a manner similar to the $1\pi_g$ orbital.

We now consider the transition energy in molecules in which the end atoms remain invariant but in which the central atom varies. By comparison of NNO to HNCO and HNNN to H_2NCN, it is expected that those molecules with the more electronegative central atom (*i.e.*, N) should possess the lower transition energies. This prediction is based on the dominance of central-atom AO character in the $2\pi_u$ MO, as demonstrated by the MWH MO eigenvectors in eq 6. The validity of this

$$O_{(1)}CO_{(2)}:\Psi(2\pi_u) =$$

$$-\begin{bmatrix}0.4981(2p_{xO_{(1)}}) - 0.7097(2p_{xC}) + 0.4981(2p_{xO_{(2)}})\\ 0.4981(2p_{yO_{(1)}}) - 0.7097(2p_{yC}) + 0.4981(2p_{yO_{(2)}})\end{bmatrix} \quad (6)$$

$$N_{(1)}N_{(2)}O:\psi(3\pi) =$$

$$-\begin{bmatrix}0.6693(2p_{xN_{(1)}}) - 0.5881(2p_{xN_{(2)}}) + 0.4542(2p_{xO})\\ 0.6693(2p_{yN_{(1)}}) - 0.5881(2p_{yN_{(2)}}) + 0.4542(2p_{yO})\end{bmatrix}$$

supposition is also confirmed in Table VII.

Table VII

A Comparison of Electronegativity and MWH Results

XCX'	*Sum of Pauling electronegativity[a] of X and X'*	*MWH energies* $1\pi_g \rightarrow 2\pi_u^*$ *(eV)*[b]	*MWH energies* $3\sigma_u \rightarrow 2\pi_u^*$ *(eV)*[b]
CO_2	6.88	7.141	8.018
HNCO	6.48	6.248	7.969
NCCl	6.20	6.262	6.542
H_2NCN	6.08	6.085	6.392
OCS	6.02	6.004	7.129
H_2CCO	5.99	6.106	7.123
HNCS	5.62	5.344	7.134
CS_2	5.16	5.004	6.282
H_2CCCH_2	5.10	5.616	6.696
XNX'			
NO_2^+	6.88	7.608	9.920
NNO	6.48	5.610	7.462
HN_3	6.08	4.916	7.104

[a] Reference 33. [b] Barycenter of MO excitations from MWH calculations.

Thus, the proposal of Walsh, as extended and correlated with MWH results in Table VII, provides qualitative predictions concerning trends in the positions of absorption bands. These trends should be useful in identifying molecular transitions, Rydberg and otherwise, which arise from excitation of electrons from $1\pi_g$ and $3\sigma_u$ molecular orbitals.

It can be seen from Table VII that the estimated energy of the $1\pi_g \rightarrow 2\pi_u^*$ excitation varies over a range of 2.225 eV (*i.e.*, from 7.141 eV in CO_2 to 4.916 eV in HN_3), while the estimated energy of the $3\sigma_u \rightarrow 2\pi_u^*$ excitation varies over a range of only 1.736 eV (*i.e.*, from 8.018 eV in CO_2 to 6.282 eV in CS_2). Although these numbers represent one-electron excitation energies (or barycenters) for the resulting electronic states, the qualitative trends should be valid. Thus, the excited states resulting from the $1\pi_g \rightarrow 2\pi_u^*$ excitation should, as a result of the higher charge-transfer nature of the $1\pi_g \rightarrow 2\pi_u^*$ MO excitation, vary over a wider energy range than those resulting from the $3\sigma_u \rightarrow 2\pi_u^*$ excitation.

(33) A. L. Allred, *J. Inorg. Nucl. Chem.*, 17, 215 (1961).

Table VIII

Fundamental Vibrational Frequencies (cm^{-1})

$D_{\infty h}$	$\nu_1(\sigma_g^+)$	$\nu_2(\pi_u)$	$\nu_3(\sigma_u^+)$						
CO_2[34]	1337	667	2349						
CS_2[34]	657	397	1523						
NO_2^+[35]	1396	571	2360						
N_3^-[36]	1360	650	2040						
$C_{\infty v}$	$\nu_1(\sigma^+)$	$\nu_2(\pi)$	$\nu_3(\sigma^+)$						
OCS[34]	859	527	2079						
N_2O[34]	1285	589	2224						
NCO^-[37]	1300	630	2170						
NCS^-[34]	750	398	2066						
NCCl[38]	714	378	2216						
NCBr[39,40]	575	342	2198						
NCI[41]	452	329	2176						
D_{2d}	$\nu_1(a_1)$	$\nu_2(a_1)$	$\nu_3(a_1)$	$\nu_4(b_1)$	$\nu_5(b_2)$	$\nu_6(b_2)$	$\nu_7(b_2)$	$\nu_8(e)$	$\nu_9(e)$
H_2CCCH_2[34]	2993	1432	1071	820	2960	1956 (r) 1980 (ir)	1389	3061	1031
	$\nu_{10}(e)$	$\nu_{11}(e)$							
	838	353							
C_{2v}	$\nu_1(a_1)$	$\nu_2(a_1)$	$\nu_3(a_1)$	$\nu_4(a_1)$	$\nu_5(b_1)$	$\nu_6(b_1)$	$\nu_7(b_1)$	$\nu_8(b_2)$	$\nu_9(b_2)$
H_2CCO[42]	3069	2151	1388	1121	3166	978	588	788	529
H_2NCN[43]	3272	2259	1586	1130	3365 (ν_7)	...	437 (ν_5)	926	538
H_2CNN[44]	3077	2102	1414	1170	3185	1109	421	564	406
C_s	$\nu_1(a')$	$\nu_2(a')$	$\nu_3(a')$	$\nu_4(a')$	$\nu_5(a')$	$\nu_6(a'')$			
HNCO[45]	3531	2274	1327	797	572	670			
HNNN[46,47]	3336	2140	1274	1150	522	672			

E. FUNDAMENTAL FREQUENCIES OF VIBRATION

The fundamental frequencies of the molecules studied here are given in Table VIII.[34-47] The symmetries of these vibrational modes determine which frequencies can couple to electronic transitions. For example, a progression in the π_u bending mode is coupled to the $^1\Pi_g \leftarrow {}^1\Sigma_g^+$ electronic transitions of both CO_2 and CS_2.

III. Experimental

A. INSTRUMENTAL MEASUREMENTS

Absorption spectra in the visible and near-ultraviolet (uv) were recorded on Cary Model 14 and 15 spectrophotometers. The cell lengths ranged from 0.01 to 10 cm; cells were of fused silica.

Absorption spectra in the vacuum ultraviolet region were obtained using a McPherson Model 225 1-m scanning monochromator. The source was a McPherson Model 630 vacuum uv lamp operated with a slow flow of hydrogen. Lithium fluoride windows were used in the light source and in the cells.

A vacuum line was attached directly to the absorption cells for ease of sampling and degassing. Pressures as low as 10^{-4} Torr were obtainable with a Welch Model 1402B vacuum pump. Pressures above 1 mm were measured with a "Speedivac" direct reading Torr gauge manufactured by Edwards High Vacuum, Ltd. Pressures below 1 mm were measured using a Veeco Model DV-1M thermocouple gauge, controlled by a RG-31X gauge, and calibrated against a Vacustat McLeod gauge from Edwards High Vacuum, Ltd. The sample cell was isolable at any desired vapor pressure or, alternatively, could be used as a continuous-flow cell for photodecomposing samples.

B. CHEMICALS AND PURIFICATION PROCEDURES

The chemicals used in this work, their origin, and purification are as follows: nitrous oxide (N_2O), 98.0% min as obtained from Matheson Chemical Co.; carbon dioxide (CO_2), 99.9995 min vol % as obtained from Matheson Chemical Co.; carbonyl sulfide (OCS), 97.5% min as obtained from Matheson Chemical Co. (the major impurity, CS_2, was removed by several trap-to-trap distillations); carbon disulfide (CS_2), obtained as the spectroscopic grade from Mallinkrodt Chemical Co; allene (H_2CCCH_2), 97% min as obtained from Matheson Chemical Co. (mass spectrographic analysis showed no obvious impurities); ketene (H_2CCO), prepared by pyrolysis of acetone in a ketene generator[48] (after passing through a trap at 0°, it was collected at −78° and purified by several trap-to-

(34) G. Herzberg, "Infrared and Raman Spectra of Polyatomic Molecules," Van Nostrand, New York, N. Y., 1945.
(35) J. W. Nobgen, A. D. McElroy, and H. F. Klodowski, *Inorg. Chem.*, 4, 1796 (1965).
(36) K. W. F. Kohlrausch and J. Wagner, *Monatsh. Chem.*, 77, 180 (1947).
(37) T. C. Waddington, *J. Chem. Soc.*, 2499 (1959).
(38) A. V. Yakovleva, *Izv. Akad. Nauk SSSR, Ser. Fiz.*, 14, 517 (1950).
(39) A. G. Maki and C. T. Gott, *J. Chem. Phys.*, 36, 2282 (1962).
(40) A. G. Maki, *ibid.*, 38, 1261 (1963).
(41) W. O. Freitag and E. R. Nixon, *ibid.*, 24, 109 (1956).
(42) W. F. Arendale and W. H. Fletcher, *ibid.*, 26, 793 (1957).
(43) W. H. Fletcher and F. B. Brown, *ibid.*, 39, 2478 (1963).
(44) C. B. Moore and G. C. Pimentel, *ibid.*, 40, 329 (1964).
(45) G. Herzberg and C. Reid, *Discuss. Faraday Soc.*, 9, 92 (1950).
(46) A. D. Dows and G. C. Pimentel, *J. Chem. Phys.*, 23, 1258 (1955).
(47) P. Gray and T. C. Waddington, *Trans. Faraday Soc.*, 53, 901 (1957).
(48) J. W. Williams and C. D. Hurd, *J. Org. Chem.*, 5, 122 (1940).

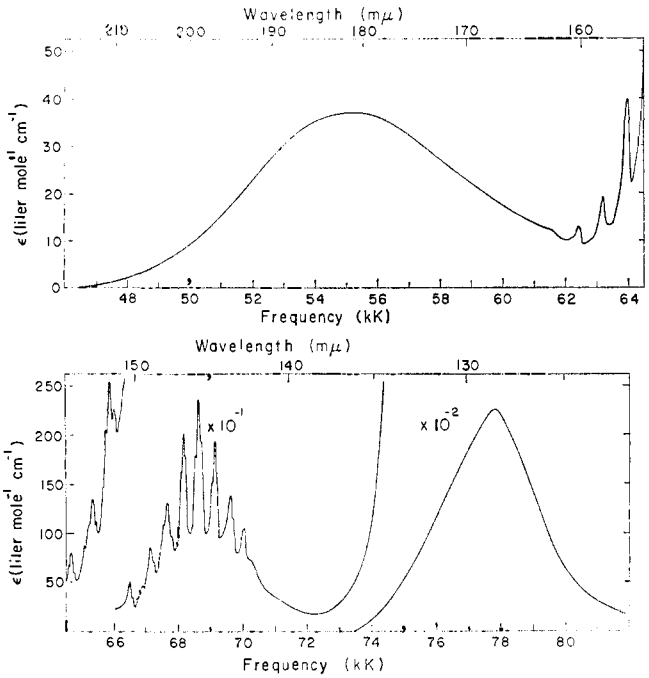

Figure 9. Absorption spectrum of nitrous oxide, N_2O.

trap distillations on a vacuum line; the spectrum of the resulting ketene was run immediately after preparation); cyanamide (H_2NCN), obtained from Eastman Kodak Co., purified by slow vacuum sublimation (all handling and storing was done in a drybox because of its hygroscopic nature); dimethyl cyanamide ($(CH_3)_2NCN$), obtained from K & K Laboratories, purified by several vacuum distillations.

The source and purification procedures of the azide (NNN^-), cyanate (NCO^-), and thiocyanate (NCS^-) salts and the corresponding acids, HNNN, HNCO, and HNCS are described in previous publications.[4-6]

C. ABSORPTION SPECTRA

Absorption spectra were measured down to 1200 Å, whenever possible. The spectrum of each molecule was recorded as often as needed to ensure reproducibility.

The spectrum of each molecule will be discussed individually. The assignments given will not necessarily be validated until section IV.

1. Nitrous Oxide

The absorption spectrum of N_2O has been reported previously;[49-58] however, satisfactory state identifications are lacking. The absorption begins very weakly at ~3065 Å and possesses maxima at 2900, 2730, 1820, 1455, and 1284 Å. The spectrum is shown in Figure 9.

a. $^1\Sigma^+ \leftarrow {}^1\Sigma^+$ Transition: 1284 Å (9.66 eV), $f = 0.36$

The high intensity of this transition indicates that it is allowed; the absorption band is very symmetrical. Zelikoff, Watanabe, and Inn[51] (ZWI) have found several weak diffuse peaks on the long-wavelength slope of this band and one sharp peak at 77,400 cm^{-1}. The sharp peak was assumed to be the first member of a Rydberg series. We have not observed these peaks, possibly because of large slit widths.

b. $^1\Pi \leftarrow {}^1\Sigma^+$ Transition: 1455 Å (8.52 eV), $f = 7.2 \times 10^{-3}$

The intensity of this band is rather low for an allowed transition; we attribute this to the fact that it derives from the parity forbidden $^1\Pi_g \leftarrow {}^1\Sigma_g^+$ transition of $D_{\infty h}$ molecules. The transition consists of a continuum on which vibrational bands are superimposed. The vibrational bands are listed in Table IX; the frequencies agree quite well with those of ZWI. The

Table IX

Primary Vibrational Frequencies in the $^1\Pi \leftarrow {}^1\Sigma^+$ Transition of N_2O

Rel intensity	λ_{max} (Å)	$\bar{\nu}$ (cm^{-1})	$\Delta\bar{\nu}$ (cm^{-1})
0.05	1623.4	61,601	
			821
0.08	1602.0	62,422	
			813
0.27	1581.4	63,235	
			766
0.48	1562.5	64,001	
			698
0.64	1545.6	64,699	
			649
2.2	1530.3	65,348	
			623
3.6	1515.8	65,971	
			598
9.6	1502.2	66,569	
			588
17.2	1489.0	67,157	
			536
28.0	1477.3	67,693	
			508
39.2	1466.3	68,201	
			520
41.0	1455.2	68,721	
			504
27.2	1444.6	69,225	
			473
17.8	1434.8	69,698	
			474
7.2	1425.1	70,172	
			470
0.80	1415.6	70,642	
			448
0.58	1406.7	71,090	

progression starts out with frequency spacings larger than 800 cm^{-1}; this spacing decreases very rapidly, indicating considerable anharmonicity. It is not possible, on the basis of the initial frequency spacing, to determine whether the active vibration is the bending mode ν_2 or the NO stretching mode ν_3, altered from ground-state values of 589 and 1285 cm^{-1}, respectively. A progression in the bending vibration is expected only if the molecule is bent in the excited state; the intensity maximum in such a progression in a linear → bent transition will not likely occur at the first member. The intensity distribution observed in this progression indicates that the molecule is bent in the excited state and that the active vibration is ν_2.

(49) Y. Tanaka, A. S. Jursa, and F. J. LeBlanc, *J. Chem. Phys.*, 32, 1205 (1960).
(50) N. Astoin, L. Lanson, and M. C. Bonnelle, *C. R. Acad. Sci. Paris*, 250, 1824 (1960).
(51) M. Zelikoff, K. Watanabe, and E. C. Y. Inn, *J. Chem. Phys.*, 21, 1643 (1953).
(52) H. Sponer and L. G. Bonner, *ibid.*, 8, 33 (1940).
(53) A. B. F. Duncan, *ibid.*, 4, 638 (1936).
(54) P. K. Sen-Gupta, *Nature*, 136, 513 (1935).
(55) O. R. Wulf and E. H. Melvin, *Phys. Rev.*, 39, 180 (1932).
(56) A. K. Dutta, *Proc. Roy. Soc., Ser. A*, 138, 84 (1932).
(57) L. Henry, *Nature*, 134, 498 (1934).
(58) S. W. Leifson, *Astrophys. J.*, 63, 73 (1926).

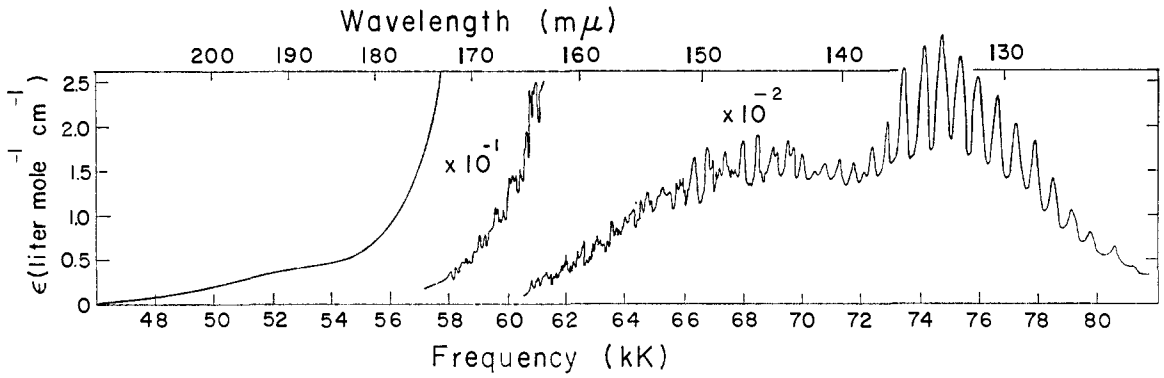

Figure 10. Absorption spectrum of carbon dioxide, CO_2.

Each vibrational band is composed of several components, the spacings between them being ~150 cm^{-1} or less. They are not totally resolved in our spectrum. It is possible that these may be rotational in origin.

c. $^1\Delta \leftarrow {}^1\Sigma^+$ Transition: 1820 Å (6.81 eV), $f = 1.4 \times 10^{-3}$

Very weak vibrational bands are superimposed on this broad continuum; however, they are too diffuse for analysis. The low intensity, large band width, and forbidden origin of the band indicates that the upper state involves considerable bond stretching and/or bending.

d. $^1\Sigma^- \leftarrow {}^1\Sigma^+$ Transition: 2730 Å (4.54 eV), $f \sim 5 \times 10^{-6}$

Sponer and Bonner[52] have observed a continuous absorption using path lengths of 33 m and several atmospheres pressure. The low intensity and continuous nature indicate that it corresponds to a forbidden transition. The most obvious assignment is the $^1\Sigma^- \leftarrow {}^1\Sigma^+$ transition; however, this must be considered tentative.

e. $^3\Sigma^+ \leftarrow {}^1\Sigma^+$ Transition: 2900 Å (4.28 eV); $f \sim 2 \times 10^{-7}$

This transition was also observed by Sponer and Bonner[52] using path lengths of 33 m and several atmospheres pressure. The observed oscillator strength is in the expected range for a multiplicity-forbidden transition of the type assigned.

f. Rydberg Transitions

Several investigators[49,51] have reported Rydberg series at wavelengths shorter than 1200 Å. The longest wavelength series converges to an ionization potential of ~12.9 eV.

2. Carbon Dioxide

The absorption spectrum of CO_2 has been considered by many investigators;[59-73] however, the identification of electronic states leaves much to be desired. The spectrum is shown in Figure 10. CO_2 is transparent in the visible and near-ultraviolet regions and exhibits three maxima in the vacuum ultraviolet region: at 1475, 1332, and 1121 Å. All of these continua possess superimposed vibrational structure.

a. $^1\Sigma_u^+ \leftarrow {}^1\Sigma_g^+$ Transition: 1121 Å (11.08 eV), $f = 0.12$

This is the strongest absorption band of CO_2. It lies beyond the short-wavelength limit of our cell windows; however, as given by Inn, Watanabe, and Zelikoff,[64] it is a broad continuum with superimposed Rydberg structure. The high intensity of the transition indicates that it is allowed. The strong bands overlying the continuum have been assigned as Rydberg series with accompanying vibrational structure. Rydberg analysis yields 13.8 eV for the first ionization potential.

b. $^1\Pi_g \leftarrow {}^1\Sigma_u^+$ Transition: 1332 Å (9.31 eV), $f = 7.5 \times 10^{-3}$

The vibrational structure associated with this transition appears, on cursory examination, to consist of a simple progression in a ~624-cm^{-1} frequency. The vibrational frequencies observed are shown in Table X. However, the irregularities in the intervals make acceptance of this proposal doubtful. Price and Simpson[68] suggested that these bands consist of two progressions in the same 1225-cm^{-1} frequency interval and that this interval corresponds to the $\nu_1(\sigma_g^+)$ normal mode of the excited state. We reject this suggestion for the following reasons.

(i) Since the transition, for correlative reasons (*vide infra*), is assigned as parity forbidden, a progression in a totally symmetric vibration can only be observed if it is based on a false origin which is vibronically allowed. There is no evidence in the spectrum for such a false origin.

(ii) The frequency intervals are not sufficiently regular[64] to validate the Price–Simpson[68] suggestion.

(59) R. N. Dixon, *Discuss. Faraday Soc.*, 35, 105 (1963).
(60) B. A. Thompson, P. Harteck, and R. R. Reeves, Jr., *J. Geophys. Res.*, 68, 6431 (1963).
(61) Y. Tanaka and M. Ogawa, *Can. J. Phys.*, 40, 879 (1962).
(62) R. N. Dixon, *Proc. Roy. Soc., Ser. A*, 275, 431 (1963).
(63) Y. Tanaka, A. S. Jursa, and F. J. LeBlanc, *J. Chem. Phys.*, 32, 1199 (1960).
(64) E. C. Y. Inn, K. Watanabe, and M. Zelikoff, *ibid.*, 21, 1648 (1953).
(65) P. G. Wilkinson and H. L. Johnson, *ibid.*, 18, 190 (1950).
(66) W. M. Preston, *Phys. Rev.*, 57, 887 (1940).
(67) A. G. Gaydon, *Proc. Roy. Soc., Ser. A*, 176, 505 (1940).
(68) W. C. Price and D. M. Simpson, *ibid., Ser. A*, 169, 501 (1938).
(69) G. Tarhenau, *Z. Phys.*, 87, 32 (1934).
(70) H. S. Henning, *Ann. Phys.*, 13, 599 (1932).
(71) H. D. Smyth, *Phys. Rev.*, 38, 2000 (1931).
(72) S. W. Leifson, *Astrophys. J.*, 63, 73 (1926).
(73) T. Lyman, *ibid.*, 27, 87 (1908).

Table X

Vibrational Frequencies in the $^1\Pi_g \leftarrow {}^1\Sigma_g^+$ Transition of CO_2

I	λ_{max} (Å)	$\bar{\nu}$ (cm^{-1})	$\Delta\bar{\nu}$ (cm^{-1})
5.9	1382.8	72,317	
6.1	1371.6	72,902	585
8.8	1360.6	73,499	597
9.5	1349.5	74,102	603
10	1337.8	74,755	653
9.1	1326.9	75,358	603
8.5	1316.0	75,976	618
7.7	1304.7	76,628	652
7.1	1293.9	77,304	676
6.0	1283.5	77,918	614
4.6	1273.1	78,548	630
3.5	1263.0	79,177	629
2.6	1253.1	79,821	644
2.1	1243.8	80,402	581
1.4	1233.9	81,042	640

An alternative explanation exists if it is assumed that the molecule is very slightly bent in the $^1\Pi_g$ state such that one degree of freedom cannot be categorized as either rotational or vibrational. In this quasi-linear situation, the vibrational frequencies will be irregular and the rotational constants, especially A, will depend sharply upon the quantum number of the bending vibration. The structure, under these conditions, could consist of a single progression in the bending vibration ν_2. The irregularities might then derive from the interaction of vibrational and rotational angular momenta. The selection rules, in this situation, are relaxed such that any number of quanta of the π_u mode becomes allowed and can couple. The observed long progression and the fact that the Franck–Condon maximum is considerably removed from the origin indicate that the upper state may be bent and that the active vibration is the bending mode ν_2.

c. $^1\Delta_u \leftarrow {}^1\Sigma_g^+$ Transition: 1475 Å (8.41 eV), $f = 6.2 \times 10^{-3}$

CO_2 is a vibrationally deficient molecule and this transition is forbidden by first-order vibronic coupling.[74] This should make the transition very improbable and it should possess a complex vibrational structure. In agreement with this, it is found that ϵ_{max} is 180 and that the vibrational structure is weak, diffuse, and apparently complex. (The rather large f compared to the small ϵ is caused by the large band width.) Other investigators have been unable to offer any analysis for these vibrational bands. The band extends from ~175 to ~139 mμ where it is lost under the stronger $^1\Pi_g \leftarrow {}^1\Sigma_g^+$ absorption. It is quite probable that the maximum at 1475 Å corresponds to the $^1\Delta_u(^1B_2) \rightarrow {}^1\Sigma_g^+$ transition, while the weaker continuum near 165 mμ corresponds to the $^1\Delta_u(^1A_2) \leftarrow {}^1\Sigma_g^+$ transition (which is forbidden in C_{2v}).

d. $^1\Sigma_u^- \leftarrow {}^1\Sigma_g^+$ Transition: 1900 Å (6.53 eV), $f \sim 1 \times 10^{-5}$

This weak, continuous absorption band corresponds to a forbidden transition. No vibrational structure appears to be associated with the transition.

(74) P. J. Gardner and M. Kasha, *J. Chem. Phys.*, **50**, 1543 (1969).

e. $^3\Sigma_u^+(^3B_2) \rightarrow {}^1\Sigma_g^+$ Transition: 2535 Å (4.89 eV)

Dixon[62] has obtained high-resolution spectra of the afterglow of CO_2 in the visible and near-ultraviolet regions. The emission has been assigned[62] as $^1\Delta_u(^1B_2) \rightarrow {}^1\Sigma_g^+$ and supposedly corresponds to the absorption maximum at 1475 Å. This represents a very large Stokes shift of ~24,000 cm^{-1} which is attributed to an emission from the minimum of an upper state, which is strongly bent (122 ± 2°), to very highly excited vibrational levels of the ground state. We are in discord with the above assignment for the following reasons: (i) the Stokes shift required for the $^1B_2$ assignment is abnormally large; (ii) the rotational analysis of Dixon[62] specifies that the excited state is B_2 but does not indicate whether it is singlet or triplet. The most reasonable assignment is $^3\Sigma_u^+(^3B_2) \rightarrow {}^1\Sigma_g^+$. This assignment places the $^3\Sigma_u^+$ state of CO_2 slightly higher than that[5] of NCO^-, in agreement with expectation. This assignment also provides a $^1\Sigma_u^+$–$^3\Sigma_u^+$ split of 6.19 eV, in good agreement with the large splitting predicted in Table V and with the calculations of Mulligan.[25] The $^3\Sigma_u^+(^3B_2)$ state is expected to be bent, thus accounting for the transitions to higher vibrational levels of the ground state. This assignment must be considered tentative.

3. Carbonyl Sulfide

OCS has been investigated previously.[49,68,75–78] The absorption spectrum, shown in Figure 11, consists of three distinct transitions with maxima at ~2237, ~1667, and ~1527 Å followed, at shorter wavelengths, by Rydberg structures.

a. $^1\Sigma^+ \leftarrow {}^1\Sigma^+$ Transition: 1527 Å (8.12 eV), $f = 0.38$

This transition consists of several diffuse bands whose frequencies are shown in Table XI. The progression, whose origin is at 63,780 cm^{-1}, corresponds to the totally symmetric stretching frequency $\nu_1(\sigma^+)$, which is 859 cm^{-1} in the ground

Table XI

Primary Vibrational Frequencies in the $^1\Sigma^+ \leftarrow {}^1\Sigma^+$ Transition of OCS

Rel intensity	λ_{max} (Å)	$\bar{\nu}$ (cm^{-1})	$\Delta\bar{\nu}$ (cm^{-1})
1.0	1567.9	63,780	
2.7	1547.2	64,633	853
2.9	1527.2	65,479	846
2.2	1509.2	66,260	781
2.1	1492.0	67,035	775
1.1	1474.7	67,810	775
0.6	1459.0	68,540	730
0.3	1443.9	69,257	717
0.2	1429.3	69,966	709

(75) (a) J. Y. Roncin, N. Damany, and B. Vodar, *Chem. Phys. Lett.*, 3, 197 (1969); (b) W. H. Breckenridge and H. Taube, *J. Chem. Phys.*, 52, 1713 (1970).

(76) L. Kopp, *Can. J. Phys.*, 45, 4011 (1967).

(77) (a) W. Lochte-Holtgreven and C. E. H. Brown, *Trans. Faraday Soc.*, 28, 698 (1932); (b) G. S. Forbes and J. E. Cline, *J. Amer. Chem. Soc.*, 61, 151 (1939); (c) K. S. Sidhu, I. G. Csizmadia, O. P. Strausz, and H. E. Gunning, *ibid.*, 88, 2412 (1966).

(78) F. M. Matsunaga and K. Watanabe, *J. Chem. Phys.*, 46, 4457 (1967).

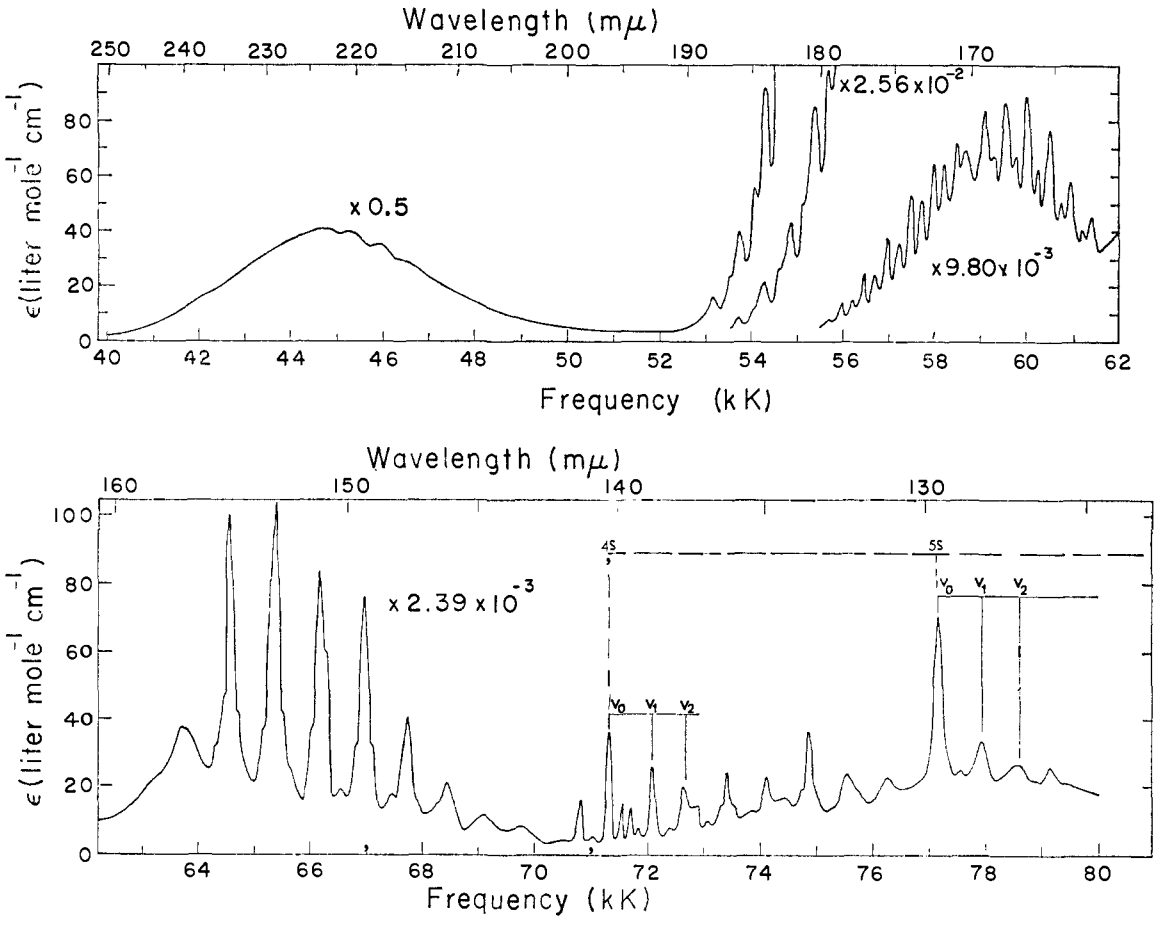

Figure 11. Absorption spectrum of carbonyl sulfide, OCS.

state. The progression becomes anharmonic toward shorter wavelengths. Each vibrational band is composed of several components which, as noted earlier, are probably due to rotational structure resulting from a slightly bent molecule. Matsunaga and Watanabe[78] have listed another progression which is interleaved with the σ^+ progression; it is difficult to determine if this is a new progression or simply rotational components of the main (*i.e.*, σ^+) progression. A Franck–Condon intensity analysis indicates that the C–O and C–S bond lengths in this excited state are 1.26 and 1.66 Å, respectively. This represents an increase of 0.16 Å in the C–O bond and 0.12 Å in the C–S bond relative to the ground state.

b. $^1\Pi \leftarrow {}^1\Sigma^+$ Transition: 1667 Å (7.44 eV), $f = 0.13$

This band consists of a continuum which reaches its maximum some 6000 cm^{-1} from the origin. Superimposed on this continuum are weak vibrational bands forming two separate progressions reaching their maxima at ~58,895 and ~60,150 cm^{-1}, respectively. These progressions, as shown in Table XII, have an average spacing of 513 cm^{-1} and are separated from each other by ~270 cm^{-1}. These must correspond to long double progressions in the bending frequency, π, which is 527 cm^{-1} in the ground state. Every quantum of the vibration is allowed in this case because the parity selection rule is relaxed in the $C_{\infty v}$ point group. Bending the molecule splits the $^1\Pi$ state into $^1A'$ and $^1A''$ states. We can assume that the two progressions correspond to the two component electronic transitions supposedly separated by a ~270-cm^{-1} energy difference.

These two degenerate components should coalesce at the linear configuration, and the Franck–Condon maxima associated with both transitions should be at the same location (*i.e.*, at the linear configuration). It is possible that interaction between the two component states might disturb this pattern, for it is known that strong interactions between the components can occur at the barrier to linearity. If so, one would probably not expect a simple pattern; furthermore, it would be extremely surprising if the bending frequencies associated with the two component electronic states were the same because the potential energy curves for the bending vibration must be different and must reflect the lifting of electronic degeneracy which occurs in the nonlinear molecule.

The vibrational pattern could, alternatively, represent two long progressions in the bending vibration of one of the component states, one of these progressions having a quantum of another vibrational frequency superimposed. Whichever interpretation is correct, the long progressions in the bending mode and the fact that the Franck–Condon maximum of each progression is at least 13 quanta removed from the origin indicate that the molecule is strongly bent in the excited state(s) in question.

c. $^1\Delta \leftarrow {}^1\Sigma^+$ Transition: 2237 Å (5.54 eV), $f = 1.8 \times 10^{-3}$

This band has a forbidden origin and is very weak (ϵ_{max} 81.6).

Table XII

Vibrational Frequencies in the $^1\Pi \leftarrow {}^1\Sigma^+$ Transition of OCS

λ_{max} (Å)	*Rel intensity*	$\Delta\bar{\nu}$ (cm^{-1})	$\bar{\nu}$ (cm^{-1})	$\bar{\nu}$ (cm^{-1})	$\Delta\bar{\nu}$ (cm^{-1}	*Rel intensity*
1875.2	0.35		53,328			
1864.7		560		53,628		0.52
1855.7	0.88		53,888		543	
1846.0		543		54,171		1.2
1837.2	2.0		54,431		548	
1827.5		551		54,719		3.2
1818.8	4.5		54,982		539	
1809.7		542		55,258		5.1
1801.0	8.1		55,524		522	
1792.8		538		55,780		10.2
1783.7	15.8		56,062		532	
1775.8		529		56,312		17.0
1767.1	27.6		56,591		519	
1759.6		515		56,831		27.3
1751.1	42.6		57,106		507	
1744.0		508		57,338		40.4
1735.7	60.0		57,614		499	
1729.0		502		57,837		57.8
1720.7	72.7		58,116		501	
1714.1		493		58,338		72.5
1706.2	80.4		58,609		557	
1697.9		474		58,895		78.1
1692.5	86.0		59,083		533	
1682.7		593		59,428		76.2
1675.7	97.5		59,676		473	
1669.4		474		59,901		75.9
1662.5	100		60,150		519	
1655.1		423		60,420		71.2
1650.9	86.3		60,573		444	
1643.0		503		60,864		57.4
1637.3	65.7		61,076		508	
1629.4		452		61,372		45.8
1625.3	50.9		61,528		497	
1616.3		491		61,869		30.1
1612.4	35.3		62,019			

Table XIII

Rydberg Series in OCS[a]

Series	A (cm^{-1})	δ	n	E (cm^{-1}) (*calcd*)	*Rel intensity*	E (cm^{-1}) (*exptl*)	$\Delta\bar{\nu}$ (cm^{-1})
$\pi \rightarrow ns(\sigma^+)$	88,807 (11.01 eV)	1.75	4	67,120	3.9	71,423	745
					2.5	72,168	686
					2.0	72,854	
			5	78,415	6.9	77,328	681
					3.3	78,009	675
					2.6	78,684	
			∞	88,807			

[a] For definitions of the quantities A, δ, and n, see eq 4.

The unseemly large oscillator strength results from the unusual breadth of this band. Several vibrational bands are superposed on the continuum; however, they cannot be analyzed because of their low intensity and diffuse nature. Price and Simpson[68] claim the observation of three bands in this region. We believe that these three bands are identical with the broadly spaced vibrational structure mentioned above. Breckenridge and Taube[75b] have reported four vibrational progressions of very weak bands in this region. They conclude that at least one of these progressions is due to "hot" bands and assign the transition as one to a bent upper state of OCS, namely $(^1\Delta)^1A'$ or $(^1\Sigma^-)^1A''$. We concur with the $^1\Delta \leftarrow {}^1\Sigma^+$ assignment.

There are no reports of the absorption spectrum of OCS in long-path-length cells. Such a study should reveal the forbidden $^1\Sigma^- \leftarrow {}^1\Sigma^+$ transition at longer wavelengths.

d. Rydberg Transitions

At wavelengths less than 1420 Å, there lies a complicated set of Rydbergs for which analyses[48,68,76] have been attempted. Tanaka, Jursa, and LeBlanc[49] have suggested that the bands at 1400.1 and 1293.2 Å are the beginning of the first Rydberg series. As shown in Table XIII, these bands do fit a $\pi \rightarrow ns$ Rydberg series with an ionization potential of ~11.01 eV;

however, our limited data make the assignment a tentative one. Each band is accompanied by vibrational members but it is not possible to decide, on the basis of frequency alone, whether the active vibration is ν_1 or ν_2. The other bands in this region are not identified here, although they are certainly of Rydberg type. The quantum defect, $\delta = 1.75$, indicates that the first *n*s Rydberg is composed of both the 4s atomic orbital from S and the 3s atomic orbitals from C and O. Kopp[76] has studied the spectrum of OCS in the region 1350–1420 Å under high resolution. His band head measurements and vibrational analysis indicate that the molecule is linear in the excited states in this region. Matsunaga and Watanabe[78] have listed the components of a Rydberg series which converges to the first doublet ionization potential (*i.e.*, 11.18 and 11.22 eV). This ionization potential agrees with the convergence limit of the photoionization curve.

4. Carbon Disulfide

The richly structured spectrum of CS_2, shown in Figure 12, has been a challenge to many investigators.[49,79-91] It is the most highly structured spectrum studied in this work. Several molecular transitions are apparent in the long-wavelength region, while the short-wavelength region is dominated by Rydberg structure. Some of the bands at long wavelengths have been identified previously.

a. $^1\Sigma_u^+ \leftarrow {}^1\Sigma_g^+$ Transition: 1970 Å (6.29 eV), $f = 1.1$

This transition has a half-width of $\simeq$2800 cm^{-1} and shows vibrational structure throughout its entirety; the potential well of the upper state must, obviously, have a rather deep minimum. Under low resolution, a progression of some 16 bands separated by $\sim$410 cm^{-1} is observed. These bands have been listed by Price and Simpson[89] and Ramasastry and Rao[85] and undoubtedly belong to the totally symmetric stretching frequency, $\nu_1(\sigma_g^+)$, reduced somewhat from its ground-state value of 657 cm^{-1}. From the complicated appearance of the vibrational structure, it is clear that more than one upper-state frequency is excited; however, the vibrational structuring is incompletely understood. Under higher resolution, each band of the 410-cm^{-1} progression splits into several components. Douglas and Zanon[81] have photographed some of these bands under high dispersion and have obtained a partial rotational analysis. The upper state appears to be the $^1B_2$ state of the bent molecule: S–C–S angle = 153° and C–S distance = 1.66 Å. This $^1B_2$ state correlates with the $^1\Sigma_u^+$ state of the linear molecule.

b. $^1\Delta_u \leftarrow {}^1\Sigma_g^+$ Transition: 3185 Å (3.89 eV), $f = 2.7 \times 10^{-4}$

The longer wavelength absorption bands of CS_2 can be separated into two systems: one extending from 3900 to 3300 Å; the other from 3300 to 2900 Å. The stronger bands lying in the region 3300–2900 Å have been studied by Liebermann[86] and Ramasastry and Rao.[85] These bands are very complex and not well understood. It appears[86] that the molecule is bent in the excited state; indeed, some of the bands at the long-wavelength end of the region have been ascribed[85] to a $^1A_2$ state. The low intensity of the transition, ϵ_{max} 35, indicates that it is forbidden. The complexity of the vibrational structure probably arises from the splitting of the $^1\Delta_u$ state into the bent $^1A_2$ and $^1B_2$ components.

c. $^1\Sigma_u^- \leftarrow {}^1\Sigma_g^+$ Transition: 3552 Å (3.49 eV), $f \sim 8 \times 10^{-5}$

The bands in the region 3900–3300 Å have been analyzed by several investigators[80,82,83,86,87] and shown to be very complex. Their low intensity indicates forbiddenness. The well-resolved bands at long wavelengths exhibit pronounced magnetic rotation[87] and Zeeman[83] effects, indicative of spin-triplet nature. High-resolution studies of these magnetic effects by Douglas and Milton[80] have shown that these are triplet parallel bands which belong to the B_2 component of a $^3A_2$ state. These bands merge into parallel bands that do not show a Zeeman effect. The high-resolution rotational analysis of Kleman[82] on these latter bands indicates a singlet excited state in which the molecule is bent. Obviously, there is at least one singlet and one triplet state in this region.

The $^1\Sigma_u^-(^1A_2)$ state is the most likely singlet-state candidate for this region. If it is responsible for the nonmagnetic bands in the 3900–3300-Å region, it must obtain intensity in the bent molecule by means of a magnetic dipole mechanism—if one is to account for parallel bands. The splitting between the $^1\Sigma_u^-$ and $^3\Sigma_u^-$ states is expected to be negligible.[25] Thus, the bands that exhibit a magnetic effect could belong to the $^3\Sigma_u^-(^3A_2)$ state. The $^3\Delta_u(^3B_2$ and $^3A_2)$ state is also expected to be near the $^3\Sigma_u^-$ and could also account for some of the bands. The similar intensities of the singlet and triplet bands can be interpreted by assuming that the singlet bands are allowed by a magnetic dipole mechanism. The mixing of the vibrational bands of these transitions undoubtedly contributes to part of the difficulties experienced in analysis.

d. $^1\Pi_g \leftarrow {}^1\Sigma_g^+$ Transition: 1720 Å (7.20 eV), $f = 2.9 \times 10^{-2}$

This transition consists of seven distinct vibrational bands, the frequencies of which are shown in Table XIV. The bands become more complex toward shorter wavelengths. The band at 1770.2 Å is very sharp, while the one at 1747.2 Å shows two heads. The bands at higher frequencies show more heads and become increasingly broader. These bands have been reported by Price and Simpson[89] and assigned as a single progression in the antisymmetric stretching frequency, $\nu_3(\sigma_u^+)$. This assignment is questionable because of the irregularities in the intervals and because the ν_3 mode would have to reduce to $\sim$800 cm^{-1} from a ground-state value of 1523 cm^{-1}, a reduction of $\sim$46%. Such a large decrease in frequency seems unlikely.

The structure seems best interpreted as follows. It is assumed that the intervals consist of two quanta of the bending

(79) G. R. Cook and M. Ogawa, *J. Chem. Phys.*, **51**, 2419 (1969).
(80) A. E. Douglas and E. R. V. Milton, *ibid.*, **41**, 357 (1964).
(81) A. E. Douglas and I. Zanon, *ibid.*, **42**, 627 (1964).
(82) B. Kleman, *Can. J. Phys.*, **41**, 2034 (1963).
(83) A. E. Douglas, *ibid.*, **36**, 147 (1958).
(84) J. H. Callomon, *Proc. Roy. Soc., Ser. A*, **244**, 220 (1958).
(85) C. Ramasastry and K. R. Rao, *Proc. Nat. Inst. Sci. India, Part A*, **18**, 621 (1952); *Indian J. Phys.*, **21**, 313 (1947).
(86) L. N. Liebermann, *Phys. Rev.*, **60**, 496 (1941).
(87) P. Kusch and F. W. Loomis, *ibid.*, **55**, 850 (1939).
(88) E. Hauptman, *Acta Phys., Pol.*, **7**, 86 (1938).
(89) W. C. Price and D. M. Simpson, *Proc. Roy. Soc., Ser. A*, **165**, 272 (1938).
(90) F. A. Jenkins, *Astrophys. J.*, **70**, 191 (1929).
(91) E. D. Wilson, *ibid.*, **69**, 34 (1929).

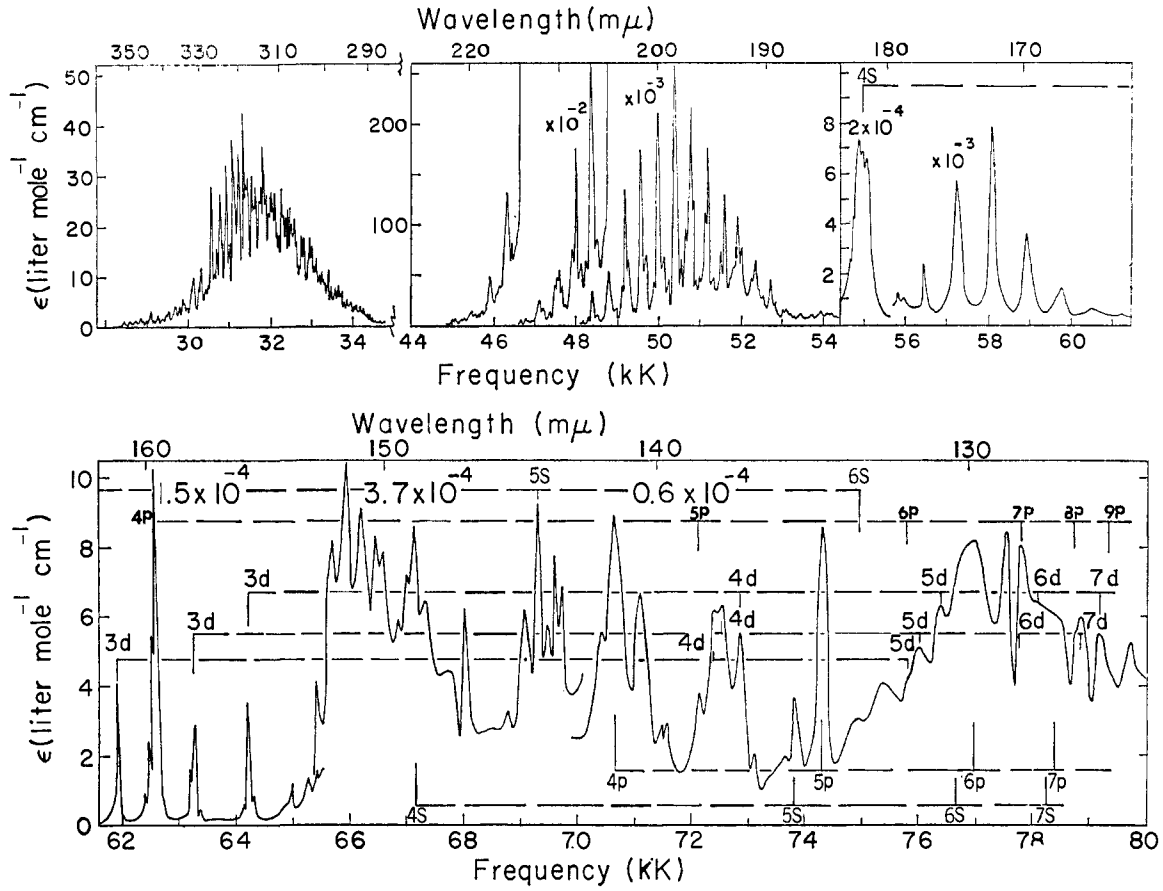

Figure 12. Absorption spectrum of carbon disulfide, CS_2.

Table XIV

Primary Vibrational Frequencies in the $^1\Pi_g \leftarrow {}^1\Sigma_g^+$ Transition of CS_2

Rel intensity	λ_{max} (Å)	$\bar{\nu}$ (cm^{-1})	$\bar{\nu} = 56{,}094 + n(397)^a$ (cm^{-1})
2.9	1770.2	56,491	56,491
5.8	1747.2	57,234	57,285
7.8	1721.2	58,099	58,079
3.7	1696.1	58,959	58,873
1.5	1673.3	59,762	59,667
0.6	1651.7	60,544	60,461
0.3	1633.9	61,203	61,255

[a] $n = 1, 3, 5, \ldots$.

Table XV

Primary Vibrational Frequencies in the $^1\Pi_u \leftarrow {}^1\Sigma_g^+$ Transition of CS_2

λ_{max} (Å)	$\bar{\nu}$ (cm^{-1})	$\Delta\bar{\nu}$ (cm^{-1})		*Rel intensity*
1539.0	64,977			0.7
1531.7	65,287	310		1.2
1527.9	65,449	162		3.7
1523.9	65,621	172	267	5.2
1521.7	65,716	95		6.4
1518.5	65,854	138	251	5.9
1515.9	65,967	113		8.2
1510.2	66,216	249		6.8
1504.7	66,458	242		6.2
1500.8	66,631	173		5.6

mode, π_u. The frequency of this mode will be essentially unchanged from its ground-state value of 397 cm^{-1}. The progression consists of only the odd members of the π_u mode since these are the only quanta allowed by selection rules. The irregularities in the frequencies result from the interaction of vibrational and electronic angular momentum. The components in each vibrational band are probably a result of Renner–Teller patterns.[30] This vibrational analysis corresponds to that of the $^1\Pi_g$ state of CO_2 and $^1\Pi$ state of OCS where long progressions in the bending frequency have been observed.

e. $^1\Pi_u \leftarrow {}^1\Sigma_g^+$ Transition: 1516 Å (8.18 eV), $f = 4.4 \times 10^{-2}$

The vibrational frequencies of this band are given in Table XV.

The complex vibrational pattern shows an apparent progression of ~250 cm^{-1}; however, the spacings are not very regular. Price and Simpson[89] were also unable to offer any explanation for this structure. At the short-wavelength edge of the transition, the progression disappears beneath a Rydberg band. The transition must arise from the excitation of an electron from one of the lower molecular orbitals, say $1\pi_u \rightarrow 2\pi_u$ or $4\sigma_g \rightarrow 2\pi_u$. The first of these excitations is parity forbidden; it produces $^{1,3}\Sigma_g^-$, $^{1,3}\Sigma_g^+$, and $^{1,3}\Delta_g$ states. The second excitation yields $^{1,3}\Pi_u$ states; the $^1\Pi_u \rightarrow {}^1\Sigma_g^+$ assignment is the most reasonable for the 1516-Å band since it is the only allowed transition feasible; however, this assignment must be considered tentative.

Table XVI

Rydberg Series in CS_2[a]

Series	*A* (cm^{-1})	δ	*n*	*Energy* (cm^{-1}, *calcd*)	*Intensity* (*f*)	*Energy* (cm^{-1}, *exptl*)	λ_{max} (Å)
$\pi \rightarrow n$s	81,400	1.97	4	54,771	6.0×10^{-2}	54,963	1819.4
(σ_g^+)	(10.09 eV)		5	69,447	9.9×10^{-3}	69,401	1440.9
			6	74,643	Weak	74,845	1336.1
			∞	81,400			
	81,560	1.23	4	67,258	1.1×10^{-2}	67,249	1487.0
	(10.11 eV)		5	73,839		73,937	1352.5
			6	76,737		76,693	1303.9
			7	78,264		78,279	1277.5
			∞	81,560			
$\pi \rightarrow n$p	81,440	1.56	4	63,008	3.6×10^{-2}	62,676	1595.5
(σ_u^+, π_u)	(10.10 eV)		5	72,167		72,239	1384.3
			6	75,873		75,763	1319.9
			7	77,732		~77,750	~1286
			8	78,794		78,796	1269.1
			9	79,458		79,441	1258.8
			∞	81,440			
	81,320	1.03	4	68,879	0.18	70,806	1412.3
	(10.08 eV)		5	74,357	0.10	74,394	1344.2
			6	76,877		76,894	1300.5
			7	78,241		~78,249	~1278
			∞	81,320			
$\pi \rightarrow n$d	81,735	0.46	3	64,726	9.2×10^{-3}	64,358	1553.8
(σ_g^+, π_g, δ)	(10.13 eV)		4	72,978		72,966	1370.5
			5	76,411		76,402	1308.9
			6	78,160		78,150	1279.6
			7	79,169		79,173	1263.1
			∞	81,735			
$\pi \rightarrow n$d	81,299	0.44	3	64,554	1.1×10^{-2}	63,359	1578.3
(σ_g^+, π_g, δ_g)	(10.08 eV)		4	72,640		72,558	1378.2
			5	76,022		75,962	1316.2
			6	77,749		77,688	1287.2
			7	78,749		78,691	1270.8
			∞	81,299			
	81,270	0.47	3	64,126	7.6×10^{-3}	62,031	1612.1
	(10.08 eV)		4	72,463		72,490	1379.5
			5	75,922		75,884	1317.8
			∞	81,270			

[a] For definitions of the quantities *A*, δ, and *n*, see eq 4.

f. Rydberg Transitions

Seven Rydberg series have been observed; they consist of two $\pi \rightarrow n$s, two $\pi \rightarrow n$p, and three $\pi \rightarrow n$d series. The analyses of these bands are given in Table XVI.

The first *n*s series exhibits a large quantum defect, $\delta = 1.97$, indicating that the first member of this series (at 1819 Å) is predominantly of sulfur 4s character. The first band of this series is weak but very wide, in agreement with the forbidden nature of the $\pi \rightarrow n$s series. It is obviously composed of several components and would constitute a very interesting high-resolution study. The second *n*s series exhibits a smaller quantum defect, $\delta = 1.23$, indicating that it has considerable 3s character from the carbon. The two series converge to 10.09 and 10.11 eV, respectively.

Both *n*p series are allowed; hence, the first members of both series are very strong and sharp. The Rydberg at 1595.5 Å is the beginning of the first series. This band is very intense, ϵ_{max} 68,000, and so sharp (half-height band width ~60 cm^{-1}) as to be almost atomic. The several heads observed on this band are probably due to wide rotational spacings attributable to the low moment of inertia of a slightly bent molecule. From the size of the quantum defect, $\delta = 1.56$, we conclude that the first member of the series is composed almost entirely of 4p character from the sulfur atoms. The first member of the second series is also very sharp and intense (ϵ_{max} 148,000). The quantum defect, $\delta \simeq 1.03$, indicates that the first member is a mixture of 4p and 3p AO's from sulfur and carbon, respectively. The two series converge to 10.10 and 10.08 eV, respectively.

The three *n*d series are also listed in Table XVI. The first two series listed, starting from the second member of each, were previously reported by Price and Simpson[89] and Tanaka, Jursa, and LeBlanc[49] who did not attempt to label the series. The agreement of our measurements with those of Price–Simpson and Tanaka–Jursa–LeBlanc is very good. In addition, we have assigned the first members of these two series and locate a third series; the first members of the series consists of the three weak bands found in the vicinity of the 1595.5-Å band. Price and Simpson[89] have assigned these as vibrational excitations associated with the 1595.5-Å band. In particular, the 1612-Å band was thought to be a hot band in the ν_1(657 cm^{-1}) ground-state frequency; the 1578.3-Å band was thought to be a vibrational band corresponding to the ν_1 mode in the excited state;

and the 1553.8-Å band was thought to be a vibrational band corresponding to the ν_3 mode in the excited state. We disagree with these assignments for the following reasons.

(i) The band at 1612.1 Å is too intense to be a hot band arising from a level some 657 cm^{-1} above the ground state.

(ii) The assignment of the 1553.8-Å band violates selection rules.

(iii) Our measurements indicate that the differences between the 1595.5- and 1578.3-Å bands and the 1595.5- and 1553.8-Å bands are 683 and 1682 cm^{-1}, respectively. If these are assigned as the ν_1 and ν_3 frequencies of the excited state, they would represent increases from the ground-state values of 657 and 1523 cm^{-1}. Such an increase in both frequencies is highly unlikely. We feel that these three bands are more properly assigned as the beginnings of the $\pi \rightarrow n$d Rydberg series. The bands are weak, in accordance with the forbiddenness of the $\pi \rightarrow n$d series. The size of the quantum defects indicates that the first members of these series are largely composed of sulfur 3d orbitals. The series converge to 10.13, 10.08, and 10.08 eV.

A strong sharp band is observed at 1403.6 Å. This band is evidently the beginning of a new Rydberg series; however, additional members were not found.

5. *Allene*

The absorption spectrum of allene, H_2CCCH_2, has been studied by Sutcliffe and Walsh.[92] The spectrum, shown in Figure 13, consists of a continuous absorption between 2500 and 1930 Å, a weak structured transition at 1850 Å, an intense structured band at 1715 Å, and considerable Rydberg structure at shorter wavelengths.

a. $^1B_2(^1\Sigma_u^+) \leftarrow {}^1A_1(^1\Sigma_g^+)$ Transition: 1715 Å (7.23 eV), $f = 0.34$

The vibrational structure of this transition is shown in Table XVII. It consists of a number of very weak and diffuse bands of

Table XVII

Primary Vibrational Frequencies in the $^1B_2(^1\Sigma_u^+) \leftarrow {}^1A_1(^1\Sigma_g^+)$ Transition of Allene

Rel intensity	λ_{max} (Å)	$\bar{\nu}$ (cm^{-1})	$\Delta\bar{\nu}$ (cm^{-1})	
1.9	1780.9	56,149		815
3.7	1755.5	59,964	339	
5.5	1745.1	57,303		8.13
8.2	1730.8	57,777	298	
8.5	1721.9	58,075	234	798
7.4	1715.0	58,309		
8.6	1707.2	58,575	287	
6.9	1698.9	58,862	257	
6.7	1691.5	59,119		769
7.3	1685.1	59,344		756
6.8	1663.9	60,100		721
5.4	1644.2	60,821		600
4.2	1628.1	61,421		510
3.0	1614.7	61,931		

which precise measurement is almost impossible. The progression of some eight bands exhibits an initial frequency difference of 815 cm^{-1} which diminishes rapidly because of anharmonicity. Six other frequency intervals ranging from 339 to 257 cm^{-1} were also observed. The main progression, initiating in a $\Delta\bar{\nu}$ of 815 cm^{-1}, is assigned as the totally symmetrical a_1 (C=C=C stretching) vibration reduced from its ground-state value of 1071 cm^{-1}. This represents a decrease of ~20%, in agreement with proportionate reductions for the same type of transition in ethylene (1623 to ~1370 cm^{-1}; 15.6%) and in ketene (1120 to ~860 cm^{-1}; 23.2%). The lower frequency vibrations probably represent the nontotally symmetrical (C=C=C bending) vibration which is 353 cm^{-1} in the ground state.

Part of the complexity of these bands arises from a Rydberg transition and its associated vibrational structure which, as discussed below, is overlapped by this transition. Sutcliffe and Walsh[92] assigned this whole band system as the $n = 3$ member of a Rydberg series. We evidently disagree with this assignment.

b. $^1E(^1\Pi_g) \leftarrow {}^1A_1(^1\Sigma_g^+)$ Transition: 1850 Å (6.70 eV), $f = 3.0 \times 10^{-2}$

This band is weak presumably because of its analog relation to the forbidden $^1\Pi_g \leftarrow {}^1\Sigma_g^+$ transition of the $D_{\infty h}$ molecules. Six well-defined vibrational bands are classified in Table XVIII;

Table XVIII

Vibrational Frequencies in the $^1E(^1\Pi_g) \leftarrow {}^1A_1(^1\Sigma_g^+)$ Transition of Allene

Rel intensity	λ_{max} (Å)	$\bar{\nu}$ (cm^{-1})	$\Delta\bar{\nu}$ (cm^{-1})
1.9	1914.1	52,244	
4.0	1890.8	52,888	644
7.4	1870.2	53,470	582
10	1849.9	54,057	587
9.6	1831.3	54,606	549
8.7	1813.0	55,157	551

these bands exhibit an initial spacing of 644 cm^{-1} and are anharmonic toward higher frequencies. At shorter wavelengths the transition submerges below the stronger $^1B_2 \leftarrow {}^1A_1$ absorption. The 644-cm^{-1} vibration does not correspond to any of the totally symmetric modes since such would require an abnormally large decrease of the ground-state frequencies in the ^1E state. It is most likely that the active vibration represents a b_1 mode (CH_2 twisting) or an e mode (C=C=C bending) which occur at 820 and 838 cm^{-1}, respectively, in the ground state. Although these modes are antisymmetric, all possible products such as $nb_1 \times E$ and $ne \times E$, where $n = 1, 2, 3, \ldots$, contain allowed components. Thus, if the active vibration is b_1 type, the upper state is probably planar; if it is e type, the upper state probably contains a bent C–C–C grouping. Investigation of the spectrum of C_3D_4 should provide definite resolution of our quandary.

c. Long-Wavelength Transitions

Continuous absorption begins at ~2600 Å and extends to ~1930 Å. At least one electronic transition, and possibly more, is involved in this continuum. Of the four states, $^1B_2$, $^1A_1$, $^1A_2$, and $^1B_1$ which arise from the 2e → 3e MO excitation

(92) L. H. Sutcliffe and A. D. Walsh, *J. Chem. Soc.*, 899 (1952).

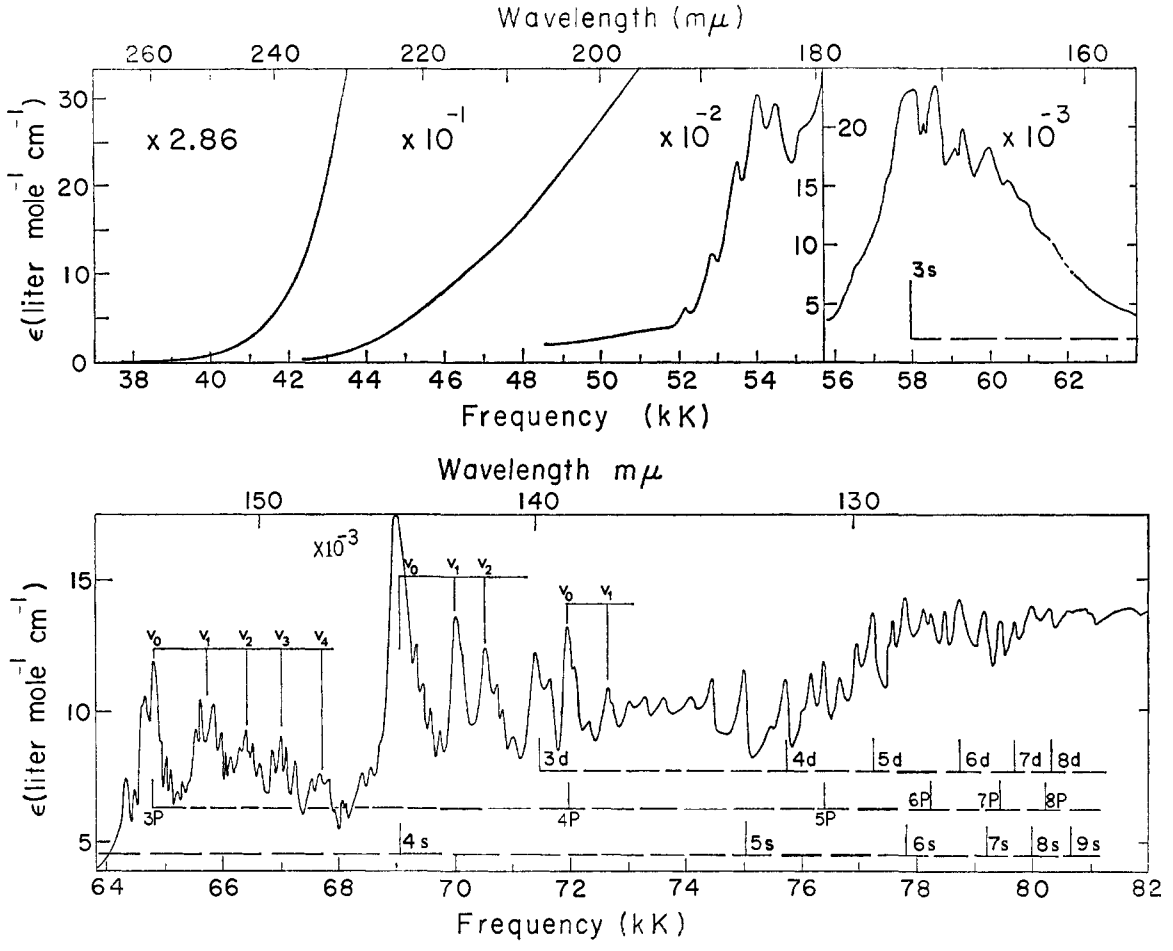

Figure 13. Absorption spectrum of allene, H_2CCCH_2.

in allene, only the $^1B_2$ state has been assigned by us so far. There is a small inflection at ~2150 Å (5.76 eV) with $\epsilon \approx 100$ which we designate as the forbidden $^1A_1(^1\Delta_u) \leftarrow {}^1A_1(^1\Sigma_g^+)$ transition. The forbidden $^1A_2(^1\Delta_u) \leftarrow {}^1A_1(^1\Sigma_g^+)$ transition may account for the weak absorption in the region 2600–2250 Å.

d. Rydberg Transitions

A large number of Rydberg bands exists at wavelengths shorter than 1600 Å. Sutcliffe and Walsh[92] have arranged these bands into nine Rydberg series consisting of three $\pi \rightarrow n$s series, four $\pi \rightarrow n$p series, and two $\pi \rightarrow n$d series. As pointed out by Herzberg,[30] some of these series are fragmentary and probably represent vibrational members of the main Rydberg bands. The Rydberg states expected are $E(\pi \rightarrow n$s), B_2 and $E(\pi \rightarrow n$p), and B_2 and $E(\pi \rightarrow n$d). Several other states are expected from the np and nd series; however, they are all forbidden. Our analysis of the Rydberg series is shown in Table XIX.

The agreement of our series with those of Sutcliffe and Walsh[92] for the np and nd series is excellent. We have extended their assigned series to one more member at short wavelengths and have assigned vibrational bands associated with the $n = 4$ member of the ns series and the $n = 3$ member of the np series. These associated vibrations are very anharmonic and probably represent the totally symmetrical stretching vibration which appears at 1071 cm^{-1} in the ground state. Each vibrational band, including the main Rydberg, is composed of several components which represents either a very low-frequency vibration or large rotational spacings. In view of the observation of similar low-frequency vibrations in the spectrum of ethylene,[92] the former explanation seems the better of the two. Vibrations associated with the $n = 3$ member of the ns series cannot be followed because of the overlap of this Rydberg with the $^1B_2$ state. However, it is presumably this Rydberg and its associated vibrations which make the region of the $^1B_2 \leftarrow {}^1A_1$ transition (1800–1600 Å) difficult to analyze. A weak band is observed 338 cm^{-1} to the red of the $n = 3$ member of the np series. This probably represents a hot band arising from one of the ground-state vibrations. It is difficult to assign this hot band with confidence; we surmise that it arises from the e (C=C=C bending) vibration which has a frequency of 353 cm^{-1} in the ground state. Both the ns and np series converge to 10.19 eV.

The $\pi \rightarrow n$d series has not been mapped by Sutcliffe and Walsh.[92] It has a very small quantum defect, $\delta = 0.01$, and converges to an ionization potential of 10.18 eV.

6. Ketene

The absorption spectrum of ketene, H_2CCO, between 3800 and 1940 Å is shown in Figure 14. The absorption spectrum below 1900 Å is presented by Price, Teegan, and Walsh.[93] Although

(93) W. C. Price, J. P. Teegan, and A. D. Walsh, *J. Chem. Soc.*, 920 (1951).

Table XIX

Rydberg Series of Allene[a]

Series	A (cm^{-1})	δ	n	E (cm^{-1}) Calcd	E (cm^{-1}) Exptl	ΔE (cm^{-1})	λ_{max} (Å)
$\pi \rightarrow n$s	82,210	1.06	3	53,053	57,803		1730.0
(a_1)	(10.19 eV)		4	69,514	69,150		1446.1
					70,092	942	1426.7
					70,671	579	1415.0
			5	75,141	75,136		1330.9
			6	77,713	77,709		1286.9
			7	79,100	79,114		1264.0
			8	79,932	79,901		1251.5
			9	80,469	80,580		1241.0
			∞	82,210			
					64,349		1554.0
$\pi \rightarrow n$p	82,190	0.70	3	61,446	64,687	338	1545.9
(b_2,e)	(10.19 eV)				65,733	1046	1521.3
					66,494	761	1503.9
					67,078	582	1490.8
					67,609	531	1479.1
			4	72,113	71,902		1390.8
					72,753	851	1374.5
			5	76,225	76,199		1312.4
			6	78,283	78,201		1278.8
			7	79,425	79,429		1259.0
			8	80,131	80,162		1247.5
			∞	82,190			
$\pi \rightarrow n$d	82,100	0.01	3	69,825	71,350		1401.5
(b_2,e)	(10.18 eV)		4	75,207	75,557		1323.5
			5	77,693	77,220		1295.0
			6	79,041	78,750		1269.8
			7	79,854	79,713		1254.5
			8	80,381	80,302		1245.3
			∞	82,100			

[a] For definition of the quantities A, δ, and n, see eq 4.

the spectrum has been investigated previously,[94-97] the state identifications remain fragmentary. We do not present our spectrum below 1940 Å because of the rapid photochemical decomposition, which we observe, into ethylene and carbon monoxide.[97] The spectrum consists of very weak diffuse bands between 4735 and 3700 Å,[94] another system of diffuse bands between 3706 and 2601 Å, a stronger transition between 2150 and 1950 Å consisting of four distinct bands, and strong and weak continua at 1700[93] and ~1550 Å,[93] respectively, upon both of which are superimposed many intense discrete Rydberg bands.

a. Long-Wavelength Transitions: 4735–3700 Å

Dixon and Kirby[94] have studied the long-wavelength absorption of ketene using path lengths up to 24 m atm. They observed an electronic transition between 4735 and 3700 Å with λ_{max} near 3700 Å (3.35 eV) which consists of prominent diffuse bands with a mean spacing of 475 cm^{-1}. These intervals have been assigned to the skeletal bending vibrations which are 588 and 529 cm^{-1} in the ground state. The long progressions in the bending modes indicate that this state is strongly bent. Dixon and Kirby have assigned this transition as $^3A_2 \leftarrow {}^1A_1$. We agree with this assignment but would like to add that the $^3B_2(^3\Sigma_u^+)$ state is also expected in this same energy range. Therefore, we assign the absorption between 4635 and 3700 Å to two transitions: $^3B_2(^3\Sigma_u^+) \leftarrow {}^1A_1(^1\Sigma_g^+)$ and $^3A_2(^3\Sigma_u^-) \leftarrow {}^1A_1(^1\Sigma_g^+)$.

b. $^1A_2(^1\Sigma_u^-) \leftarrow {}^1A_1(^1\Sigma_g^+)$ Transition: 3226 Å (3.84 eV), $f = 2.3 \times 10^{-4}$

This band consists of a number of diffuse peaks which are pressure dependent.[94,97] Dixon and Kirby have assigned this band as the $^1A_2 \leftarrow {}^1A_1$ transition and the vibrational spacings of ~365 cm^{-1} as a progression in the bending mode. The transition corresponds to the forbidden $n \rightarrow \pi^*$ transition of aldehydes and ketones which is usually found between 3400 and 2500 Å. The red-shift in ketene occurs because of the conjugation between the "nonbonding" electrons on the oxygen and the in-plane π orbital of the central carbon atom (see Figure 4).

c. $^1B_2(^1\Delta_u) \leftarrow {}^1A_1(^1\Sigma_g^+)$ Transition: 2130 Å (5.82 eV), $f = 9.9 \times 10^{-3}$

This transition is weak because it related to the forbidden $^1\Delta_u \leftarrow {}^1\Sigma_g^+$ transition. The four vibrational bands observed, with an average spacing of 1040 cm^{-1}, are shown in Table XX. The intensity distribution indicates that the transition has an

(94) R. N. Dixon and G. H. Kirby, *Trans. Faraday Soc.*, 62, 1406 (1966).
(95) K. Knox, R. G. Norrish, and G. Porter, *J. Chem. Soc.*, 1477 (1952).
(96) G. C. Lardy, *J. Chim. Phys.*, 21, 353 (1924).
(97) R. G. W. Norrish, H. G. Crone, and O. Saltmarsh, *J. Chem. Soc.*, 1533 (1933).

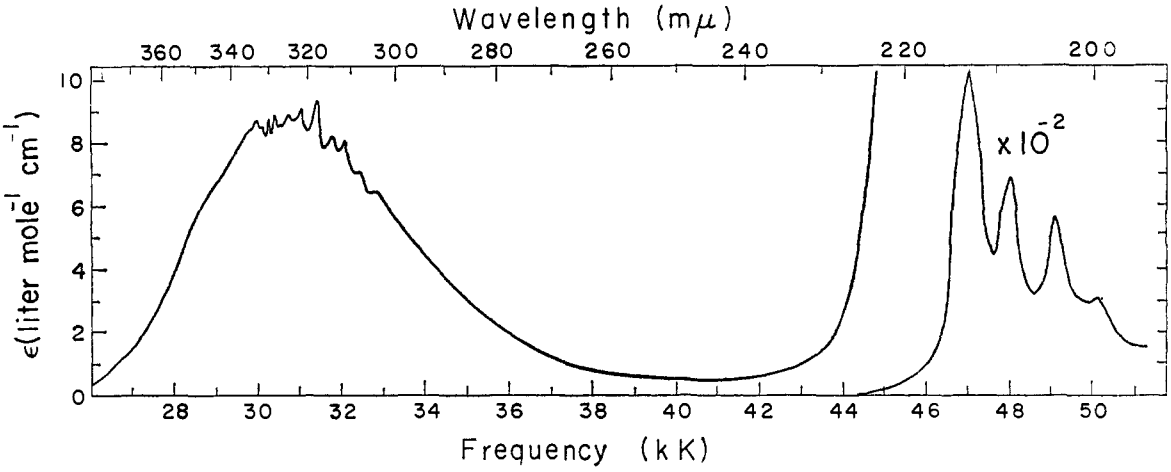

Figure 14. Absorption spectrum of ketene, H_2CCO.

Table XX

Vibrational Frequencies in the $^1B_2(^1\Delta_u) \leftarrow {}^1A_1(^1\Sigma_g^+)$ Transition of Ketene

Rel intensity	λ_{max} (Å)	$\bar{\nu}$ (cm^{-1})	$\Delta\bar{\nu}$ (cm^{-1})
7.7	2132.4	46,896	
4.5	2085.9	47,942	1046
3.8	2039.8	48,972	1030
2.5	1999.3	50,017	1045

allowed origin at 46,896 cm^{-1} and that the geometry of the excited state is similar to that of the ground state. This vibrational structure corresponds to the ~1200-cm^{-1} progression in the 1960–1850-Å region of acetone, where there is evidence[93] that it represents the totally symmetrical hydrogen-bending frequency of the CH_3 group reduced from its ground-state value of 1357 cm^{-1}. Thus, the 1040-cm^{-1} progression of ketene probably represents the symmetrical CH deformation frequency which is 1386 cm^{-1} in the ground state. If one considers the MO's involved in this transition $4b_2 \rightarrow 6a_1$ (both MO's are in the plane of the hydrogens and possess some electron density on them), it is evident that the most likely active vibration is the CH deformation mode.

d. Short-Wavelength Transitions: λ <1900 Å

A good description of the spectrum below 1900 Å has been given by Price, Teegan, and Walsh.[93] For this reason, our discussion will be brief. A strong continuum, ϵ_{max} ~10,000, appears with maximum at ~1700 Å (7.29 eV). The high intensity of this absorption band indicates that it is strongly allowed; it is, therefore, assigned as the $^1B_2(^1\Sigma_u^+) \leftarrow {}^1A_1(^1\Sigma_g^+)$ transition. A weaker continuum, ϵ_{max} ~4000 with λ_{max} ~1550 Å (8.00 eV), is assigned as the allowed $^1B_2(^1\Pi_g) \leftarrow {}^1A_1(^1\Sigma_g^+)$ transition. This transition is weaker than the former because it is derived from the forbidden $^1\Pi_g \leftarrow {}^1\Sigma_g^+$ transition. Both of these continua are overlapped by numerous intense discrete Rydberg bands. The first Rydbergs begin at ~1829 Å. This region of the spectrum is very similar to that of ethylene which has a continuous absorption with maximum at 1630 Å and first strong Rydberg at ~1745 Å. The ketene spectrum is red-shifted from ethylene by ~2600 cm^{-1} because of the conjugation and delocalization of electrons from three $p\pi$ atomic orbitals rather than two. Price, Teegan, and Walsh[93] have listed a $\pi \rightarrow ns$ Rydberg series, including vibrational members associated with the main bands, which converges to an ionization potential of 9.60 eV. The quantum defect of this series is 1.07.

7. *Cyanamide and Dimethyl Cyanamide*

a. Cyanamide

In spite of the low molecular weight, cyanamide (H_2NCN) exists as a solid at room temperature; the melting point is 46–47°. The vapor pressure is surprisingly low (reported as 3.0 mm[43] at 110°) and is indicative of strong intermolecular hydrogen bonding. The question of whether the molecule exists in the amide form (H_2NCN) or the carbodiimide form (HNCNH) has been the subject of several investigations; recent work[43] has shown that the molecule exists almost entirely in the amide form.

The only reported ultraviolet absorption spectrum of cyanamide vapor is by Imanishi and Tachi[98] who employed temperatures ranging from ambient to ~100° in order to obtain sufficient vapor densities. Their spectrum was analyzed in terms of the presence of ~100% of the imide form. Using an absorbing path length of 10 cm and temperatures ranging from 60 to 110°, we were able to record the exact spectrum presented by Imanishi and Tachi, only to discover afterwards that the spectrum is that of NH_3 gas. Thus, the published spectrum[98] of cyanamide vapor is simply the 2168–1700-Å absorption band of ammonia gas.[30] The ammonia is formed from the photochemical and/or thermal decomposition of cyanamide and most likely follows a reaction such as

$$2H_2NCH \longrightarrow NH_3 + N{\equiv}C{-}\underset{\displaystyle H}{\underset{|}{N}}{-}C{\equiv}N \qquad (7)$$

The second product is unstable and polymerizes rapidly to form a white deposit on the cell windows. Thus, no true spectra of cyanamide vapor are available.

(98) S. Imanishi and T. Tachi, *J. Chem. Soc. Jap., Ind. Chem. Sect.*, 63, 492 (1942).

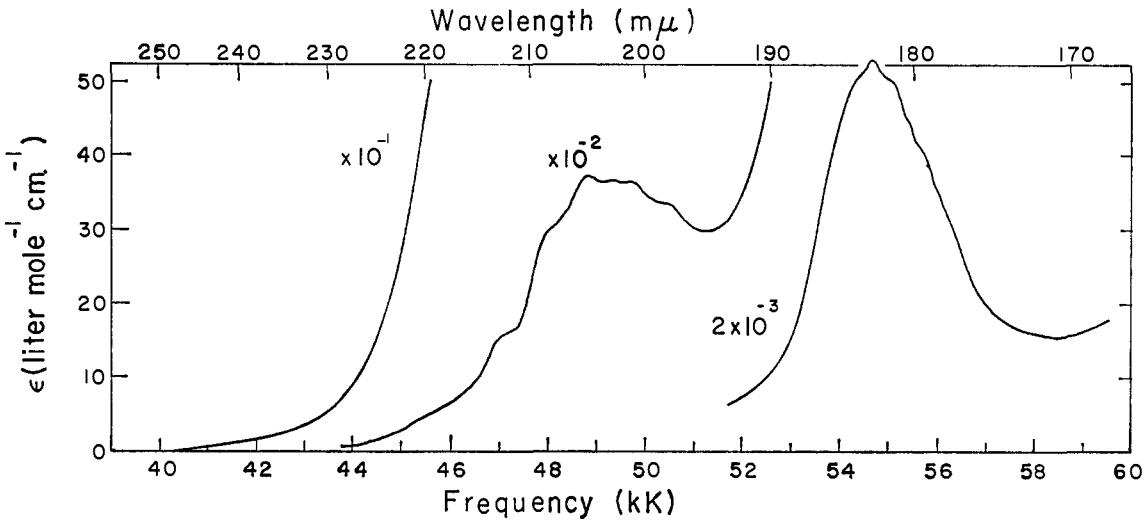

Figure 15. Absorption spectrum of dimethyl cyanamide, $(CH_3)_2NCN$.

b. Dimethyl Cyanamide

$(CH_3)_2NCN$ is a liquid at room temperature; however, no ultraviolet spectra of the vapor have been reported. The absorption spectrum between 2500 and 1700 Å is shown in Figure 15. We observe a continuous absorption at λ <1700 Å with no obvious maxima. It is probable that excitation in either one or both of the bands observed in the near-ultraviolet region leads to direct dissociation.

The strong band with λ_{max} 1830 Å (6.78 eV) and $f = 0.32$ is assigned as the allowed $^1B_2(^1\Sigma_u^+) \leftarrow {}^1A_1(^1\Sigma_g^+)$ transition. Vibrational bands were observed near the maximum and on the short-wavelength side of this absorption; however, they are too weak and diffuse for proper characterization.

The weaker absorption band with λ_{max} 2047 Å (6.05 eV) and $f = 5.8 \times 10^{-2}$ is assigned as the allowed $^1B_2(^1\Delta_u) \leftarrow {}^1A_1(^1\Sigma_g^+)$ transition. It is weak because of the forbidden nature of the parent transition. This transition exhibits diffuse vibrational structure (see Table XXI) which initiates in a quantum of

Table XXI

Primary Vibrational Frequencies in the $^1B_2(^1\Delta_u) \leftarrow {}^1A_1(^1\Sigma_g^+)$ Transition of Dimethyl Cyanamide Vapor

Rel intensity	λ_{max} (Å)	$\bar{\nu}$ (cm^{-1})	$\Delta\bar{\nu}$ (cm^{-1})
0.7	2264.9	44,152	
			1594
1.2	2186.0	45,746	
			1348
3.3	2123.4	47,094	
			983
6.0	2080.0	48,077	
			782
7.5	2046.7	48,859	
			744
7.3	2016.0	49,603	
			732
7.1	1986.7	50,335	
			615
6.8	1962.7	50,950	

~1491 cm^{-1} and which exhibits considerable anharmonicity. This frequency probably corresponds to the totally symmetric a_1 (CH_3 deformation) mode which is 1465 cm^{-1} in the ground state.[99]

A very weak absorption band was observed at 2700 Å (4.59 eV) with ϵ_{max} ~6. This band has the contour and appearance of the forbidden $^1A_1(^1\Sigma_u^-) \leftarrow {}^1A_1(^1\Sigma_g^+)$ transition and is assigned as such.

The $^1B_2(^1\Pi_g) \leftarrow {}^1A_1(^1\Sigma_g^+)$ transition has not been observed in this spectrum. It is reasonable to assume that it lies in the dissociative continuum above 6.78 eV.

8. *Cyanogen Halides*

The absorption spectra of the cyanogen halides were reported by some earlier workers;[100-103] more recently, King and Richardson[104] have examined the spectra under high resolution down to 1250 Å. The spectra of the three cyanogen halides NCCl, NCBr, and NCI are very similar except for large shifts to longer wavelengths in the order I > Br > Cl. The spectra consist of two weak unstructured absorption bands of more or less equal intensities in the long-wavelength region, two intense discretely structured absorption bands at shorter wavelengths, and several Rydberg transitions which appear at still shorter wavelengths. King and Richardson[104] have discussed these spectra in considerable detail. We would like to present an alternate interpretation of some of the observed bands.

a. $^1\Sigma^- \leftarrow {}^1\Sigma^+$ Transition

The longest wavelength absorptions of NCI, NCBr, and NCCl occur with λ_{max} at 2300, 1990, and 1775 Å and oscillator strengths of 4.8×10^{-3}, 2.5×10^{-3}, and 4.8×10^{-3}, respectively. These bands appear as low-intensity continua with no apparent vibrational structure. This transition, the so-called A-system, is assigned by King and Richardson[104] to the $2\pi \rightarrow 5\sigma$ MO excitation which produces a $^1\Pi$ excited state. We disagree with this assignment for the following reasons.

(i) Even though this transition is forbidden in the $D_{\infty h}$ point group, it is allowed in $C_{\infty v}$. In molecules such as cy-

(99) F. B. Brown and W. H. Fletcher, *Spectrochim. Acta*, **19**, 915 (1962).

(100) W. C. Price and A. D. Walsh, *Trans. Faraday Soc.*, **41**, 381 (1945).
(101) D. E. Gillam, *ibid.*, **29**, 1132 (1933).
(102) R. M. Bager and S.-C. Woo, *J. Amer. Chem. Soc.*, **53**, 2572 (1931).
(103) R. B. Mooney and H. G. Reid, *Nature*, **128**, 271 (1931); *Proc. Roy. Soc. Edinburgh*, **52**, 152 (1931).
(104) G. W. King and A. M. Richardson, *J. Mol. Spectrosc.*, **21**, 339, 353 (1961).

anogen halides which are very asymmetrical, the $^1\Pi$ state should have a considerably higher intensity than is observed.

(ii) The 5σ MO lies several electron volts above the 3π MO's. For this reason, the $2\pi \rightarrow 3\pi$ MO excitation should lie at much lower energies than the $2\pi \rightarrow 5\sigma$ MO excitation.

We believe that this transition should be assigned, instead, as a forbidden $^1\Sigma^- \leftarrow {}^1\Sigma^+$ transition of $2\pi \rightarrow 3\pi$ MO excitation type. The $^1\Sigma^-$ state correlates with the n,π^* state of carbonyl compounds. In line with this, the absorption $^1\Sigma^- \leftarrow {}^1\Sigma^+$ has been found to shift to higher energies upon changing the solvent from *n*-heptane to water, in agreement with the observed shifts in the $n \rightarrow \pi^*$ transitions of carbonyl-containing compounds.

b. $^1\Delta \leftarrow {}^1\Sigma^+$ Transition

The next higher energy transition is also unstructured and very weak; the maxima occur at 1890, 1800, and 1700 Å in NCI, NCBr, and NCCl, respectively. The oscillator strength for NCI has been reported[38] as 2.9×10^{-3}. The corresponding bands in NCBr and NCCl are of approximately this same intensity. King and Richardson have assigned this transition, the so-called α system, as either the $1\pi \rightarrow 5\delta$ or $2\pi \rightarrow 3\pi$ MO excitations. We disagree with the former assignment because the 1π MO is deeply buried in the filled MO levels and such an excitation would be at considerably higher energy. We are in accord with the second assignment, but, more specifically, we identify the band as the forbidden $^1\Delta \leftarrow {}^1\Sigma^+$ transition.

c. $^1\Sigma^+ \leftarrow {}^1\Sigma^+$ and $^1\Pi \leftarrow {}^1\Sigma^+$ Transitions: $10^{-2} < f < 10^{-1}$

The first strong absorptions occur in two distinct bands at shorter wavelengths. These are denoted by King and Richardson as absorptions to the B and C excited states. They have given the electronic origins for NCI, NCBr, and NCCl, respectively, as 1598, 1509, and 1364 Å (B system) and 1576, 1465, and 1343 Å (C system) with relative B/C intensities of 3:2, 2:1, and 3:4. Both of these regions show very sharp vibrational structure. King and Richardson have identified the progressions as the symmetrical ν_1 and ν_3 stretching modes of σ^+ symmetry. They have assigned the B and C transitions as $2\pi \rightarrow (n+1)s\sigma$ Rydberg-type electronic excitations in which the Rydberg orbitals are localized on the halogens. The resulting states are $^1\Pi$ and $^3\Pi$. We would like to point out the following.

(i) The Ryberg transitions are expected to be of higher energy than either the $^1\Sigma^+ \leftarrow {}^1\Sigma^+$ or the $^1\Pi \leftarrow {}^1\Sigma^+$ transitions. This has been the case for all other molecules considered here. It is highly improbable that such Rydberg transitions would be observed at lower energy than the $^1\Sigma^+ \leftarrow {}^1\Sigma^+$ and $^1\Pi \leftarrow {}^1\Sigma^+$ transitions.

(ii) If the B and C transitions are first members of a Rydberg series, other members should be found. This is the case only for NCI, in which only one possible higher member of the postulated series was found.[104]

We attribute the B and C absorption regions to the $^1\Sigma^+ \leftarrow {}^1\Sigma^+$ and $^1\Pi \rightarrow {}^1\Sigma^+$ transitions, the band of higher intensity being that to the $^1\Sigma^+$ state. It is quite probable that the Rydberg states proposed by King and Richarsdon lie also in this same region. It would not be unreasonable to assume that the transitions may overlap.

d. Rydberg Transitions

Several other transitions have been observed by King and Richardson at shorter wavelengths and assigned as Rydberg transitions. The first ionization potential of NCI, NCBr, and NCCl is reported as 10.98, 11.95, and 12.49 eV, respectively.

9. *Diazomethane*

The absorption spectrum of H_2CNN has been studied in the visible and near-ultraviolet regions[105, 106] and under high resolution in the vacuum region.[107, 108] The spectrum consists of a very weak band at ~3950 Å, a stronger continuum with a maximum at ~2175 Å, strong discrete absorption bands near 1900 Å, strong but diffuse bands near 1750 Å, and numerous Rydberg-type transitions. Rather than reproduce this spectrum, we refer the reader to the high-resolution work of Herzberg[107] and Merer.[108]

a. $^1A_2(^1\Sigma_u^-) \leftarrow {}^1A_1(^1\Sigma_g^+)$ Transition: 3950 Å (3.14 eV), $f \sim 1 \times 10^{-4}$

The longest wavelength transition is a continuum with very weak diffuse vibrational bands superimposed on it; these bands are too diffuse for analysis. The intensity of this band is approximately that expected for the $^1\Sigma_u^- \leftarrow {}^1\Sigma_g^+$ transition.

b. $^1B_g(^1\Delta_u) \leftarrow {}^1A_1(^1\Sigma_g^+)$ Transition: ~2300 Å (~5.90 eV)

A second absorption continuum lies between 2650 and 2000 Å. No vibrational structure has been observed in this region. It is tentatively assigned as the $^1\Delta_u \leftarrow {}^1\Sigma_g^+$ transition.

c. Short-Wavelength Transitions: λ <2000 Å (>6.20 eV)

The 1900-Å region consists of strong discrete transitions. The rotational analysis of Merer[108] has shown that there are three distinct transitions in this region: two Rydbergs and one molecular transition of $^1B_2 \leftarrow {}^1A_1$ species. Another intense band system occurs at 1757 Å (7.06 eV) with very diffuse structure. No assignment has been given for this band. From the energetic positions and intensities of these bands, we tentatively assign the former as the $^1B_2(^1\Pi_g) \leftarrow {}^1A_1(^1\Sigma_g^+)$ transition and the latter as the $^1B_2(^1\Sigma_u^+) \leftarrow {}^1A_1(^1\Sigma_g^+)$ transition.

d. Rydberg Transitions

Several transitions in the vacuum region have been assigned[107, 108] to Rydberg excitations. In particular, two $\pi \rightarrow np$ series and one extended and very clear $\pi \rightarrow nd$ series have been mapped. The first ionization potential is reported to be at 9.00 eV.

10. *Mercury Halides*

The absorption spectra of $HgCl_2$, $HgBr_2$, and HgI_2 vapor have

(105) R. K. Brinton and D. H. Volman, *J. Chem. Phys.*, **19**, 1394 (1951).
(106a) J. F. Ogilvie, *Photochem. Photobiol.*, **9**, 65 (1969).
(106b) F. W. Kirkbride and R. G. W. Norrish, *J. Chem. Soc.*, 119 (1933).
(107) G. Herzberg, *Proc. Roy. Soc., Ser. A*, **262**, 291 (1961).
(108) A. J. Merer, *Can. J. Phys.*, **42**, 1242 (1964).

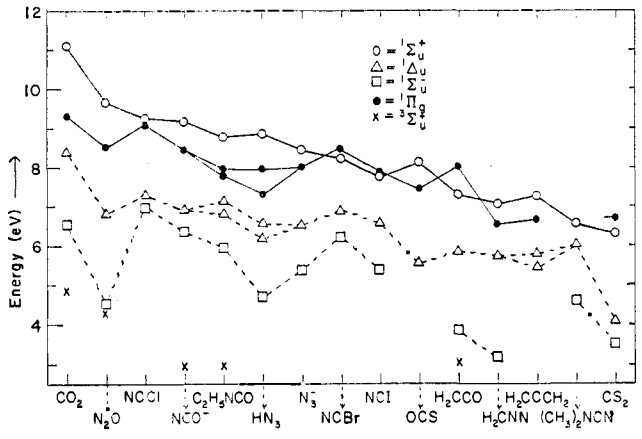

Figure 16. Correlation diagram for excited electronic states (see caption to Table XXIII).

been investigated[109-113] in the near- and vacuum ultraviolet regions; however, state identifications are lacking. We have investigated these spectra down to ~1250 Å using a 10-cm heated cell at 60° < T < 120°. The spectra of these molecules are not analogous to others discussed here. For example, in the spectrum of HgI_2 vapor between 3200 and 1250 Å there are at least ten electronic transitions. Some of these transitions appear to be from excitations localized either on the Hg or halogen atoms. These spectra will be discussed in a subsequent publication.

11. Cyanate and Isocyanate Species

The phosphorescence spectra, phosphorescence lifetimes, and absorption spectra of the cyanate salts of Na^+, K^+, Cd^{2+}, Ag^+, Hg^{2+}, and Pb^{2+} and of HCNO, CH_3NCO, CH_3CH_2NCO, and C_6H_5NCO have been measured; they are discussed in ref 5 in a manner fully compatible with the points of view adopted here.

12. Azido Species

The absorption spectra of the azide salts of Na^+, Li^+, and Ba^{2+} and of HNNN and *n*-amylazide have been measured; they are discussed in ref 6 in a manner fully compatible with the points of view adopted here.

13. Thiocyanate Species

The phosphorescence spectra, phosphorescence lifetimes, and absorption spectra of the thiocyanate salts of K^+, Ba^{2+}, Zn^{2+}, Cd^{2+}, Pb^{2+}, and Ag^{2+} and of HNCS have measured and are discussed in ref 4 in a manner fully compatible with the points of view adopted here.

IV. Discussion

The state identifications are serialized in this section, and the specific assignments made in section III are, to a large extent, vindicated. The gist of the identification procedure is contained in the correlations of Table XXII and Figure 16.

(109) S. Bell, *J. Mol. Spectrosc.*, 23, 98 (1967).
(110) S. Bell, R. D. McKenzie, and J. B. Coon, *ibid.*, 20, 217 (1966).
(111) H. Sponer and E. Teller, *Rev. Mod. Phys.*, 13, 106 (1941); *J. Chem. Phys.*, 7, 382 (1939).
(112) M. Wehrli, *Naturwiss.*, 25, 734 (1937); *Helv. Phys. Acta*, 13, 153 (1940); 11, 340 (1938).
(113) K. Wieland, *Z. Phys.*, 76, 801 (1932); 77, 157 (1932).

Table XXII is a listing of the energies, intensities, and suggested assignments of the electronic absorption bands of all the isoelectronic molecules. At the top of this table are listed the five point groups considered and the correlations of their symmetry representations in the various molecules. The molecules are listed in the left column. The symmetry representation of each state can be found by looking at the top of its respective column for the species belonging to the point group of the molecule. Since data for a large number of molecules such as this can be more easily visualized diagrammatically, some effort in this regard has been made in Figure 16. The ordering of molecules in Figure 16 follows the approximate computed barycenter of the $\pi \rightarrow \pi^*$ states. When the symmetry representations of the electronic states are correlated throughout the point groups considered, certain unique and descriptive features arise for each correlatory series. These are the properties that form the strongest basis for the assignment of electronic states given here. We will now discuss the assignments, and the validating arguments, for each species of electronic state.

A. $^1\Sigma_g^+$ STATE AND CORRELATING SPECIES

1. Geometry

The structure of the ground-state species is shown in Figure 1. Fundamental frequencies of vibration are listed in Table VIII. The longest bonds are those which involve a second-row atom and an atom from the third, fourth, or fifth rows. This is related to the fact that the AO's of the heavier atom are of high principal quantum number; as a result, they are very large and diffuse and their overlap with the AO's of second-row atoms is smaller.

2. Binding Energy

Using the total energies of the molecules obtained from the MWH calculations and the energies of the constituent atoms from Siegbahn,[114] it is possible to evaluate a qualitative order of binding energy for the ground states of these molecules. This ordering actually represents the amount of energy released when the molecule or ion is formed from the corresponding free "atoms" ("atoms," which in some cases, are positively or negatively charged). The ordering obtained is $NO_2^+ > H_2CCCH_2 > CS_2 > N_2O > HN_3 > HNCS > OCS > NCl > H_2CCO > NCBr > CO_2 > NCCl > H_2NCN > HNCO > H_2CNN > SCN^- > HNCN^- > NNN^- > NCO^- > NCN^{2-}$. This ordering indicates that the neutral molecule with the lowest binding energy should be diazomethane. In agreement with this, it is known that the C–N bond in H_2CNN is very weak and that the N–N bond has more triple-bond character[115] than the C–O bond in H_2CCO or the C–N bond in H_2NCN. Indeed, photolysis of H_2CNN yields $N_2(^1\Sigma_g^+)$ and singlet CH_2 radical. It should be noted also that CO_2 is predicted to be more unstable than either OCS or CS_2.

3. Bonding

The triatomic chain is linear in the ground states of all of these molecules. This linearity is a consequence of the steep increase in energy of the $^1\Sigma_g^+$ state (see Figures 7 and 8)

(114) K. Siegbahn, *et al.*, *Nova Acta Regiae Soc. Sci. Upsal., Ser. IV*, 20, 1 (1967).
(115) J. M. André, M. C. André, G. LeRoy, and J. Weiler, *Int. J. Quantum Chem.*, 3, 1013 (1969).

which occurs upon bending the molecule. This, in turn, is a result of a similar steep rise of the highest energy filled MO [$1\pi_g(4b_2)$ MO, see Figure 3].

The doubly degenerate sets of π MO's span the entire linear triatomic group. When an H atom is added to this linear chain, it assumes an off-axis position such that the $1s_H$ MO can bind to the former π MO component which is now situated in the newly defined plane. If two H atoms are added to the molecule, they bond to the same end of the chain but on different sides of the triatomic axis; the molecule remains planar. Thus, in a molecule such as HNCS (or H_2CCO), the mutually perpendicular π MO's remain intact in the CS (or CO) bond region but only the out-of-plane π MO remains intact in the NC (or CC) bond region. In allene, the four H atoms lie in mutually perpendicular planes with two H atoms at each end of the chain. Only one component of each set of π MO's remains intact in each CC bond region; these are mutually perpendicular to each other and to the plane of the two adjacent H atoms.

B. $^1\Sigma_u^+$ STATE AND CORRELATING SPECIES

The $^1\Sigma_u^+$ state, with electronic orbital angular momentum $\Lambda = 0$ about the internuclear axis, arises from the $1\pi_g(1a_2) \rightarrow 2\pi_u(2b_1)$ MO excitation. The $^1\Sigma_u^+ \leftarrow {}^1\Sigma_g^+$ transition belongs to the class of "V ← N" transitions.[116] These transitions are expected to have particularly high intensities when compared to other intravalency-shell transitions and to have rather high energies—generally approximating those of the lowest energy Rydberg series members. In molecules with off-axis substituents, this transition should remain intact but should be restricted to excitation between the two mutually parallel pure π-orbital components. The transition should be polarized parallel to the molecular axis and should involve considerable charge transfer from the two end atoms to the central atom (see Figure 3). The total energy plots of Figures 7 and 8 predict that the triatomic chain will remain linear in the $^1\Sigma_u^+$ state.

The composite of the experimental inferences from intensities, energies, and vibrational analyses are in complete agreement with the properties expected for an V ← N assignment of this band. Furthermore, this is the only observed absorption band which is clearly allowed in all molecules and which does not split into two components in molecules of lower symmetry. We believe that the V ← N (*i.e.*, $^1\Sigma_u^+ \leftarrow {}^1\Sigma_g^+$) transition assignment for this absorption band is unique.

1. Intensity

The most distinctive feature of the absorption bands assigned as $^1\Sigma_u^+ \leftarrow {}^1\Sigma_g^+$ is their extremely high absorption intensity.

a. $D_{\infty h}$ Species

The V ← N transition should be easiest to identify in these molecules (*i.e.*, CO_2, CS_2, and NNN^-), for it is expected to be the only lower energy orbitally allowed excitation. In agreement with this, the absorption bands which we assign as $^1\Sigma_u^+ \leftarrow {}^1\Sigma_g^+$ (see Table XXII) are by far the most intense of all observed absorption bands. In both CO_2 and CS_2, the experimental oscillator strength[117] is two orders of magnitude larger than that of any other absorption and provides a virtually unquestionable identification. In NNN^-, the experimental oscillator strength of the transition assigned as V ← N is three times larger than the next most intense absorption band. This finding agrees with prediction; however, the oscillator strengths for N_3^- are taken from thin film spectra and, since they may be influenced by solid state factors, the data can be questioned.

b. $C_{\infty v}$ and D_{2d} Species

In these molecules, the transitions to $^1\Pi$ and ^1E states should be allowed also; however, since these transitions derive from the forbidden $^1\Pi_g \leftarrow {}^1\Sigma_g^+$ transition of the $D_{\infty h}$ entities, they are expected to be considerably weaker than the transitions to the $^1\Sigma^+$ and $^1B_2$ states which correlate with $^1\Sigma_u^+(D_{\infty h})$. In agreement with these predictions, all of the experimental oscillator strengths for the bands assigned as transitions to the $^1\Sigma^+$ and $^1B_2$ states are larger than those appropriate to the bands which are assigned as excitations to the $^1\Pi$ and ^1E states (see Table XXII). In the cyanogen halides, the corresponding assigned bands have relative $^1\Sigma^+/{}^1\Pi$ intensities of 3:2, 2:1, and 4:3 for NCI, NCBr, and NCCl, respectively.

c. C_{2v} and C_s Species

In these molecules, many other transitions become allowed; however, the absorption band which is assigned as $^1\Sigma_u^+$-$(^1B_2, {}^1A')$ ← $^1\Sigma_g(^1A_1, {}^1A')$ retains its superior intensity in all cases.

Comparison of the experimental oscillator strengths with those calculated in Table IV shows that agreement between the two is excellent. The calculations indicate an increase in the oscillator strengths for the series $CO_2 < OCS < CS_2$, which is also the case experimentally. This increase in f can be attributed to the proportionality of the transition moment to the equilibrium internuclear distances[116], r_e, which also follow the ordering $CO_2 < OCS < CS_2$. This same trend is observed in the calculated and experimental oscillator strengths of several other series of molecules (*e.g.*, $NNN^- < NCO^- < NCS^-$ and HNNN < HNCO < HNCS) and is a direct result of the increased dipole strength of the transition in molecules with longer bond lengths.

2. Energy

Another distinctive feature of this transition should be its energetic position with respect to the other excitations. The calculations of Mulligan[25] on CO_2 predict the $^1\Sigma_u^+$ state to be the highest energy state of those which result from the $1\pi_g \leftarrow 2\pi_u$ and $3\sigma_u \leftarrow 2\pi_u$ MO excitations. The energy of the state assigned as $^1\Sigma_u^+$ can be seen in Figure 16. The experimental energy ordering of this state in the various molecules is in good agreement with the VESCF CI calculations of Table V, with the barycenter energies from MWH calculations, and with the electronegativity considerations quoted in Table VII. In all cases where Rydberg series have been identified, the state assigned as $^1\Sigma_u^+$ is found to lie in approximately the same energy region as the first members of such series. For example, in CS_2 and OCS the first Rydbergs occur ~2000 cm^{-1} higher than the short-wavelength edge of the transition assigned as $^1\Sigma_u^+ \leftarrow {}^1\Sigma_g^+$; in CO_2, H_2CCCH_2, H_2CCO, C_2H_5NCO, and HNNN the Rydberg bands are

(116) R. S. Mulliken, *J. Chem. Phys.*, 7, 14, 20 (1939).

(117) The maximum extinction coefficient quoted for CS_2 in Table XXIII is 250,000. This value refers to the maximum of the bands. The maximum in the underlying continuum is considerably lower, $\epsilon \sim 35{,}000$.

Table XXII

Energies and Intensities of Electronic Absorption Bands[a]

$D_{\infty h}$ $C_{\infty v}$ D_{2d} C_{2v} C_s	$^1{}_u\Sigma^-(f)$ $^1\Sigma^-(f)$ $^1B_1(f)$ $^1A_2(f)$ $^1A''(z)$	$^1\Delta_u(f)$ $^1\Delta(f)$ $^1A_2(f)$ $^1A_2(f)$ $^1A''(z)$	$^1A_1(f)$ $^1B_2(z)$ $^1A'(x,y)$	$^1\Sigma_u{}^+(z)$ $^1\Sigma^+(z)$ $^1B_2(z)$ $^1B_2(z)$ $^1A'(x,y)$	$^1\Pi(f)$ $^1\Pi(x,y)$ $^1E(x,y)$ $^1A_2(f)$ $^1A''(z)$	$^1B_2(z)$ $^1A'(x,y)$	$^3\Sigma_u{}^+(f)$ $^3\Sigma^+(f)$ $^3B_2(f)$ $^3B_2(f)$ $^3A'(f)$
N_2O ($C_{\infty v}$)	4.54 eV[m] $f \sim 5 \times 10^{-6}$	6.81 eV $\epsilon = 37$ $f = 1.4 \times 10^{-3}$		9.66 eV $\epsilon = 22{,}500$ $f = 0.36$	8.52 eV $\epsilon = 2300$ $f = 7.2 \times 10^{-3}$		4.28 eV[m] $f \sim 2 \times 10^{-7}$
CO_2 ($D_{\infty h}$)	6.53 eV $\epsilon = 0.38$ $f \sim 1 \times 10^{-5}$	8.41 eV $\epsilon = 180$ $f \sim 6.2 \times 10^{-3}$		11.08 eV[b] $\epsilon = 43{,}500$ $f = 0.12$	9.31 eV $\epsilon = 342$ $f \sim 7.5 \times 10^{-3}$		4.89 eV[c]
OCS ($C_{\infty v}$)		5.54 eV $\epsilon = 81.6$ $f = 1.8 \times 10^{-3}$		8.12 eV $\epsilon = 41{,}840$ $f = 0.38$	7.44 eV $\epsilon = 8980$ $f = 0.13$		
CS_2 ($D_{\infty h}$)	3.49 eV $\epsilon \sim 2.5$ $f \sim 8 \times 10^{-5}$	3.89 eV $\epsilon = 35$ $f = 2.7 \times 10^{-4}$		6.29 eV $\epsilon = 2.5 \times 10^5$ $f = 1.1$	7.20 eV $\epsilon = 7800$ $f = 2.9 \times 10^{-2}$		
H_2CCCH_2 (D_{2d})	5.45 eV $\epsilon \sim 30$ $f \sim 1 \times 10^{-3}$		5.76 eV $\epsilon \sim 100$ $f \sim 3 \times 10^{-3}$	7.23 eV $\epsilon \sim 23{,}200$ $f = 0.34$	6.70 eV $\epsilon = 3020$ $f = 3.0 \times 10^{-2}$		
H_2CCO (C_{2v})	3.84 eV $\epsilon = 8.90$ $f \sim 2.3 \times 10^{-4}$		5.82 eV $\epsilon = 1028$ $f = 9.9 \times 10^{-3}$	7.29 eV[d] $\epsilon \sim 10^4$ $f \sim 0.3$		8.00 eV[d] $\epsilon \sim 4 \times 10^3$ $f \sim 1 \times 10^{-1}$	3.35 eV[e] 24 m atm
$(CH_3)_2NCN$ (C_{2v})	4.59 eV $\epsilon = 6.0$ $f \sim 2 \times 10^{-4}$		6.05 eV $\epsilon \sim 3750$ $f = 5.8 \times 10^{-2}$	6.78 eV $\epsilon = 27{,}000$ $f = 0.32$		>6.78 eV	
NCO^- ($C_{\infty v}$)	6.36 eV[f] $\epsilon = 650$ $f = 2.3 \times 10^{-2}$	6.92 eV[f] $\epsilon = 1190$ $f = 4.1 \times 10^{-2}$		9.17 eV[f] $\epsilon = 5740$ $f = 0.20$	8.43 eV[f] $\epsilon = 5310$ $f = 0.18$		3.44 eV[f] $\epsilon = 3.8 \times 10^{-3}$ $f = 1.3 \times 10^{-7}$
C_2H_5NCO (C_s)	5.96 eV[f] $\epsilon = 60$ $f = 2.1 \times 10^{-3}$	6.82 eV[f] $\epsilon = 680$ $f = 2.4 \times 10^{-2}$	7.13 eV[f] $\epsilon = 870$ $f = 3.0 \times 10^{-2}$	8.77 eV[f] $\epsilon = 8800$ $f = 0.30$	7.80 eV[f] $\epsilon = 2200$ $f = 7.6 \times 10^{-2}$	7.93 eV[f] $\epsilon = 4800$ $f = 0.17$	3.44 eV[f] $\epsilon = 3.2 \times 10^{-5}$ $f = 1.1 \times 10^{-9}$
NNN^- ($D_{\infty h}$)	5.39 eV[g] $f = 2 \times 10^{-3}$	6.52 eV[g] $f = 0.5$		8.43 eV[g] $f = 3.0$	8.00 eV[g] $f = 1.0$		
HNNN (C_s)	4.70 eV[g] $\epsilon = 20$ $f = 6.0 \times 10^{-4}$	6.20 eV[g] $\epsilon = 450$ $f = 9 \times 10^{-3}$	6.56 eV[g] $\epsilon = 740$ $f = 1.5 \times 10^{-2}$	8.84 eV[g] $\epsilon = 15{,}000$ $f = 0.3$	7.29 eV[g] $\epsilon = 6800$ $f = 1 \times 10^{-2}$	7.94 eV[g] $\epsilon = 20{,}000$ $f = 0.3$	

NCS^- ($C_{\infty v}$)	5.64 eV[h] $\epsilon \sim 10^{-2}$ $f \sim 3 \times 10^{-5}$					~3.44 eV[h] $f = 3.90 \times 10^{-6}$
HNCS (C_s)	5.06 eV[h]	6.29 eV[h]				~3.44 eV[h]
NCCl ($C_{\infty v}$)	6.98 eV[i] $f = 4.8 \times 10^{-3}$		7.29 eV[i] $f \sim 3 \times 10^{-3}$	9.23 eV[i] $10^{-1} > f > 10^{-2}$	9.09 eV[i] $10^{-1} > f > 10^{-2}$	
NCBr ($C_{\infty v}$)	6.23[i] $f = 2.5 \times 10^{-3}$		6.89 eV[i] $f \sim 3 \times 10^{-3}$	8.22 eV[i] $10^{-1} > f > 10^{-2}$	8.46 eV[i] $10^{-1} > f > 10^{-2}$	
NCI ($C_{\infty v}$)	5.39 eV[i] $f = 4.8 \times 10^{-3}$		6.56 eV[i] $f \sim 2.9 \times 10^{-3}$[j]	7.76 eV[i] $10^{-1} > f > 10^{-2}$	7.87 eV[i] $10^{-1} > f > 10^{-2}$	
H_2CNN (C_{2v})	3.14 eV[k] $\epsilon = 3.0$ $f \sim 1 \times 10^{-4}$		5.70 eV[l]	7.06 eV[l]	6.53 eV[l]	

[a] Only the terminal state of the absorptive act is shown; the ground state is taken as the zero of energy. Energies and extinctions refer to band maxima, except for the $^1\Sigma^+ \leftarrow {}^1\Sigma^+$ and $^1\Pi \leftarrow {}^1\Sigma^+$ transitions of the cyanogen halides for which band origins from ref 104 are listed. When interpreting the polarizations in parentheses, one should take note of the coordinates used in Figure 1. All of the absorption data are from the vapor state with the exception of NCO^-, NNN^-, and NCS^- for which solution and thin-film spectra were used. For this reason, it is difficult to compare the intensities of the transitions in these ions to those of the vapor spectra; the ions are surely effected by solute–solvent interactions. [b] Reference 64. [c] Reference 62. [d] Reference 93. [e] Reference 94. [f] Reference 5. [g] Reference 6. [h] Reference 4. [i] Reference 104. [j] Reference 38. [k] Reference 106. [l] References 107 and 108. [m] Reference 52.

actually superimposed on the continuum of the transition assigned as $^1\Sigma_u^+ \rightarrow {}^1\Sigma_g^+$. The state assigned as $^1\Sigma_u^+$ is the highest energy observed excited state in all molecules except CS_2, NCBr, NCI, H_2CCO, and $(CH_3)_2NCN$ in which case the $^1\Pi_g$ state is slightly higher. For CS_2, NCBr, and NCI the larger more diffuse atomic orbitals of the heavier elements used in constructing the molecular orbitals should lead to an effective decrease in electron repulsions. Thus, the whole manifold of $\pi \rightarrow \pi^*$ states should shift to lower energies. This is apparent from the fact that the computed barycenter of the $\pi \rightarrow \pi^*$ states follows the trend, $CS_2 < OCS < CO_2$ and NCI < NCBr < NCCl. On the other hand, the energy of the $^1\Pi_g$ state resulting from the $\sigma \rightarrow \pi^*$ excitation is not expected to be as variable as that of the $\pi \rightarrow \pi^*$ states (see Figure 16); the energy of this state should remain much more constant than does that of the $^1\Sigma_u^+$ state throughout the series of molecules studied. Thus, for certain molecules, it is not unexpected that the energy of the $^1\Sigma_u^+$ state should lie slightly below that of the $^1\Pi_g$ state.

It is evident from Figure 16 that the state assigned as $^1\Sigma_u^+$ varies over a wider energy range than all other states studied. It varies between a high of 11.08 eV (CO_2) and a low of 6.29 eV (CS_2). This sensitivity to the potential supplied by the individual atoms in the molecule is related to the electronegativities of these atoms and the part which they play in determining the energy of a transition which transfers charge from the end atoms to the central atom.

3. *Vibrational Structure*

All of the bands assigned as $^1\Sigma_u^+ \leftarrow \Sigma_g^+$ are very symmetrical and very broad (*e.g.*, in CS_2 the half-width is $\simeq$2800 cm^{-1}), and the vibronic intensity maximum is always located near the band center. Thus, the potential energy well for the assigned $^1\Sigma_u^+$ state must have a very deep minimum at large r_e. In agreement with this, a Franck–Condon analysis of the absorption band of OCS which we assign as $^1\Sigma^+ \leftarrow {}^1\Sigma^+$ (the analysis followed the methods outlined by Coon, *et al.*[118]) indicates an elongation of the C–S and C–O bond lengths by 0.12 and 0.16 Å, respectively, relative to their ground-state values.

Since the V ← N band should be allowed in all molecules considered, the totally symmetrical vibrations should be most actively coupled.

a. N_2O, $(CH_3)_2NCN$, and CH_3CH_2NCO

The transition assigned as $^1\Sigma_u^+ \leftarrow {}^1\Sigma_g^+$ in these molecules appears as an intense very symmetrical peak with weak diffuse superimposed vibrational structure. This structure has been analyzed[5] for CH_3CH_2NCO and assigned as the totally symmetric deformation mode of the linear NCO group.

b. CO_2, HN_3, and H_2CCO

The corresponding transition in these molecules consists of a strong continuum overlapped by intense Rydbergs. For CO_2 and HN_3, weak vibrational bands are observed but analysis is not clear.

(118) J. B. Coon, R. E. DeWames, and C. M. Loyd, *J. Mol. Spectrosc.*, 8, 285 (1962).

c. H_2CCCH_2

The totally symmetrical stretching frequency and several lower frequency vibrations are observed; however, analysis is complicated by a Rydberg band which is superimposed on the same region.

d. CS_2, OCS, and Cyanogen Halides

These molecules exhibit very sharp intense vibrational structure throughout the region assigned to the V ← N band. Thus, it seems that only those molecules which contain atoms from the third, fourth, ... rows of the periodic table exhibit a sharp vibrational structure in this band. In CS_2 the predominant vibrational progression has been assigned as the totally symmetrical stretching frequency; however, lower frequency vibrations are also excited and are not fully understood. Rotational analysis[81] of the CS_2 band system provides a $^1B_2(^1\Sigma_u^+) \leftarrow {}^1A_1(^1\Sigma_g^+)$ assignment, in agreement with our own. In OCS, the frequency observed also pertains to the totally symmetric vibration; however, other low-frequency unassigned vibrations do occur. The vibrational structure in the cyanogen halides has been assigned[104] as ν_1 and ν_3, both of which are totally symmetrical.

Progressions in the totally symmetrical vibrations are observed in all cases, and the assignment as the allowed $^1\Sigma_u^+ \leftarrow {}^1\Sigma_g^+$ transition is supported.

C. $^1\Pi_g$ STATE AND CORRELATING SPECIES

The doubly degenerate $^1\Pi_g$ state possesses electronic orbital angular momentum $\Lambda = 1$ about the symmetry axis. The $^1\Pi_g \leftarrow {}^1\Sigma_g^+$ transition derives from the $3\sigma_u(3b_2) \leftarrow 2\pi_u(6a_1$ and $2b_1)$ MO excitation. This transition corresponds, in the atomic case, to the $np\sigma \rightarrow np\pi$ AO excitation which is Laporte forbidden; this forbiddenness is retained in $D_{\infty h}$ molecules in the form of the parity rule. When allowed, as it is in molecules of symmetry other than $D_{\infty h}$, this transition should be polarized perpendicular to the molecular axis and should involve a very small amount of charge transfer from the end atoms to the central atom. The total energy plots of Figures 7 and 8 predict that the degeneracy of the $^1\Pi_g$ state will usually resolve into two components: the $^1B_2$ state which is bent and the $^1A_2$ state which is nearly linear.

The unusual characteristics of allowedness *vs.* forbiddenness, degeneracy splitting, and vibronic coupling which should be associated with this transition provide, we believe, a unique basis for its assignment. All of these characteristics lead to the $^1\Pi_g$ assignments which we have made: the $^1\Pi_g$ state is the only state to which a transition is forbidden in $D_{\infty h}$ and allowed in all other point groups and to which two allowed component transitions occur in molecules of C_s symmetry.

1. Intensity

The transition assigned as $^1\Pi_g \leftarrow {}^1\Sigma_g^+$, and its analog in molecules of lower symmetry, is found to be the second most intense absorption band in all molecules studied. (The most intense band is that assigned as V ← N in the previous section.)

a. $D_{\infty h}$ Species

The $^1\Pi_g \leftarrow {}^1\Sigma_g^+$ transition is forbidden by dipole selection rules in $D_{\infty h}$. The oscillator strength of the band assigned to this transition is $10^{-3} < f < 10^{-2}$ in both CO_2 and CS_2. This intensity is considerable; it is attributable to either a vibronic coupling involving π_u and/or σ_u^+ vibrations, or to a serious departure from $D_{\infty h}$ symmetry in the excited state, or both. The only exceptional molecule is N_3^-; the intensity of the correlating transition in this molecule is very high, but, since this is a solid-state spectrum and since other influences intervene here, we treat this datum lightly.

b. $C_{\infty v}$ and D_{2d} Species

The transition to the $^1\Pi_g$ analog state of these molecules ($^1\Pi$ and ^1E states, respectively) is allowed; its intensity, however, should remain comparably moderate for genealogical reasons. These conclusions agree with experiment. Since the $^1\Sigma^+ \leftarrow {}^1\Sigma^+(C_{\infty v})$ and $^1B_2 \rightarrow {}^1A_1(D_{2d})$ transitions discussed in the previous section are the only other allowed transitions expected in these molecules, the $^1\Pi_g \rightarrow {}^1\Sigma_g^+$ analog transitions are, we believe, readily identified in these systems.

c. C_{2v} Species

The $^1\Pi_g$ state should split into $^1A_2$ and $^1B_2$ components in C_{2v} molecules; however, of the two possible transitions, only the $^1B_2 \leftarrow {}^1A_1$ transition should be allowed. In accord with this, we find only one absorption band of moderate intensity in the appropriate energy range in C_{2v} molecules.

d. C_s Species

The $^1\Pi_g$ state is expected to split into $^1A''$ and $^1A'$ components in C_s molecules; transitions to both of these states should be allowed and both should be observed. We observe both transitions in these C_s molecules. The more intense of the two transitions is the one which is analog to the $^1B_2 \leftarrow {}^1A_1$ transition of the C_{2v} entities; the oscillator strengths for this transition run as high as $f \approx 0.3$ (in HNNN).

2. Energy

The energetic position of the $^1\Pi_g$ state and its splitting in the lower symmetry point groups is a useful diagnostic tool. The $^1\Pi_g$ state is usually the second highest energy state, the $^1\Sigma_u^+$ state being highest; however, as mentioned earlier, the order of these two states is inverted in certain molecules in which the manifold of $\pi \rightarrow \pi^*$ states shifts to lower energies. The $3\sigma_u \rightarrow 2\pi_u$ excitation involves very little charge transfer; it should not be affected, therefore, to the same extent as the $\pi \rightarrow \pi^*$ states by variations in the potential imposed by the individual atoms. In accord with this, the small variation in the energy of the band assigned to the $^1\Pi_g \rightarrow {}^1\Sigma_g^+$ transition throughout the whole series of molecules is remarkable. As shown in Figure 16, it varies from a high of 9.31 eV in CO_2 to a low of 6.5 eV in H_2CNN.

Both allowed components of the split $^1\Pi_g$ state have been identified in the molecules which are of C_s symmetry. In the C_{2v} molecules, the one allowed component has been observed, making the assignment reasonably secure.

The energy ordering of this transition in the various molecules, as predicted from the MWH calculations (see Table

VII), is in good agreement with the experimental ordering of Figure 16.

3. Vibrational Structure

The vibrational structure of this band is most interesting.

a. $D_{\infty h}$ Species

In CO_2 and CS_2, where the $^1\Pi_g \leftarrow {}^1\Sigma_g^+$ transition is forbidden, coupling with the π_u and σ_u^+ normal modes is the only vibronic coupling which can confer allowedness. Vibrational analyses of the assigned bands indicate that the frequencies are much too low to be σ_u^+; they appear to correspond, instead, to the π_u mode. In CS_2, a distinct progression, consisting only of odd members of the π_u mode, is observed in the assigned band. In the corresponding band of CO_2, it is assumed that the upper state is slightly bent so that one degree of freedom cannot be categorized as either rotational or vibrational. The selection rules are thus relaxed, allowing every quantum of the bending mode to appear. This quasi-linear situation would cause the vibrational frequencies to be irregular, thereby accounting for the irregularities in the observed intervals. In both of these molecules, the frequency of the π_u mode in the excited state is virtually unchanged from that in the ground state.

b. $C_{\infty v}$ and D_{2d} Species

In these molecules where transitions to the $^1\Pi$ and ^1E states are expected to be allowed, coupling of any number of vibrational quanta of π or e modes is allowed. In OCS two progressions in the π-bending mode are observed in the assigned band. In this case every single vibrational quantum jump is found in both progressions. The frequency separation of the two progressions does not correspond to any known ground-state interval and could represent a splitting of the $^1A''$ and $^1A'$ components of the $^1\Pi$ state of the bent molecule. These upper states are very strongly bent; the Franck–Condon maxima are quite far removed ($\simeq$7000 cm^{-1}) from seemingly forbidden origins.

In N_2O, a very prominent progression attributed to the bending mode ν_2 is observed in the assigned band; considerable anharmonicity occurs at higher frequencies and the Franck–Condon maximum is far removed from the origin. Other lower frequency bands are also observed in N_2O, but their assignment is not obvious. Both $\nu_1(\sigma^+)$ and $\nu_3(\sigma^+)$ are observed in the cyanogen halides. In the corresponding transition of allene, a progression which consists of every quantum of the bending frequency, e, is observed, with the intensity maximum again far removed from the origin.

c. C_{2v} Species

The assigned $^1B_2(^1\Pi_g) \leftarrow {}^1A_1(^1\Sigma_g^+)$ absorption band of H_2CCO and H_2CNN is overlapped by strong Rydberg bands. The H_2CCO band shows only continuous absorption while the H_2CNN band exhibits a discrete vibrational structure on which rotational analysis provides[108] a $^1B_2 \leftarrow {}^1A_1$ assignment.

d. C_s Species

In HNNN and CH_3CH_2NCO, the transitions assigned as the two components of the split $^1\Pi_g \leftarrow {}^1\Sigma_g^+$ transition (*i.e.*, $^1A'' \leftarrow {}^1A'$ and $^1A' \leftarrow {}^1A'$) appear as strong continua with vibrational structure observable only in CH_3CH_2NCO. This structure is weak and diffuse; however, the spacings are similar to those of the $\nu_4(a')$ ground-state vibration.

Thus, in all molecules except the cyanogen halides, the absorption bands assigned as $^1\Pi_g \leftarrow {}^1\Sigma_g^+$ exhibit distinct vibrational structure containing the π_u bending vibration as the most prominent mode or show some evidence for the presence of the π_u mode. In all cases, the vibrational analysis supports the $^1\Pi_g \leftarrow {}^1\Sigma_g^+$ assignment, and, in some cases, it makes this assignment unique.

D. $^1\Delta_u$ STATE AND CORRELATING SPECIES

The forbidden $^1\Delta_u \leftarrow {}^1\Sigma_g^+$ transition derives from the $^1\pi_g(1a_2$ and $4b_2) \rightarrow 2\pi_u(6a_1)$ MO excitation. The $^1\Delta_u$ state is doubly degenerate with $\Lambda = 2$. The total energy plots of Figures 7 and 8 suggest that the $^1\Delta_u$ state should invariably resolve into two components—a $^1B_2$ state of a bent molecule and a $^1A_2$ state of an almost linear molecule—because the excited $^1\Delta_u$ state is not stable with respect to molecular bending deformations. The descriptive features of this transition, as derived from group theory, should permit reasonably secure identification. The $^1\Delta_u \leftarrow {}^1\Sigma_g^+$ transition is the only one which is forbidden in $D_{\infty h}$, $C_{\infty v}$, and D_{2d} and which should show one allowed component in C_{2v} and two allowed components in C_s.

1. Intensity

The intensity characteristics of the transition assigned as $^1\Delta_u \leftarrow {}^1\Sigma_g^+$ are different from all other absorptions considered and provide an unmistakable means of assignment.

a. $D_{\infty h}$, $C_{\infty v}$, and D_{2d} Species

The assigned absorption band is undoubtedly electric-dipole forbidden in $D_{\infty h}$, $C_{\infty v}$, and D_{2d}. Furthermore, in D_{2d}, it splits into two-component transitions both of which appear to be forbidden. If we consider magnetic dipole radiation, electric quadrupole radiation, and first-order vibronic coupling as the primary means by which an electric-dipole forbidden transition gains intensity, we find that in $D_{\infty h}$ all three methods should be inoperative; in $C_{\infty v}$ the first mechanism should be no value; and, in the two resolved D_{2d} transitions, vibronic coupling should be allowed for both, magnetic dipole absorption should be allowed for one, and electric quadrupole radiation should be allowed for the other. Thus, $D_{\infty h}$ molecules must resort to second-order vibronic coupling in order to gain transition intensity for such an absorption band. However, from the predictions of Figures 7 and 8, it is entirely plausible that the linear triatomic chain is bent in the $^1\Delta_u$ state, thus relaxing the stringent selection rules specified above and conferring the observed intensity.

It is found experimentally that the oscillator strengths are very low, ranging from 6.2×10^{-3} in CO_2 to 2.7×10^{-4} in CS_2 as shown in Table XXII.

b. C_{2v} and C_s Species

In these molecules, the assigned transition should split into two components, both of which should be allowed in C_s and only one of which should be allowed in C_{2v}. Despite this allowedness, the experimental intensities remain low

(maximum $f = 5.8 \times 10^{-2}$). However, these small f values do accord with the forbidden genealogy of the assigned process. The computed oscillator strengths for the states are given in Table IV; they concur with the above qualitative considerations and they are in satisfactory agreement with experiment. Thus, general intensity considerations concur in the $^1\Delta_u$ assignment.

2. Energy

The energy of the $^1\Delta_u$ state, as predicted by Mulligan,[25] should be lower than that of the $^1\Pi_g$ and $^1\Sigma_u^+$ states but higher than that of the $^1\Sigma_u^-$ state. From Figure 16 it can be seen that the energy of the band assigned as $^1\Delta_u$ concurs with these predictions. Its energy is significantly lower than the first Rydberg series members. The energy of the state assigned as $^1\Delta_u$ varies over a wide range, going from a high of 8.41 eV (CO_2) to a low of 4.06 eV (CS_2). The transition energy decreases consistently by a large amount in the series $CO_2 > OCS > CS_2$ indicating the sensitivity to the electronegativity of the two end atoms (from which charge should transfer to the central atom in the course of a $^1\Delta_u \leftarrow {}^1\Sigma_g^+$ transition). The two allowed components expected in C_s and the one allowed component expected in C_{2v} have been identified experimentally.

3. Vibrational Structure

Owing to the extreme variances in the selection rules for the $^1\Delta_u \leftarrow {}^1\Sigma_g^+$ transition in the various point groups considered, it is expected that the characteristics of this transition will vary considerably. These features are of much value in following this transition in the various molecules.

a. $D_{\infty h}$ Species

The $^1\Delta_u \leftarrow {}^1\Sigma_g^+$ transition is expected to be electric dipole forbidden in $D_{\infty h}$ molecules. The band assigned as this transition is very broad (*e.g.*, the half-width in CO_2 is $\simeq$9000 cm^{-1}), the extinction coefficient is low, and the origin appears to be forbidden. The transition is also expected to be forbidden by magnetic dipole, electric quadrupole, and first-order vibronic coupling selection rules. Indeed, it must resort to second-order vibronic coupling or to bending in the upper state in order to gain allowedness. As stated earlier, there is experimental evidence for such a bending of the upper state of the assigned absorption band. In CO_2 and CS_2 the absorption band possesses very complicated vibrational structure which is not well understood. The complexity of these bands probably arises from the splitting of the assumed $^1\Delta_u \leftarrow {}^1\Sigma_g^+$ transition into the allowed $^1B_2 \leftarrow {}^1A_1$ and forbidden $^1A_2 \leftarrow {}^1A_1$ components whose vibrational structure overlaps in certain regions. Indeed, the very breadth of the CO_2 band suggest the presence of two transitions.

b. $C_{\infty v}$ Species

The absorption band in these molecules is very similar to that in the $D_{\infty h}$ species; however, it should be forbidden only by electric dipole selection rules in the $C_{\infty v}$ point group. In OCS and N_2O, the absorption band appears as a low broad continuum (*e.g.*, the half-width is $\simeq$5000 cm^{-1} for OCS and $\simeq$7400 cm^{-1} for N_2O) with weak diffuse vibrational structure superimposed on it. The cyanogen halides exhibit no vibrational structure in this absorption band.

c. D_{2d} Species

The transition is expected to be forbidden; in agreement with this, the assigned transition in allene exhibits only a low broad continuum with no vibrational structure. The low broad continuum evidently contains the two forbidden split components of the $^1\Delta_u \leftarrow {}^1\Sigma_g^+$ transition, that is, $^1A_2 \leftarrow {}^1A_1$ and $^1A_1 \leftarrow {}^1A_1$.

d. C_{2v} Species

The expected single allowed component of this band in C_{2v} has been identified in all cases. In H_2CNN, the absorption is found to be broad and continuous. In $(CH_3)_2NCN$, it exhibits weak diffuse vibrational bands which have been assigned as the totally symmetric CH_3 deformation mode. In H_2CCO, four distinct vibrational bands are observed; their intensity distribution indicates an allowed origin. This progression in H_2CCO is assigned as the symmetrical CH deformation frequency and is very similar to corresponding vibrational structure observed in one of the absorption bands of acetone.

e. C_s Species

In C_s, the expected two allowed components are observed. They are very broad and cover a large region of the spectrum. Both components are also observed in CH_3CH_2NCO; they are continuous, with no observable vibrational structure. In HN_3, the lower component transition, which we assign as $^1A'' \leftarrow {}^1A'$, exhibits two interleaved progressions in the symmetrical N–N–N stretching frequency; the displacement between the progessions corresponds to one of the N–N–N bending modes. The higher energy component of this band, which we assign as $^1A' \leftarrow {}^1A'$, shows a single progression in the a'' bending frequency of N–N–N.

The vibrational assignments and band shapes are those expected for $^1\Delta_u \leftarrow {}^1\Sigma_g^+$ and correlating transitions.

E. $^1\Sigma_u^-$ STATE AND CORRELATING SPECIES

The $^1\Sigma_u^-$ state results from the MO excitation $1\pi_g(4b_2) \rightarrow 2\pi_u(2b_1)$ and has $\Lambda = 0$. This transition is expected to have particularly low intensities compared to other intravalency shell excitations. The total energy plots of Figures 7 and 8 suggest that the triatomic chain is bent to $\sim$140° in this excited state. In molecules with off-axis substituents, the transition should take place from the occupied in-plane "π" MO to the unoccupied "π" MO perpendicular to the molecular plane. The $^1\Sigma_u^- \leftarrow {}^1\Sigma_g^+$ transition should correspond to the forbidden $n \rightarrow \pi^*$ transition of aldehydes and ketones. In the molecules considered here, the analog of the nonbonding electrons on the oxygen atom of the aldehydes and ketones are either "bonding" or "antibonding" with the in-plane "π" orbital on the central atom as shown in Figure 4. Thus, the "nonbonding" character is lost.

The distinguishing features of weak intensity and low energy agree with experiment and point to the $^1\Sigma_u^-$ assignment. This is the only singlet $\leftarrow$ singlet transition which should be forbidden in all point groups except C_s and which should not split into two components in the low-symmetry

molecules. The features of the assigned absorption concur with these predictions.

1. Intensity

The $^1\Sigma_u^- \leftarrow {}^1\Sigma_g^+$ transition is electric dipole forbidden in all point groups except C_s where it should be polarized perpendicular to the molecular plane. It is also forbidden by magnetic dipole, electric quadrupole, and first-order vibronic coupling selection rules in $D_{\infty h}$; in $C_{\infty v}$, the first and third methods are allowed; in D_{2d}, the latter two are available; in C_{2v}, all three methods are allowed.

a. $D_{\infty h}$, $C_{\infty v}$, D_{2d}, and C_{2v} Species

The high degree of forbiddenness expected for the $^1\Sigma_u^- \leftarrow {}^1\Sigma_g^+$ transition is manifest in the low intensity of the bands assigned to this transition. For example, the highest oscillator strength observed is 4.8×10^{-3} (in NCCl and NCI). An absorption path length of 33 m and several atmospheres pressure was used[52] to observe the transition in N_2O. The corresponding transition has not been observed in OCS and allene; an investigation in long path lengths would be most interesting.

b. C_s Species

In C_s molecules, where the $^1A''(^1\Sigma_u^-) \leftarrow {}^1A'(^1\Sigma_u^+)$ transition is allowed, the maximum extinction in the assigned bands is only 60.1 mol^{-1} cm^{-1}.

The calculated oscillator strengths for the allowed analog transitions (see Table IV) are in good agreement with experimental values. Thus, the low intensity of the bands assigned to the $^1\Sigma_u^- \leftarrow {}^1\Sigma_g^+$ transition is in full accord with the theoretical predictions.

2. Energy

The calculations of Mulligan[25] predict that the $^1\Sigma_u^-$ state should be the lowest energy excited singlet state. From Figure 16, it is apparent that this is indeed the case for the transition assigned as $^1\Sigma_u^- \leftarrow {}^1\Sigma_g^+$. The energy varies over a smaller range than the other $\pi \rightarrow \pi^*$ states (*i.e.*, $^1\Delta_u$ and $^1\Sigma_u^+$) ranging between 6.53 eV in CO_2 to 3.14 eV in H_2CNN. However, this is still a wider range than that covered by the $^1\Pi_g$ state.

3. Vibrational Structure

For most of the molecules studied the absorption assigned as $^1\Sigma_u^- \leftarrow {}^1\Sigma_g^+$ appears as a weak continuous absorption band with a forbidden origin and no vibrational structure. The only molecules with structure are the following.

H_2CCO and H_2CNN. Very weak diffuse vibrational bands have been observed in these molecules; however, analysis is not feasible.

CS_2. A very complex vibrational structure is observed in the $^1\Sigma_u^- \leftarrow {}^1\Sigma_g^+$ transition of CS_2. This structure is not completely understood; however, the bands are very sharp and well resolved.

HNCO. A long progression in the bending mode has been observed in the corresponding transition of HNCO.

HNNN. The transition in HNNN exhibits two diffuse interleaved progressions in the a′ antisymmetric N–N–N stretching mode which are separated by one of the bending modes.

The contours of these absorption bands and the fact that most of them are continuous and show only very weak diffuse vibrational structure indicate that the transition is forbidden, in agreement with the $^1\Sigma_u^- \leftarrow {}^1\Sigma_g^+$ assignment.

F. TRIPLET STATES

The manifold of triplet states is of particular importance in photochemistry. Owing to the low extinction coefficients of triplet ← singlet absorption bands and the fact that phosphorescence of triplet → singlet character usually occurs only from the lowest energy triplet state, it is difficult to obtain information on the triplet mainfold. The calculations of Mulligan[25] predict the order of energies: $^3\Sigma_u^+ < {}^3\Delta_u < {}^3\Sigma_u^- < {}^3\Pi_g$. The singlet–triplet intervals $^3\Sigma_u^- - {}^1\Sigma_u^-$ and $^3\Pi_g - {}^1\Pi_g$ are expected to be negligible; the $^3\Delta_u - {}^1\Delta_u$ interval is expected to be considerably larger; and the interval $^3\Sigma_u^+ - {}^1\Sigma_u^+$ is predicted to be very large. Thus, the $^3\Pi_g$, $^3\Sigma_u^- \leftarrow {}^1\Sigma_g^+$ transitions should lie at high energies and should be masked by strong singlet ← singlet absorptions; the $^3\Sigma_u^+$, $^3\Delta_u \leftarrow {}^1\Sigma_g^+$ transitions should lie at lower energies and might be observable.

The lowest triplet state of N_2O has been observed[52] in an absorption path length of 33 m at several atmospheres pressure; that of H_2CCO[94] has been observed at 24 m atm. A triplet state has also been observed[80,87] in CS_2 using high-resolution studies of magnetic rotation and Zeeman effects. The lowest triplet states of HNCO, C_2H_5NCO, NCO^- salts, NCS^- salts, and NNN^- salts have been observed[4,5] in either absorption, emission, or both. The lowest triplet of CO_2 has been observed[62] in emission. As seen in Figure 16, the energies of these states lie well below the lowest energy excited singlet state, $^1\Sigma_u^-$. From the experimental and computational evidence,[4,5] there is little doubt of the spin-forbidden nature of this transition. The reasons for the triplet assignment are the following.

(a) The extinction coefficients observed for the absorptive transition are extremely low for singlet ← singlet transitions but in the expected range for singlet ← triplet transitions.

(b) The decay lifetimes observed in the emissive transition are much too long to be of a fluorescence nature; they must represent intrinsic molecular phosphorescence decay from a triplet state.

(c) The lifetimes of the anion luminescences appear to decrease as the atomic number of the associated metal cation increases. This seems to be the "external heavy-atom spin-orbit coupling effect" so common to molecular phosphorescence.

(d) The extinction coefficients of the anion absorptions appear to increase as the atomic number of the associated metal cation increases, demonstrating, again, the same spin-orbit effect specified in (c).

(e) VESCF CI calculations performed here (see Table V), as well as those of Mulligan,[25] indicate that the lowest energy electronic state of all these molecules is a triplet state. This, of course, would also be the qualitative prediction based on the simple application of Hund's rules.

(f) Studies of the magnetic rotation and Zeeman effects in CS_2 have proven that the lowest excited state is a triplet.

Having established the probable triplet character of this lowest energy transition, the next question concerns the nature

of the orbital excitation involved. The most telling evidence relating to the orbital excitation type is provided by the correspondence of observed phosphorescence lifetimes with those obtained from spin-orbit coupling calculations.[5] Experimental phosphorescence lifetimes of CH_3NCO and NaOCN are approximately 2 and 0.2 sec, respectively. The calculated lifetime of the $^3\Sigma_u^+ \rightarrow {}^1\Sigma_g^+$ transition in linear NCO^-, in bent NCO^-, and in HNCO is ~0.12 sec, which corresponds closely to experiment. The calculated lifetime of the $^3\Delta_u \rightarrow {}^1\Sigma_g^+$ and $^3\Sigma_u^- \rightarrow {}^1\Sigma_g^+$ transitions is $\sim 10^3$ times shorter than the experimental lifetime.[5] Thus, we predict that the orbital-excitation type is $\pi_x \rightarrow \pi_x^*$ or $\pi_y \rightarrow \pi_y^*$ (*i.e.*, $^3\Sigma_u^+ \rightarrow {}^1\Sigma_g^+$).

The luminescence of the NCO^- ion and its salts is very similar to that of the alkyl isocyanates; indeed, the decay times τ_p are somewhat longer. In the case of phenyl isocyanate, there seems to be little doubt that the transition is of $\pi \rightarrow \pi^*$ type. In view of the out-of-plane nature of the π and π^* orbitals of the phenyl isocyanate, it follows that the $\pi_x \rightarrow \pi_x^*$ and $\pi_y \rightarrow \pi_y^*$ nature of the corresponding transition in the cyanate grouping is validated.

A Stokes shift of ~7000 cm^{-1} between the maxima of the corresponding absorption and phosphorescence bands of NCO^- is taken as evidence of the bent nature of the excited state. If the excited state is assigned as $^3\Sigma_u^+$, our calculations indicate that the energy of this state should decrease upon bending the triatomic chain. The phosphorescence, therefore, might be labeled more properly as $^3A'(C_s) \rightarrow {}^1\Sigma^+(C_{\infty v})$.

Thus, in all cases where the emission is observed,[4,5] it seems well established that the lowest triplet state is of $^3\Sigma_u^+$ species. The assignment is less certain in N_2O and H_2CCO where only absorption has been observed. However, by analogy with the examples cited above, the lowest energy excited state should be $^3\Sigma_u^+(D_{\infty h})$, $^3\Sigma^+(C_{\infty v})$, $^3B_2(D_{2d})$, $^3B_2(C_{2v})$, or $^3A'(C_s)$.

G. RYDBERG STATES

Rydberg series have been mapped for CS_2, OCS, allene, and HN_3. These series yield 10.10, 11.01, 10.19, and 11.15 eV, respectively, for the lowest ionization potentials (*i.e.*, removal of an electron from the $1\pi_g$ MO's). These ionization potentials are in excellent agreement with those obtained by other methods, as shown in Table VI. Of the several computational methods used, the MWH calculations are found to give the best first ionization potentials.

V. Conclusion

This work contains the identification of a large number of electronic absorption and emission bands in the spectra of 16 valence-electron molecules and ions. These identifications are based on three attitudes: (1) a correlation of symmetry representations and various properties of the electronic states such as intensity, energy, vibrational structure, etc., throughout the gamut of molecular point groups; (2) a correlation of the experimental and calculated electronic properties of the various molecules; and (3) the use of specific assignments obtained by vibrational and/or rotational analysis of some individual absorption bands, usually by other authors.

In view of the large number of correlations and assignments that have been made here, it is expected that certain ones will and should be questioned. In specific, Table XXII contains the assignment of 73 transitions (not counting Rydberg's!) in 17 molecules and ions. Those transition assignments we consider most tentative are

N_2O: $^1\Sigma^- \leftarrow {}^1\Sigma^+$; $^3\Sigma^+ \leftarrow {}^1\Sigma^+$
CO_2: $^3\Sigma_u^+(^3B_2) \rightarrow {}^1\Sigma_g^+$
OCS: $\pi \rightarrow n$s Rydberg series
CS_2: $^1\Pi_u \leftarrow {}^1\Sigma_g^+$; the $n = 3$ members of the three $\pi \rightarrow n$d Rydberg series
H_2CCCH_2: $^1A_1(^1\Delta_u) \leftarrow {}^1A_1(^1\Sigma_g^+)$; $^1A_2(^1\Delta_u) \leftarrow {}^1A_1(^1\Sigma_g^+)$
H_2CCO: $^1B_2(^1\Pi_g) \leftarrow {}^1A_1(^1\Sigma_g^+)$
NCCl, NCBr, NCI: $^1\Pi \leftarrow {}^1\Sigma^+$; $^1\Sigma^+ \leftarrow {}^1\Sigma^+$
H_2CNN: $^1B_2(^1\Pi_g) \leftarrow {}^1A_1(^1\Sigma_g^+)$; $^1B_2(^1\Sigma_u^+) \leftarrow {}^1A_1(^1\Sigma_g^+)$

Finally, the greatest vindication of the assignments we make lies in their reasonableness and their conformity to symmetry correlations for such a large number of molecules.

Acknowledgments. We wish to thank Dr. H. J. Maria for his helpful discussions concerning the interpretation of experimental data and Dr. C. J. Ballhausen and Dr. C. J. Seliskar for critically reading the entire manuscript.